THE ALUMINUM/OXYGEN ELECTROCHEMICAL CELL:
A NOVEL APPROACH TO CHEMICAL CONVERSION AND ENERGY STORAGE

A Dissertation

Presented to the Faculty of the Graduate School

of Cornell University

In Partial Fulfillment of the Requirements for the Degree of

Doctor of Philosophy

by

Wajdi Issam A Al Sadat

December 2017

THE ALUMINUM/OXYGEN ELECTROCHEMICAL CELL: A NOVEL APPROACH TO CHEMICAL CONVERSION AND ENERGY STORAGE

Wajdi Issam A Al Sadat, Ph. D.

Cornell University 2017

The highly reactive superoxide (O_2^-) is produced during the galvanostatic discharge of metal/O_2 electrochemical cells. In combination with high energy density metal anodes, metal/O_2 batteries provide exceptional energy density capacity. By properly selecting a catalytic electrolyte for the cell and exploiting the nucleophilic properties of the superoxide, we demonstrate the ability to deploy the system for energy production and low-value chemicals upgrade/conversion.

The examined Al/O_2 electrochemical system uses Al as the anode and an imidazolium-based ionic liquid/$AlCl_3$ salt electrolyte. Compared to other high energy density metals, Al is more abundant, inherently safer to handle and has higher volumetric capacity. The selected electrolyte has been shown to complex with thermodynamically stable chemicals and catalyze their conversion.

Herein we report an Al/O_2+CO_2 electrochemical cell with the ability to capture and convert CO_2 to useful C_2 species, oxalate, while enhancing the discharge capacity of the cell. We, also, report the deployment of the Al/O_2 electrochemical cell to oligomerize, isomerize and carboxylate hydrocarbon feedstocks, providing an alternative to the classical energy-intensive hydrocarbon refining and fuel producing processes.

BIOGRAPHICAL SKETCH

Wajdi Al Sadat was born in Saudi Arabia. He received his B.S. in Chemical Engineering from Louisiana State University in 2001. Before joining Cornell, Wajdi worked for 12 years in the oil and gas industry (Saudi Aramco) and has been involved in the design, construction, operation and decommissioning of oil and gas production and processing plants. He completed his M.S. in Chemical Engineering at King Fahd University of Petroleum & Minerals in 2009 as a part-time student. In 2010, he joined the R&D Center as a member of the Carbon Management team and was instrumental in demonstrating the feasibility of Onboard Carbon Capture. Wajdi earned his Ph.D. in 2017 from the Robert Frederick Smith School of Chemical and Biomolecular Engineering at Cornell University under the supervision of Prof. Lynden A. Archer working on a novel conversion system of low-value feedstocks (including CO_2) based on the metal/O_2 electrochemical cell.

Dedicated to my family; especially my wife.

ACKNOWLEDGMENTS

Asking Prof. Lynden Archer to advise and guide me through my Ph.D. was one of the best decisions I made in my life. His grasp of fundamentals and ability to eloquently ask the most important questions never ceased to amaze me. Though I joined Cornell with a different experience, and even research interests, from his group members he still accepted me in. Although the research project we agreed to tackle was high risk, he trusted that I am the right candidate to tackle it. Every time the results and progress take a turn for the worse, I remember what he said on our first meeting, “all flowers bloom, in their own time.”

I would like to thank my thesis committee members, Prof. Jefferson Tester and Prof. Jin Suntivich for their guidance and for asking the questions that were not obvious to me. I had the chance to take courses with both of them and I am grateful that I was able to apply the principles they taught me in my own research. I would like to thank the CBE faculty members that taught us the first-year core courses (Professors Donald Kock, Yong Joo, Susan Daniel, Fernando Escobedo, Tobias Hanrath, Julius Lucks and Claude Cohen.) They really helped us see what we’re made of and what we can do.

I am thankful to Archer Group members for their support and for asking the right questions. I know I asked too many questions and they were very patient with me. Even though we had varying research interests, I enjoyed and learned a lot from our group meetings. I am particularly grateful to Dr. Shaomao Xu who put in the time and effort to help me start my lab work.

I am grateful to the support and training I received at the shared Cornell facilities including KAUST-Cornell Center for Energy and Sustainability, Cornell Center for Materials Research (CCMR), Cornell NMR Facility and Center for Nanomaterials Engineering & Technology (CNET). The discussions and interactions with the people managing those facilities have been instrumental to my research. I would to particularly thank Ivan Keresztes, Anthony Condo, Brenda Fischer, Jon Shu, Mick Thomas, Darren Dale and Maura Weathers.

The love and support of my family kept me sane. I couldn't have done this without their help. Most importantly, I am grateful for and to my wife for her support and for understand how important this work is to me.

TABLE OF CONTENTS

LIST OF FIGURES

electrolyte. Detected hydrocarbons are denoted on the TIC (blue, green and red for saturated, unsaturated and carboxylated hydrocarbons, respectively). The insert table lists the yield of the main components. The inset presents the different components of an electrochemical cuvette with limited hydrocarbon/electrolyte exposure.

Figure 2.12. GC-MS TIC of 1-decene discharged in an Al/80%CO_2 cell. The electrolyte is based on 2:1($AlCl_3$:EMImCl). The 1-decene had limited exposure to the electrolyte. Detected hydrocarbons are denoted on the TIC (blue, green and red for saturated, unsaturated and carboxylated hydrocarbons, respectively). The insert table lists the yield of the main components. The inset presents the different components of an electrochemical cuvette with limited hydrocarbon/electrolyte exposure.

Figure S2.1. RGA-MS of electrochemical cell headspace. The spectra are for n-decane discharged under O_2, n-decane mixed with 2:1 ($AlCl_3$:EMImCl) electrolyte under O_2 and n-decane without the electolyte. Logarithmic scale was use to account for the large intensity difference between O_2 and hydrocarbons.

Figure S2.2. RGA-MS difference of the electochemical cell's headspace. The spectra shows the difference between the Al/O_2 cell discharged with n-decane and only mixed with n-decane. The electrolyte is based on 2:1 ($AlCl_3$:EMImCl). The inset lists the yields of the main components generated when Al/O_2 electochmical cell is disharged.

Figure S2.3. GC-MS Total Ion Count (TIC) chromatogram of top n-decane layer. N-decane was mixed with 1:2.3 ($AlCl_3$:EMImCl) electrolyte and exposed to O_2. Only n-decane was detected with no indication for fractionation, isomerization, branching or up-conversion.

Figure S2.4. GC-MS TIC of bottom 1:2.3 ($AlCl_3$:EMImCl) electrolyte layer. The electrolyte was mixed with n-decane and exposed to O_2. Only n-decane was detected with no indication for fractionation, isomerization, branching or up-conversion.

Figure S2.5. GC-MS TIC of top 1-decene layer. 1-decene was mixed with 1:2.3 ($AlCl_3$:EMImCl) electrolyte and exposed to O_2. No indication of conversion or hydrogenation.

Figure S2.6. GC-MS TIC of bottom 1:2.3 ($AlCl_3$:EMImCl) electrolyte layer. The electrolyte was mixed with 1-decene and exposed to O_2. No indication of conversion or hydrogenation.

Figure S2.7. GC-MS TIC of n-decane discharged in an Al/80%CO_2 cell. The hydrocarbon was discharged using 2:1 ($AlCl_3$:EMImCl) electrolyte. The spectrum is identical to the Al/O_2 case.

Figure S2.8. GC-MS TIC of 1-decene discharged in an Al/80%CO_2 cell. The hydrocarbon was discharged using 2:1 ($AlCl_3$:EMImCl) electrolyte. The spectrum is identical to the Al/O_2 case.

Figure S2.9. Positive-ion DART-MS spectra of top n-decane layer. The hydrocarbon was mixed with 2:1 ($AlCl_3$:EMImCl) electrolyte without discharge. The circled numbers refer to number of carbon atoms in an alkane.

Figure S2.10. Positive-ion DART-MS spectra of bottom 2:1 ($AlCl_3$:EMImCl) electrolyte layer. The electrolyte was mixed with n-decane under O_2. The circled numbers refer to number of carbon atoms in the hydrocarbon. Blue, green and yellow refer to saturated, unsaturated and ionic liquid (IL)-associated species.

Figure S2.11. Positive-ion DART-MS spectra of discharged n-decane in an Al/O_2 cell. The electrolyte is based on 2:1 ($AlCl_3$:EMImCl). The circled numbers refer to number of carbon atoms in the hydrocarbon. Blue, green and yellow refer to saturated, unsaturated and ionic liquid (IL)-associated species.

Figure S2.12. Positive-ion DART-MS spectra of discharged n-decane in an Al/80%CO_2 cell. The electrolyte is based on 2:1 ($AlCl_3$:EMImCl). Inset spectra show zoomed-in spectra and detected carboxylic-containing species.

Figure S2.13. Positive-ion DART-MS spectra of discharged 1-decene in an Al/80%CO_2 cell. The electrolyte is based on 2:1 ($AlCl_3$:EMImCl). Inset spectra show zoomed-in spectra and detected carboxylic-containing species.

Figure S2.14. ^{1}H-NMR of 2:1 ($AlCl_3$:EMImCl) electrolyte with n-decane. The spectra are for the electrolyte discharged with n-decane in an Al/O_2 cell and of top and bottom layers of mixed n-decane and electrolyte exposed to O_2. The signal at 2.05 and 2.84ppm are associated with acetone and water solvents, respectively. The inset table lists the ratio of methylene and methine to methyl protons.

Figure S2.15. ^{1}H-NMR of 1-decene and 2:1 ($AlCl_3$:EMImCl) electrolyte. The spectra are for 1-decene mixed and mixed/discharged with 2:1 ($AlCl_3$:EMImCl) electrolyte in an Al/O_2 cell. The signal at 2.05 and 2.84ppm are associated with acetone and water solvents, respectively.

Figure S2.16. ^{1}H-NMR of 1:2.3 ($AlCl_3$:EMImCl) electrolyte and n-decane. The spectra are for the electrolyte discharged with n-decane in an Al/O_2 cell and of top and bottom layers of mixed n-decane and electrolyte exposed to O_2. The signal at 2.05 and 2.84ppm are associated with acetone and water solvents, respectively. The inset table lists the ratio of methylene and methine to methyl protons.

Figure S2.17. ^{1}H-NMR of 1-decene and 1:2.3 ($AlCl_3$:EMImCl) electrolyte. The spectra are for 1-decene mixed and mixed/discharged with the electrolyte in an Al/O_2 cell. The signal at 2.05 and 2.84ppm are associated with acetone and water solvents, respectively. The inset table lists the ratio of methylene and methine to methyl protons.

Figure S2.18. ^{1}H-NMR for chemically produced superoxide with hydrocarbons. The spectra are for n-decane and 1-decene with chemically generated superoxide using K_2O and Dicyclohexano-18-crown-16. The signal at 2.05 and 2.84ppm are associated with acetone and water solvents, respectively. * corresponds to protons associated with Dicyclohexano-18-Crown-6.

Figure S2.19. ^{1}H-NMR of Al/O_2+CO_2 (80%CO_2) cell. The spectra are for 2:1 ($AlCl_3$:EMImCl) electrolyte discharged with n-decane and 1-decene in an Al/O_2+CO_2 (80%CO_2) cell. The inset shows the hydrocarbon introduced inside a capillary in the electrochemical cell. The signal at 2.05, 2.84 and 7.6ppm are associated with acetone, water and chloroform solvents, respectively.

Figure S2.20. ^{27}Al-NMR of 2:1 ($AlCl_3$:EMImCl) electrolyte. The spectra are for the electrolyte with and without n-decane and after discharge in an Al/O_2 cell.

LIST OF TABLES

LIST OF ABBREVIATIONS

$AlCl_3$ – Aluminum chloride

CCUS – Carbon capture, utilization and sequestration

CV – Cyclic voltammetry

DART – Direct analysis in real time

EDXS – Energy Dispersive X-Ray Spectroscopy

EMImCl – 1-ethyl-3-methylimidazolium chloride

FTIR – Fourier Transform Infrared

GC– Gas chromatography

IL – Ionic liquid

LCA – Life Cycle Assessment

MS – Mass spectrometry

NMP – N-methyl-2-pyrrolidone

NMR – Nuclear magnetic resonance

O_2^- – Superoxide

PVDF – Polyvinylidene floride

RGA – Residual gas analysis

SEM – Scanning electron microscopy

TGA – Thermogravimetric analysis

TIC – Total ion count

XPS – X-ray photoelectron spectroscopy

PREFACE

Starting this thesis research, the intention was to develop a CO_2 capture system based on the metal/O_2 electrochemical cell platform. As we detail in Chapter 1, previous studies investigated the effect of CO_2 on metal/O_2 systems, primarily using Li and Na metals. In addition to the existing challenges facing Li/O_2 and Na/O_2 electrochemical cells, which include the formation of hazardous dendrite, decline in efficiency due to metal loss and electrolyte degradation, the incorporation of CO_2 complicates those systems even further. The main reaction products in Li/O_2+CO_2 or Na/O_2+CO_2 cells were carbonates and bicarbonates, which are difficult to electrochemically reverse in a rechargeable system and not valuable as a feedstock. In addition, building full-size CO_2 capture plants based on Li/O_2 or Na/O_2 cells would be difficult to justify based on economic feasibility (with such rare metals) and safety (with highly reactive metals) reasons.

The rationale behind the first part of this thesis project (Chapter 1) was to build a CO_2 capture system using an inherently safer, cheaper and high-energy metal for easier industrial adoption. Al was of particular interest since it possesses all of those traits. To our knowledge, Al/O_2 systems were never investigated for CO_2 capture and were primarily investigated using aqueous electrolytes. Going back to literature, including previous work conducted within the Archer Group, the imidazolium ionic liquid-based electrolyte with aluminum chloride presented a promising alternative considering its superior Al electrodeposition and electrochemical and thermal stability. Remarkably, when discharging the Al/O_2+CO_2 cell using $AlCl_3$:imdzolium-ionic liquid electrolyte and excess CO_2-to-O_2 ratio showed the formation of aluminum oxalate as the primary discharge product, a useful class of chemicals for many industries/markets. The

discharge capacity increased by 15 folds by the introduction of CO_2. Life Cycle Assessment (LCA) showed that the Al/O_2+CO_2 cell present net reduction of CO_2 emissions after accounting for Al metal production emissions. This gives the Al/O_2+CO_2 cell an edge combining the carbon capture and conversion as well as high energy storage. We believe that the electrolyte system is unique in that it binds to and activates CO_2 as well as demonstrates optimum electrochemical performance.

The rationale behind the second part of the thesis project (Chapter 2) is to study the ability and mechanism of Al/O_2 electrochemical cell to convert/upgrade other low-value feedstocks. Some of the feedstocks and associated conversion processes that were considered include methane activation/polymerization, natural gas polymerization/upgrade, alkanes polymerization/upgrade, alkenes polymerization/upgrade, elemental sulfur conversion/addition to other feedstocks, removal of sulfur-containing hydrocarbons (such as dibenzothiophene), removal of nitrogen-containing hydrocarbons, conversion of low-value refinery distillates and others. Considering the time constraint, the second part of the thesis project focuses on the conversion/upgrade of alkanes and alkenes, including in the presence of CO_2. Remarkably, the galvanostatic Al/O_2 cell has the ability to oligomerize and isomerize low-octane rating hydrocarbons, mimicking the energy-intensive and expensive alkylation and reforming processes in traditional refining processes. As detailed in Chapter 2, the galvanostatically generated superoxide specie facilitates the oligomerization and isomerization of hydrocarbons. The $AlCl_3$:imdzolium-ionic liquid electrolyte enables the transport of different electrochemical species, electrostripping of the Al anode as well as catalytic activation of the hydrocarbon feedstock. We demonstrate that the Al/O_2 electrochemical cell with the $AlCl_3$:imidazolium electrolyte has the ability upgrade and combine multiple feedstocks. Redesigning the

electrochemical cell, we demonstrate oligomerization and isomerization as well as carboxylation of hydrocarbons when discharging the Al/O_2 cell under hydrocarbons and CO_2.

This dissertation follows the "paper option" format in accordance with the 2017 Thesis and Dissertation Guide, published by the Cornell University's Graduate School. The first paper is titles "The O_2-Assisted Al/CO_2 Electrochemical Cell: A System for CO_2 Capture/Conversion and Electric Power Generation" and the second paper is titled "Oligomerization, Isomerization and Carboxylation of Alkanes and Alkenes with Galvanostatically-Generated Superoxide in the Al/O_2 Electrochemical Cell."

CHAPTER 1

The O_2-Assisted Al/CO_2 Electrochemical Cell: A System for CO_2 Capture/Conversion and Electric Power Generation

1.1 Abstract

Economical and efficient carbon capture, utilization and sequestration (CCUS) technologies are a requirement for successful implementation of global action plans for reducing carbon emissions and for mitigating climate change. Such technologies are also essential for long-term use of fossil fuels while reducing the associated carbon footprint. We demonstrate an O_2-assisted Al/CO_2 electrochemical cell as a new approach for sequestering CO_2 emissions and, at the same time, generating substantial amounts of electrical energy. We report on the fundamental principles that guide operation of such cells using multiple intrusive electrochemical and physical analytical methods, including Chronopotentiometry, Cyclic Voltammetry (CV), Direct Analysis in Real Time Mass Spectrometry (DART-MS), Energy Dispersive X-ray Spectroscopy (EDXS), X-ray Photoelectron Spectroscopy (XPS), and coupled Thermal Gravimetric Analysis (TGA)-Fourier Transform Infrared (FTIR) Spectrometry, and on this basis demonstrate that an electrochemical cell that utilizes metallic aluminum as anode and a carbon dioxide-oxygen gas mixture as the active material in the cathode provides a path towards electrochemical generation of a valuable (C_2) species and electrical energy. Specifically, we show that the cell first reduces O_2 at the cathode to form superoxide intermediates. Chemical reaction of the superoxide with CO_2 sequesters the CO_2 in the form of aluminum oxalate, $Al_2(C_2O_4)_3$, as the dominant product. Based on an analysis of the overall CO_2-footprint, which considers emissions associated with the production of aluminum anode and the CO_2 captured/abated by the Al/CO_2-O_2 electrochemical cell,

we conclude that the proposed process offers an important strategy for net reduction of CO_2 emissions.

1.2 Introduction

Balancing the increasing world energy demand with the need to economically reduce carbon dioxide emissions is one of the most defining challenges of our time (*1*). Most world energy forecasts show that fossil fuels will continue to play a major role in meeting worldwide energy demands for the foreseeable future, particularly in the transportation and power generation sectors (*2, 3*). To capitalize on the exceptional, high energy density of fossil fuels, the incorporation of carbon capture, utilization and sequestration (CCUS) technologies is essential to reduce global CO_2 emissions (*4*). Large scale adoption of classical CCUS technologies (e.g. absorption, adsorption, membranes) is currently limited by the additional energy requirements associated with CO_2 capture, resulting in higher cost of energy, and difficulties to transport and sequester the captured CO_2 (*5*). Recently, CO_2 capture has been demonstrated for mobile sources, capitalizing on the waste energy of combustion engines (*6*). Conversion of CO_2 to useful chemicals and fuels is understood to be a requirement for the commercial success of a CCUS process, but has proven to be very difficult because of the thermodynamic and kinetic stability of CO_2. Of the catalysts recognized to enable the chemical formation of C-C bonds from CO_2, $AlCl_3$ is considered an effective Friedel-Crafts catalyst. Olah, et al. (*7*) reported the carboxylation of benzene with CO_2, $AlCl_3$ and Al metal and demonstrated through Density Functional Theory the $AlCl_3$ activation of CO_2 forming $AlCl_3$-CO_2 complexes, which react with benzene to produce its carboxylate. A similar reaction path has been proposed for the carboxylation of toluene with CO_2 and $AlCl_3$ (*8*). The conversion of CO_2 to oxalates (a feedstock to useful

chemicals supporting various markets/industries) has been demonstrated electrocatalytically using a copper complex by Angamuthu et al. (*9*).

The metal/CO_2 electrochemical cell has been proposed as a novel approach for capturing CO_2 from mixed CO_2/O_2 gas streams, particularly using metallic Li (*10-12*), Na (*13, 14*) and Mg (*13*) anodes of high energy densities, while generating electrical energy. An important finding from these studies is that the presence of O_2 is important for enabling the chemical reduction and thereby capture of CO_2. Such metal/O_2-CO_2 electrochemical capture systems, may be operated in either secondary (rechargeable) or primary (non-rechargeable) configurations. In a secondary cell, reduced CO_2 species react with oxidized metal ions to form the metal carbonate or bicarbonate and electricity during cell discharge. Recharging the cell would ideally reverse the reaction, consuming electrical energy to release the captured CO_2 and O_2 and regenerate the metal anode. Adoption of such secondary electrochemical systems in a CCUS process would therefore facilitate separation and concentration of CO_2 as demonstrated in Fig. 1.1(a). Another configuration of interest is the primary electrochemical cell, where the metal anode is consumed to produce electrical energy and discharge products, which can be harvested (from the electrode, electrolyte and other cell components) and regenerated to concentrate the CO_2 or converted to valuable chemicals if the discharge forms C_n ($n \geq 2$) products (Fig. 1.1(b)).

Aluminum is an attractive anode material for electrochemical capture and conversion of CO_2 both because of its relatively low cost and lower reactivity, in comparison to Li and Na, which makes electrochemical systems involving Al inherently safer and potentially easier to manufacture. As the third most abundant element in the Earth's crust (*15*), Al is also available in regions all over the world. The material has a high specific energy

(electrochemical equivalence of 2980 Ah/kg (*16*)), which means that its electrochemical conversion by CO_2 may also be used to generate large quantities of electrical energy.

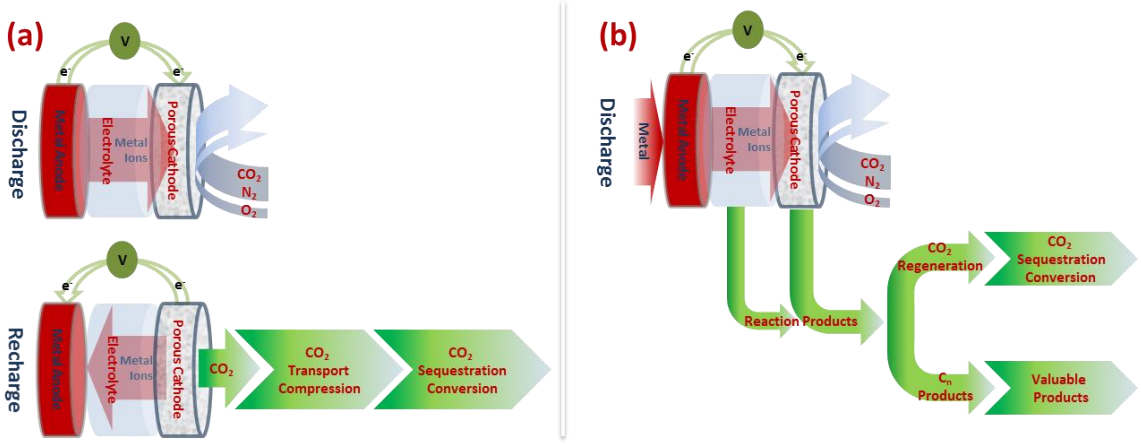

Fig. 1.1. Architectures of metal/CO_2 electrochemical cells as capture systems. (**a**) Secondary metal/CO_2 electrochemical cell where CO_2 is concentrated by recharging. (**b**) Primary metal/CO_2 electrochemical cell where captured CO_2 is concentrated or converted to C_n ($n \geq 2$) valuable products.

In Al electrochemical systems, room-temperature ionic liquids present attractive alternatives to alkaline and saline (aqueous and non-aqueous) electrolytes, which are associated with parasitic corrosion and hydrogen evolution problems (*17-20*). The ionic liquid/salt melt of 1-ethyl-3-methylimidazolium chloride ([EMIm]Cl)/aluminum chloride ($AlCl_3$) is particularly important because of its thermal and electrochemical properties (*21*). The electrochemically prevalent species can be designated by adjusting the ratio of $AlCl_3$ to [EMIm]Cl (*22-23*). An equimolar mixture will have $AlCl_4^-$ as the primary anion. Basic melts, where the [EMIm]Cl molar ratio is higher than $AlCl_3$, include Cl^- and $AlCl_4^-$ as the anions. Acidic melts, with higher $AlCl_3$ to [EMIm]Cl ratio have $AlCl_4^-$ and $Al_2Cl_7^-$ as the prevailing ions and are demonstrated to have higher conductivity (*24*) and lower viscosity (*25*). Aluminum batteries based on these electrolytes have recently attracted considerable attention. In aluminum-ion batteries, the acidic [EMIm]Cl/$AlCl_3$ melt has been used in conjunction with sulfur (*26*) V_2O_5 (*27, 28*), $LiFePO_4$ (*29*) and carbon-based (*30*) cathodes. Lin, M. et. al (*30*) demonstrated an ultrafast rechargeable aluminum ion battery based on the intercalation/de-intercalation of $AlCl_4^-$ in graphitic carbon electrodes. Though the capacity of the battery was limited to about 60 $mAh/g_{Graphite}$, the columbic efficiency was maintained at 97% at high applied current density.

1.3 The Al/O_2-CO_2 Cell

Herein we report an Al/CO_2-O_2 electrochemical cell based on an [EMIm]Cl/$AlCl_3$ electrolyte melt and show that this cell design is effective for both capturing CO_2 and for upconverting the captured CO_2 to a C_2 species, an oxalate, without the need for a catalyst or high temperature cell operation. Al/O_2 electrochemical cells based on an acidic [EMIm]Cl/$AlCl_3$ melt have been reported to produce approximately $158mAh/g_{Carbon}$ of electrical energy during cell discharge at around 0.7V under a current

density of 0.2mA/g_{Carbon} (*24*). More recently, Gelman et al. (*31*) demonstrated an Al/O_2 battery based on 1-ethyl-3-methylimidazolium oligo-fluoro-hydrogenate ($EMIm(HF)_{2.3}F$) electrolyte producing substantially higher discharge capacity (7450mAh/g_{Carbon}) at around 1.0V under current density of about 79mA/g_{Carbon}. Here we show that in addition to providing a process for CO_2 capture and conversion, an Al/CO_2-O_2 cell based on [EMIm]Cl/$AlCl_3$ can deliver very high discharge capacities (as high as 13000mAh/g_{Carbon}) at a discharge voltage of around 1.4V when discharged at a fixed rate of 70mA/g_{Carbon}.

Using aluminum as an anode in the electrochemical cell enabled the production of electrical energy when galvanostaticly discharging under specific gases, which are allowed to diffuse in the electrolyte through the porous cathode. Under constant current, oxidation of the aluminum anode and reduction of the diffused gases on the electrically conductive cathode produced a potential plateau indicative of the electrochemical reaction taking place. Postmortem analysis of the discharged cells was carried out using different techniques to identify the reaction products and showed congruence in the results. DART-MS was used to identify the main reaction products from the ionized fragments. EDXS and wide-scan XPS were used to compare the atomic ratios of aluminum, oxygen and carbon and high-resolution XPS was used to identify the bonds of those atoms. Coupled TGA-FTIR was used to compare the discharged cathodes with the primary potential reaction product.

1.4 Electrochemical Methods

Voltage profiles from galvanostatic discharge of Al electrochemical cells operated under Ar, O_2, CO_2 and mixtures of CO_2/O_2 are reported in Fig. 1.2. Discharging the Al

cell under pure O_2 (denoted 100%O_2) produced considerable electrical energy (about 890mAh/g_{Carbon}) at about 1.4V. The capacity increased by about 15 fold when CO_2 was introduced at a molar ratio of 80:20 compared to O_2 (denoted 80%CO_2). Discharging Al under pure CO_2 or Ar produced no/negligible electrical energy, with the only noticeable discharge voltage plateau at lower potential of about 0.3V. Cyclic voltammetry (Fig. 1.2 insert) revealed a matching reduction peak around 1.5V for Al/100%O_2 and Al/80%CO_2 systems, corresponding to the discharge potential. No corresponding oxidation peak, however, was detected to the 1.5V reduction peak. The redox couple peaks at 0.45-0.55V correspond to the lower discharge potential (0.3V), which was noticed regardless of the gas environment.

1.5 Direct Analysis in Real Time (DART) Mass Spectroscopy

The main negative and positive ion mode fragments/ionized species detected in pristine cathodes and cathodes discharged under 100%O_2 and 80%CO_2 were identified (Table 1.1S). As expected, the strongest signals were produced by fragmentation/ionization of the ionic liquid and salt considering their abundance. Table 1.S2 lists the negative and positive ion mode species detected by DART Mass Spec and corresponding theoretical signatures. Cl_2^- and HCl_2^- produced the strongest signals. $AlCl_4^-$ was detected, but not $Al_2Cl_7^-$, which is believed to have been fragmented. Fragments of the salt complexed with moisture in the air and produced species $AlCl_3(OH)^-$, $AlCl_2(OH)_2^-$ and $AlCl(OH)_3^-$. Fragmentation of the [EMIm]Cl produced $C_6H_{11}N_2^+$, $C_5H_9N_2^+$, $C_4H_7N_2^+$ and $C_3H_4N_2^+$ indicating the loss of chlorine, methyl and ethyl groups. The $C_6H_{11}N_2Cl_2^-$ species were detected from the ionization of [EMIm]Cl with an additional chlorine. Those species were produced similarly from undischarged cathodes and cathodes discharged under 100%O_2 and 80%CO_2. The same fragments/species were reported of the [EMIm]Cl/$AlCl_3$ melt using other mass spec techniques, including Fast Atom

Bombardment (*32*), Secondary Ion (*33*), Collision Induced Dissociation (*34*) and Pyrolysis Gas Chromatography (*35*) Mass Spec.

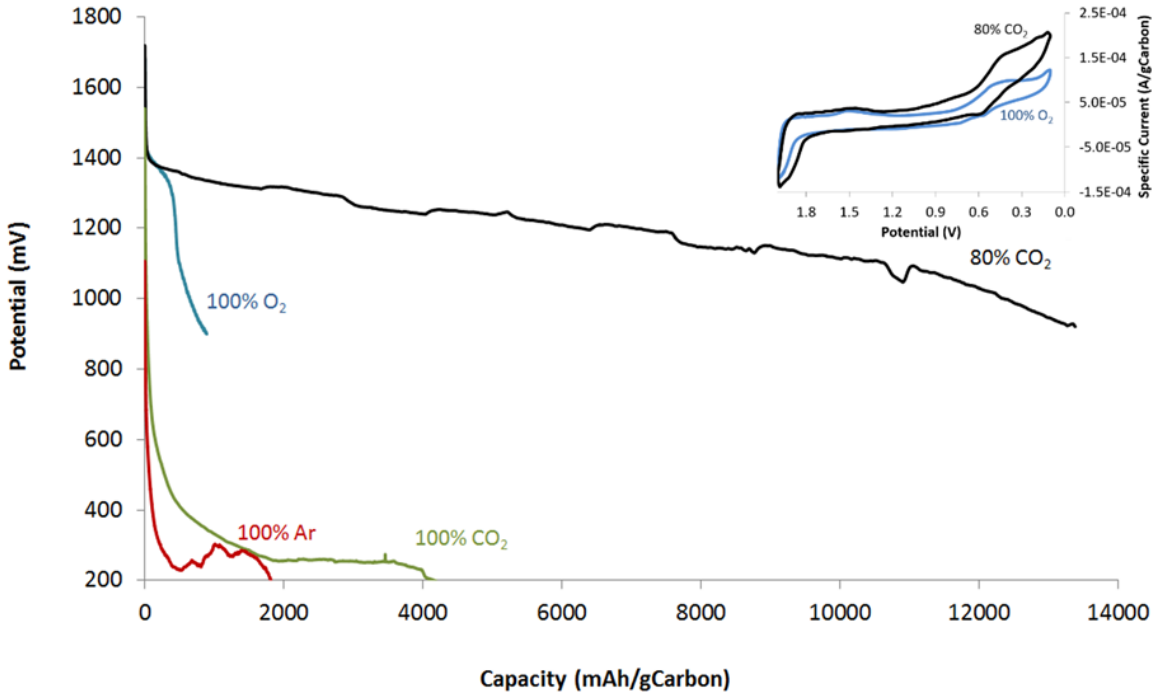

Fig. 1.2. Electrochemical performance of Al cell under different gas conditions. Galvanostatic discharge of Al under Ar, 100%CO_2, 100%O_2 and 80%CO_2 using [EMIm]Cl:$AlCl_3$ electrolyte of ratio 1:2 and current density of 70mA/g_{Carbon}. **Insert:** Cyclic voltammetry for 3-electrode cell under 100%O_2 and 80%CO_2 with 0.1mV/sec sweep rate.

Remarkably, what sets cathodes discharged under 80%CO_2 apart is the detection of $Al_2(C_2O_4)_3$ fragments and ionized species with the electrolyte melt. Aluminum oxalate fragments to produce $Al(C_2O_4)^+$, $Al(C_2O_4)_2^-$, $Al(C_2O_4)(C_2O_3)^+$ and $Al(C_2O_4)O^-$ as demonstrated in Tables 1.S1 and 1.S2. Aluminum oxalate also ionizes and complexes with $AlCl_3$ and [EMIm]Cl to produce $AlCl_2(C_2O_4)^-$, $C_6H_{11}N_2(C_2O_4)^-$, $(C_6H_{11}N_2)_3(C_2O_4)^+$ and $(C_6H_{11}N_2)_2(C_2O_4)Cl^-$. The intensity of the oxalate fragments were much lower than electrolyte species, where only the main peaks were detectable.

1.6 Scanning Electron Microscopy (SEM) – Energy Dispersive X-Ray Spectroscopy (EDXS)

Distinct differences were noted between cathodes discharged under 80%CO_2 and 100%O_2 (Table 1.1). Reaction products formed rugged micron-size particles on the stainless steel mesh cathodes discharged under 80%CO_2. Cathodes discharged under 100%O_2, on the other hand, showed submicron bead-like structures. The reaction products seemed to be distributed throughout the electrodes, though not completely covering them. It is not clear if the acetonitrile wash removed part of the reaction products form the electrodes.

Even after the acetonitrile wash, weak N and Cl signals are observed in the discharged and undischarged stainless steel cathodes by EDXS (Table 1.S3), most likely from remaining electrolyte. Whereas the Al atomic percentage in discharged cathodes was close to 10%, the undischarged cathode revealed values close to 1%. In the case of discharged cathodes, the atomic percentage of Al exceeded the stoichiometric values

Table 1.1. SEM and EDXS Results. Images of discharged stainless steel cathodes (under 80%CO_2 and 100%O_2) and undischarged cathode, after acetonitrile wash. The atomic ratios of O, C and Al are listed after discounting Al based on Cl and C based on N in the electrolyte. X marks the spot of the ED x-ray.

	SEM		O/Al	C/Al	C/O
Al/80%CO_2 Cathode	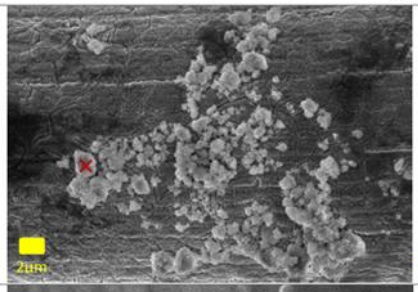	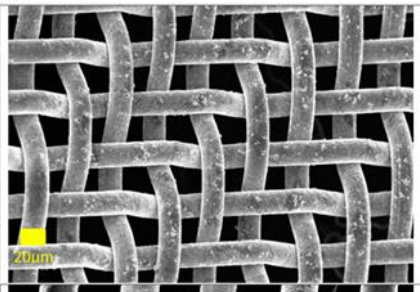	7.11	4.04	0.57
Al/100%O_2 Cathode	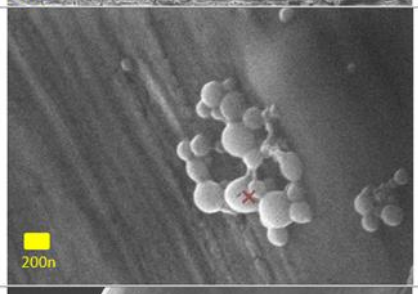	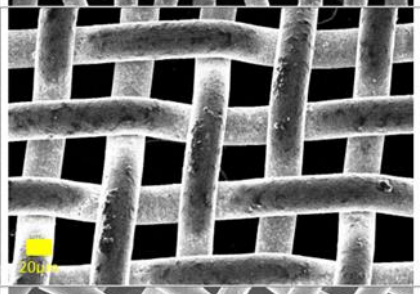	2.58	0.77	0.30
Undischarged Cathode	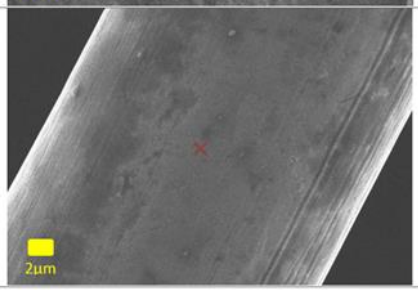	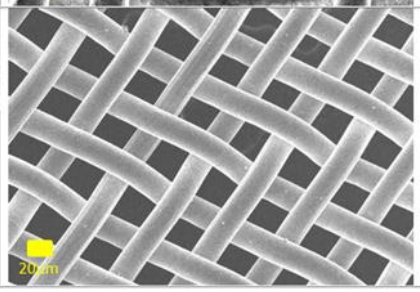	3.59	0.76	0.21

expected in the electrolyte when comparing to Cl atomic percentage, suggesting that Al is part of the reaction product depositing on the electrode. To discount the Al signal from the remaining electrolyte, the Al atomic percentage was adjusted based on the Cl signal and electrolyte stoichiometric value. Similarly, C was discounted based on the detected N and the corresponding electrolyte stoichiometry. The O to Al, C to Al and C to O atomic ratios are clearly larger for the cathodes discharged under 80%CO_2 (Table 1.1) and close to stoichiometric values of aluminum oxalate (6, 3 and 0.5, respectively). For the cathodes discharged under 100%O_2, the measured ratios are as expected consistent with stoichiometric values for aluminum oxide (1.5, 0 and 0, respectively). In contrast, for the undischarged cathodes, the ratios are close to the stoichiometric values for aluminum hydroxide (3, 0 and 0, respectively), suggesting that part of the remaining aluminum chloride reacts with moisture in the air during the short sample transfer. Both carbon and oxygen were detected in pristine stainless steel electrodes (not soaked in the electrolyte), which could explain the slightly higher ratios compared to aluminum in discharged cathodes.

1.7 X-Ray Photoelectron Spectroscopy

Wide survey scans (Table 1.S4) were performed to estimate surface atomic ratios and high resolution scans were conducted for Al 2p, O 1s and C 1s to determine more precise chemical bonding information. Table 1.2 reports the high resolution spectra and bonds assigned to the deconvoluted peaks; multiple bonds were assigned to some peaks. Two doublet Al 2p ($2p_{3/2}$ and $2p_{1/2}$) peaks were detected in discharged and pristine electrodes at 74eVs, which could be assigned to chloride (*36*) and hydroxide (*37*) compounds, and 77eVs, assigned to oxide (*38*) and oxalate (*39*) compounds. Two peaks at 531 and 534eVs were detected for O 1s and are attributed to hydroxides (*40*), oxides (*41*) and the two oxygen bonds (Al-O-C and C=O) in oxalate (*39, 41*). Seven different carbon

Table 1.2. High resolution XPS spectra and atomic ratios associated with aluminum oxalate. High resolution spectra (vs. number of counts) for Al 2p, O 1s and C 1s. Red doted-lines for experimental data and solid lines for fitted curves. Numbers are assigned to the different bonds and corresponding XPS peaks. Atomic ratios of specific bonds associated with aluminum oxalate, derived from coupling overall atomic ratios (from wide survey scans) with contributions of specific binding energies (from high resolution scans)

	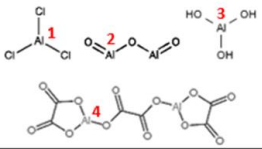	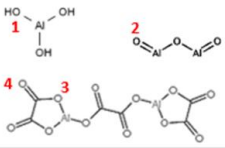	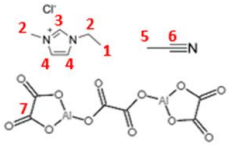			
	Al 2p ($2p_{3/2}$ and $2p_{1/2}$ doublets)	O 1s	C 1s	$\frac{O_{534eV}}{Al_{77eV}}$	$\frac{C_{286eV}}{Al_{77eV}}$	$\frac{C_{286eV}}{O_{534eV}}$
Al/80%CO_2 Cathode	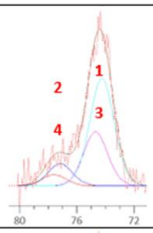	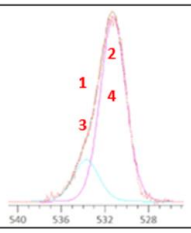	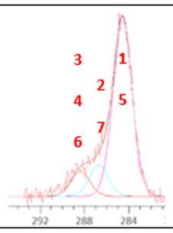	6.60	4.51	0.68
Al/100%O_2 Cathode	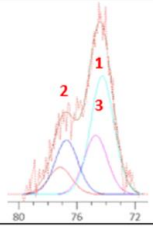	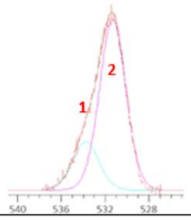	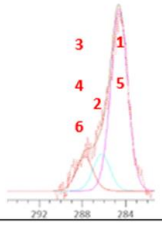	2.26	0.74	0.33
Undischarged Cathode	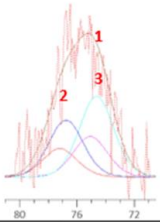	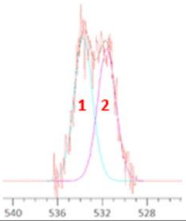	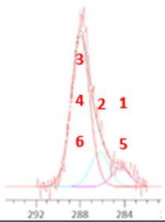	1.18	0.69	0.58
Aluminum Oxalate	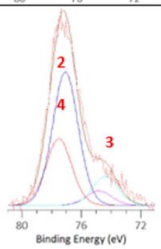	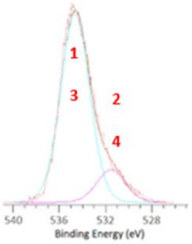	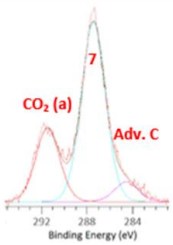	4.94	2.64	0.54

bonds can be attributed to the three C 1s peaks at 284, 286 and 288eVs originating from the ionic liquid (*42-44*), remaining acetonitrile (*45*) and oxalate (*39*).

Our findings are similar to those reported by Young et al. (*39*) from their XPS analysis of aluminum oxalate tetrahydrate, with the exception that binding energies are consistently around 2eV higher than those observed in our study. We suspect that the difference in binding energies originates from differences in referencing of the spectra, which is particularly important for nonconductive materials. The study by Young indicated that XPS degrades aluminum oxalate to form aluminum oxides. We conducted XPS on chemically synthesized aluminum oxalate samples purchased from Sigma Aldrich to compare with the results from electrochemically created material. These results are also included in Table 1.2. It is apparent that the C 1s spectra did not show the 288eV peak, but rather displays a peak at 291eV, which could be attributed to surface adsorbed CO_2 and CO (*39*). The C 1s 284eV peak is attributed to remaining adventitious carbon since it is difficult to sputter powders.

The high resolution peak contributions were used in conjunction with atomic ratios from wide surveys to predict discharge compounds. Table 1.2 shows the atomic ratios of oxygen to aluminum, carbon to aluminum and carbon to oxygen for specific bonds. O 534eV to Al 77eV ratio can be used to evaluate presence aluminum oxalate since the peaks associated with those binding energies are linked to the Al-O-C bond. The ratios are clearly higher for the cathode discharged under 80%CO_2 compared to the cathode discharged under 100%O_2 or undischarged electrode. The ratio for the cathode discharged under 80%CO_2 is higher than the stoichiometric value of 3.0 and can be attributed to the presence of aluminum-oxygen complexes (notorious of this electrolyte melt in the presence of O_2 gas (*32*)) which are linked to the same oxygen and aluminum

peaks. Comparing the C 286eV peak (associated with oxalate) to Al 77eV and O 534eV peaks demonstrate higher ratios of carbon for the cathode discharged under 80%CO_2 compared to 100%O_2 and undischarged electrode. The C 286eV to Al 77eV ratio higher than stoichiometric value of 3.0 in aluminum oxalate could be attributed to the presence of remaining ionic liquid on the surface since the same carbon peak is attributed to methyl and ethyl group in the ionic liquid. The C 286eV to O 534eV ratio is lower than stoichiometric value of 1.0 for oxalate and can be explained by the presence of oxides attributed to the same oxygen peak. Comparing the contribution of the same peaks for acquired aluminum oxalate, the O 534eV to Al 77eV and C 286eV to Al 77eV ratios are close to the stoichiometric values. The C 286eV to O 534eV ratio is slightly lower the stoichiometric value and could be explained by the presence of aluminum oxide as reported by Young et al. (*39*).

1.8 Thermogravimetric Analysis (TGA) Coupled Fourier Transform Infrared (FTIR) Spectroscopy

Cathodes discharged under 80%CO_2, 100%O_2 and undischarged cathode exhibited similar TGA profiles, with a significant mass loss occurring around 530°C (Fig. 1.3). This mass loss is attributed to the thermal decomposition of the ionic liquid (*46*). Only the cathode discharged under 80%CO_2 featured an additional defined dip at around 280°C. The TGA was coupled with FTIR to analyze the composition of the thermally degraded products as demonstrated in Fig. 1.3. All cathodes showed the evolution of CO_2 and H_2O through out the TGA experiment, from sample-adsorbed CO_2 and H_2O during sample loading and degraded species. Focusing on the region of asymmetric stretch of CO_2 (2349cm^{-1}), both the undischarged cathode and the cathode discharged under 100%O_2 clearly show CO_2 is evolved and that the evolution plateaus up to 600°C.

The cathode discharged under 80%CO_2 also shows the evolution of CO_2 reaching a plateau and then a spike that is associated with the 280°C TGA drop, which is

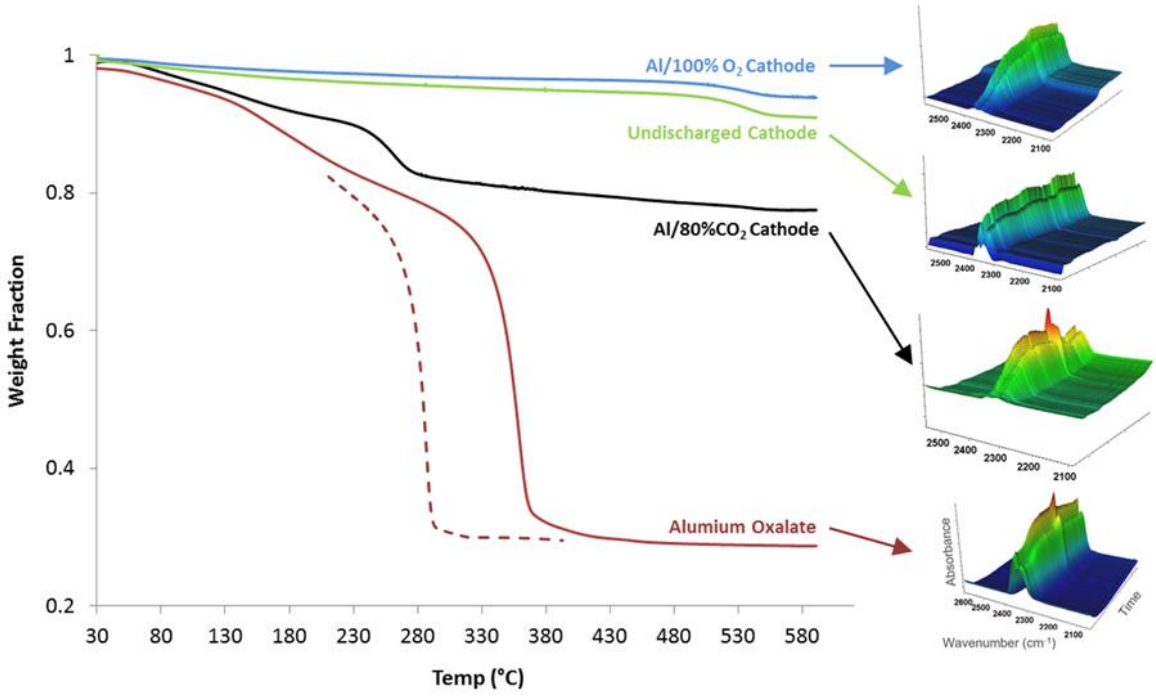

Fig. 1.3. TGA coupled FTIR. TGA curves and coupled time-resolved FTIR spectra for discharged cathodes (under 80%CO_2 and 100%O_2), undischarged cathode and chemically synthesized aluminum oxalate. Ramp-up rates 5°C/min and 0.05°C/min for solid and dashed lines, respectively.

hypothesized to result from degradation of discharge-deposited aluminum oxalate. The TGA-FTIR experiment was duplicated for the chemically synthesized aluminum oxalate to test this hypothesis. Significantly, the results show a similar thermal profile, including the spike, confirming that a significant release of CO_2. The TGA results, however, show the weight drop occurring around 350°C. The difference in the temperature could be attributed to the bigger size of chemically synthesized aluminum oxalate particles (>10μm by SEM) compared to the deposited in Al/80%CO_2 electrochemical cell (~1 μm by SEM). Decreasing the TGA ramp-up rate provides a simple strategy for accommodating mass transfer differences between smaller and larger sample aggregate sizes. This expectation was confirmed by reducing the scan rate to 0.05°C/min whereupon the weight drop was seen to shift to 280°C. Young et al. (*39*) reported the decomposition of aluminum oxalate tetrahydrate between 300 and 320°C (10°C/min ramp-up rate). The acquired aluminum oxalate sample also showed the evolution of CO (2099cm^{-1}) at very low intensity compared to CO_2.

1.9 Preliminary System Analysis

When recharging Al/80%CO_2 or Al/100%O_2 electrochemical cells using stainless steel cathodes, the recharge potential exhibits a shuttling-like behavior where it reaches a plateau and fluctuates radically. Similar behavior is well known for Li/S (*47*) and Na/S (*48*) batteries, where current is continuously consumed in a parasitic redox loop involving interconversion of metal polysulfide species of different orders dissolved in the electrolyte. In the case Al/80%CO_2 and Al/100%O_2, shuttling is tentatively attributed to a similar loop involving interconversion of different aluminum chloride species present in the electrolyte. These behaviors can be contrasted with what is seen when the cathode is replaced by Ketjenblack-casted carbons, where the Al electrochemical cell showed good recyclability achieving and maintaining about

200mAh/g_{Carbon} for more than 50 cycles. The cell recyclability, however, corresponds to an intercalation/deintercalation process and was seen under CO_2, O_2, CO_2/O_2 and Ar. Based on these results, we conclude that a CO_2 capture/conversion system based on Al/80%CO_2 electrochemical cell may be most easily operated in a primary mode in which the Al anode is continuously fed to the cell (Fig. 1.1(b)) and oxidized/consumed to form aluminum oxalate. Oxalic acid is used as a bleaching agent in the pharmaceutical and fiber industries, as a cleaning agent and as a precipitant in metal smelters. Demand for oxalic acid in these application has been increasing in recent years to support different sectors with an estimated worldwide demand of 230 000tonnes in 1998 (*49*). Oxalic acid can also be used as a feedstock to the production of dimethyl oxalate (*9*) and eventually ethylene glycol, where the global production was estimated at 20 Million tonnes in 2010 (*50*).

To evaluate the effectiveness of the proposed primary Al/80%CO_2 electrochemical cell as a CO_2 sequestration technology, Life Cycle Assessment (LCA) maybe used. LCA presents a structured approach to evaluate environmental impacts throughout a product's lifecycle (from raw material, production and waste management, etc.) (*51*). It enables balancing CO_2 emissions associated with the Al anode production to abated CO_2 converted by the electrochemical cell from flue streams. In this paper we extend an LCA for aluminum metal production to act as a preliminary LCA for the Al/80%CO_2 electrochemical cell. Aspects related to efficiencies, electrolyte production/replacement, flue gas pretreatment and other features are yet to be incorporated. An LCA study that was conducted by The Aluminum Association, inline with ISO 1404/14044, estimated average genetic CO_2 emission values for North American aluminum industry based on input from 25 companies (*52*). The study accounted for CO_2 emissions from the four main process steps for Al metal production:

bauxite mining, alumina refining, aluminum electrolysis and primary aluminum production. An average of 7.88kgCO_2/kgAl was estimated for the combined steps of aluminum production and associated processes (Fig. 1.4).

Integrating the Al/80%CO_2 electrochemical cell in a flue gas stream, we estimate a total of 9.31kgCO_2/kg/Al to be captured and abated (Fig. 1.4). We calculate 4.89kgCO_2/kgAl to be separated based on the proposed discharge reaction. Generated electric power from the battery replacing other energy sources results in overall reduction of CO_2 emissions. If the battery replaces natural gas sources, reduction of 1.97kgCO_2/kgAl can be credited to the system, based on a theoretical energy of 3.58kWh/kgAl and CO_2 emissions of 0.55kgCO_2/kWh associated with natural gas (*53*). We propose that the main discharge product of the battery can be converted to oxalic acid. Fischer, et al. (*54*) demonstrated the relatively simple production of $H_2C_2O_4$ from ZnC_2O_4. We propose that $Al_2(C_2O_4)_3$ can be converted to $H_2C_2O_4$ and Al_2O_3, reducing CO_2 emissions associated with oxalic acid produced in industry through classical methods. One of the established methods to producing oxalic acid in industry is through the oxidation of propene with nitric acid, where CO_2 is produced in equimolar quantities to the oxalic acid (*55*). If Al/80%CO_2 electrochemical cell is used to produce $H_2C_2O_4$ instead of propene oxidation, CO_2 abatement can be estimated at 2.45kgCO_2/kgAl. The overall balance of CO_2 shows that the primary Al/80%CO_2 electrochemical system reduces emissions from flue streams after accounting for emissions from Al metal production (Fig. 1.4(a)). If Al_2O_3 produced from $Al_2(C_2O_4)_3$ conversion to $H_2C_2O_4$ is recycled back to the Al production facility, aluminum can be produced, considerably reducing CO_2 emissions associated with the bauxite mining and alumina refining steps. This results in even higher CO_2 reduction (3.52kgCO_2/kgAl) of the overall system as demonstrated in Fig. 1.4(b). This outlines a

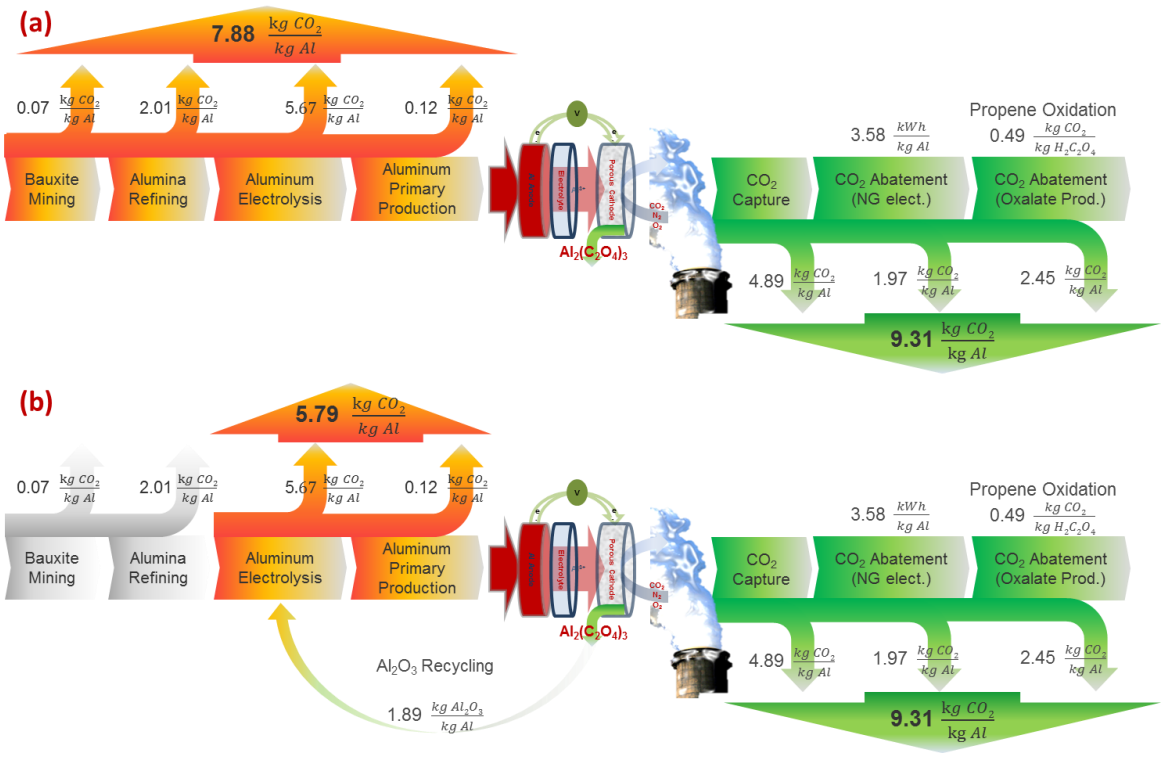

Fig. 1.4. Preliminary System Analysis. (**a**) Overall balance of CO_2 emissions captured/abated by the primary Al/80%CO_2 electrochemical system contrasted with emissions of aluminum metal production. (**b**) Overall balance of CO_2 emissions, allowing the recycling of Al_2O_3 for production of aluminum metal.

preliminary LCA and a rigorous study is to be conducted to account for emissions associated with electrolyte replacement (depends on degradation rate), moisture removal from flue gases, oxalic acid production from aluminum oxalate and other aspects.

1.10 Discussion

The galvanostatic discharge at relatively high potential (1.4V) and CV experiments suggest that O_2 reduction is the main electrochemical process in the Al/CO_2-O_2 cell. Similar potential plateaus for Al discharged under pure O_2 or CO_2/O_2 mixture underlines that the main electrochemical process involves the reduction of O_2, expectedly forming superoxide species ($O_2^{\bullet-}$). Direct electrochemical reduction of CO_2 does not take place but rather through the chemical reduction by the superoxide species.

Similar results have been reported previously when incorporating CO_2 to Li/O_2 and Na/O_2 batteries, demonstrating an increase in discharge capacity while maintaining the same discharge potential plateau. In ethylene carbonate/diethyl carbonate (EC/DEC) electrolyte, the incorporation of 50% CO_2 into Li/O_2 batteries increased the discharge capacity by three folds while maintaining the same discharge potential (*10*). The proposed discharge mechanism involves the reduction of O_2 to form the superoxide radical that in turn chemically reduces CO_2 to form CO_4^{2-} and then $C_2O_6^{2-}$ radicals resulting in the formation of Li_2CO_3 as the main discharge product (*56*). In tetraethylene glycol dimethyl ether (tetraglyme), Li/CO_2-O_2 (2:1 ratio) was demonstrated to be rechargeable to limited number of cycles, forming Li_2CO_3 as the main discharge product (*11*). In Na/O_2 batteries, the introduction of CO_2 in ratios between 40 and 60% compared to O_2 increased the capacity by two to three folds depending on the electrolyte system (*13*). Na_2CO_3 and $Na_2C_2O_4$ were reported as the main discharge products in tetraglyme

and ionic liquid electrolytes, respectively. Rechargeability was demonstrated when stabilizing the propylene carbonate electrolyte with ionic liquid-tethered silica nanoparticles where $NaHCO_3$ was the main discharge product (*14*).

Analytically, using DART-MS, SEM-EDXS, XPS and TGA-FTIR, it is shown that the principal discharge product of the Al/CO_2-O_2 cells is aluminum oxalate ($Al_2(C_2O_4)_3$). Accordingly, building on the hypothesized reaction mechanisms for Li/CO_2-O_2 and Na/CO_2-O_2 batteries, we propose the following reaction mechanism for the Al/CO_2-O_2 electrochemical cell:

$2\ Al \leftrightarrow 2\ Al^{3+} + 6\ e^-$

$6\ O_2 + 6\ e^- \leftrightarrow 6\ O_2^{\bullet-}$

$3\ CO_2 + 3\ O_2^{\bullet-} \leftrightarrow 3\ CO_4^{\bullet-}$

$3\ CO_4^{\bullet-} + 3\ O_2^{\bullet-} \leftrightarrow 3\ CO_4^{2-} + 3\ O_2$

$3\ CO_4^{2-} + 3\ CO_2 \leftrightarrow 3\ C_2O_4^{2-} + 3\ O_2$

$2\ Al^{3+} + 3\ C_2O_4^{2-} \leftrightarrow Al_2(C_2O_4)_3$

Overall Reaction: $2\ Al + 6\ CO_2 \leftrightarrow Al_2(C_2O_4)_3$

Protonic impurities could present a challenge when using [EMIm]Cl/$AlCl_3$ as an electrolyte because the electrochemically generated super oxide ($O_2^{\bullet-}$) could react with impurities in the electrolyte melt (*57*). A strong nucleophilic reagent such as $O_2^{\bullet-}$ is reported to react with and degrade the EMI^+ cation (*58-59*). Despite such possible side reactions, the introduction of CO_2 in higher ratios than O_2 demonstrated that $O_2^{\bullet-}$ reduces CO_2 to produce oxalates. It is believed that the CO_2 complexing with $AlCl_3$ in the electrolyte facilitates the chemical reduction of CO_2 by the superoxide and the eventual formation of oxalate.

The proposed O_2-assisted Al/CO_2 electrochemical cell demonstrates a new approach for converting CO_2 from a flue gas streams to useful products while producing considerable electrical energy. The preliminary LCA, which compares the captured/abated CO_2 by the proposed primary Al/CO_2-O_2 system to emissions associated with the production of the Al anode, showed a net reduction of CO_2 emissions. Current work is planned to better understand the rate performance/kinetics of the system (enabling comparison with classical CO_2 capture/conversion techniques) as well as study different electrolytes (the most sensitive part of the system, particularly to water) and other metal anodes.

1.11 Materials and Methods

1.11.1 Electrolyte Preparation and Material Handling

The electrolyte was prepared by slowly mixing 1-ethyl-3-methylimidazolium chloride ([EMIm]Cl) (Sigma Aldrich, >95%) with aluminum chloride ($AlCl_3$) (Sigma Aldrich, 99.99%). Acidic electrolyte melt (1:2 [EMIm]Cl:$AlCl_3$) was primarily used in this study. No major differences in electrochemical performance were noticed for electrolyte melts between ratios 1:2.1 and 1:1.5 ([EMIm]Cl:$AlCl_3$). The electrolyte was vacuum heated at 130°C for 15 minutes to remove/reduce water and oxygen complexes before applying to the battery. Chemically synthesized aluminum oxalate hydrate (Alfa Aesar, 99%) was vacuum heated overnight at 120°C to drive out hydrates. All materials used in the study were stored/prepared in an Ar-filled glovebox (MBraun. Labmaster). Electrochemical cells were also assembled in an Ar-filled glovebox. Electrode and electrolyte samples for postmortem analysis were obtained after disassembling cells inside the glovebox and transferring in Ar-filled vials for analysis outside the glovebox.

1.11.2 Electrochemical Cells Assembly

Al/CO_2-O_2 cells were assembled with CR2032 coin-type cells that were perforated on the cathode side (15.8mm diameter). Ketjenblack (AkzoNobel EC600JD) was dissolved with Polyvinylidene floride (PVDF) binder (8:2 carbon to binder ratio) in N-methyl-2-pyrrolidone (NMP) solvent, ball milled and cast on carbon paper (Toray TGP-H-030). The cathodes were dried in vacuum oven overnight at 100°C. Typical loading of cathodes was 0.5-1.0mg_{Carbon}/cm^2. For comparison, other electrodes such as carbon paper, stainless steel mesh and nickel foam were tested with/without the porous carbon with comparable electrochemical performance. However, the use of porous carbon (providing considerably high surface area for the reduction reaction) was essential to reduce the overpotential in the system during discharge and obtain a high potential plateau. Al foil (Alfa Aesar, 99.99% 0.1mm thick) were used as the anode after mechanical cleaning with silicon carbide sandpaper and washing with acetonitrile. Whatman GF/D glassfiber was used as separator and was soaked with 100µL electrolyte. Custom-designed chambers were used to place battery cells, exposing them to premixed gases at 1 atm. Cuvette-type cells were used to conduct cyclic voltammetry and allow harnessing the electrolyte (1mL) after discharge for postmortem analysis.

1.11.3 Electrochemical Experiments

Galvanostatic discharge experiments were conducted using a Neware CT-3008 battery testers at a fixed current density of 70mA/g_{Carbon}. Cyclic Voltammetry (CV) was performed using Solartron Frequency Response Analyzer (model 1252) with a three-electrode configuration and a fixed 0.1mV/sec scan rate. Ketjenblack on carbon paper was used as the working electrode. Tn wire (Alfa Aesar 99.99% 1.0mm diameter) was used as the counter electrode. The reference electrode constituted an Al wire (Alfa Aesar, 99.999% 2.0mm diameter) immersed in the same electrolyte. Counter and

reference electrodes were mechanically cleaned with silicon carbide sandpaper and washed with acetonitrile.

1.11.4 Direct Analysis in Real Time (DART) Mass Spectrometry

High-resolution mass spectrometry (HRMS) analyses were carried out on a Thermo Scientific Exactive Orbitrap Mass Spec system equipped with an Ion Sense DART ion source. MestReNova software was used to analyze the mass spec results and compare them to predicted spectra. DART mass spectroscopy enables the analysis of products on discharged cathodes in their native states without the need for sample preparation. Exposing cathodes to the ion source fragments/ionizes the different species.

1.11.5 Scanning Electron Microscopy (SEM) and Energy Dispersive X-Ray Spectroscopy (EDXS)

SEM (Keck SEM) was conducted using Zeiss 1550 Field Emission (Schottky field emitter). EDXS was carried out with Bruker QUANTAX 200 and with XFlash®6 SDD and energy resolution of <126eV at Mn-K-alpha line. For SEM-EDXS postmortem analysis, batteries were discharged using stainless steel mesh cathodes to be able to differentiate the reaction products from porous carbon electrodes. Discharged cathodes were washed with acetonitrile inside the Ar glovebox to remove excess electrolyte.

1.11.6 X-Ray Photoelectron Spectroscopy (XPS)

Samples were analyzed using a Surface Science Instruments SSX-100 with operating pressure ~$2x10^{-9}$ Torr. Monochromatic Al K-alpha X-rays (1486.6eV) were used with beam diameter of 1mm. Photoelectrons were collected at a 55° emission angle. A hemispherical analyzer determined electron kinetic energy, using a pass energy of 150V for wide/survey scans, and 50V for high resolution scans. Samples were ion etched

using 4kV Ar ions, rastered over 2.25mm x 4mm area with total ion beam current of 2μA, to remove adventitious carbon. Spectra were referenced to adventitious C 1s at 284.5eV. CasaXPS software was used for XPS data analysis with Shelby backgrounds. C 1s and O 1s were assigned single peaks for each bond. Al 2p were assigned double peak ($2p_{3/2}$ and $2p_{1/2}$) for each bond with 0.44eV separation. Residual standard deviation was maintained close to 1.0 for the calculated fits. For XPS postmortem analysis, batteries were discharged using stainless steel mesh cathodes to be able to differentiate reaction products from carbon electrodes. Discharged cathodes were washed with acetonitrile inside the Ar glovebox to remove excess electrolyte.

1.11.7 Thermogravimetric Analysis (TGA) coupled Fourier Transform Infrared (FTIR) Spectroscopy

TGA was carried out using TA Instruments TGA Q500 up to 600°C at 5°C/min unless otherwise stated. The FTIR spectrum was obtained by Thermo Scientific Nicolet iZ10 spectrometer with TGA sampling accessory. Evolved gases were flushed through the TGA-FTIR chambers with N_2 (10mL/min with VWR peristaltic pump terminating at a liquid seal). OMNIC software was used to construct 3D (absorbance and wavenumber vs. time) plots of FTIR spectra. TGA-FTIR was conducted on Ketjenblack-based cathodes that were washed with acetonitrile to remove excess electrolyte.

1.11.8 Base Case Tests

Considering the sensitivity of the electrolyte system and to account for any interaction with air, moisture and impurities, the DART-MS, SEM-EDXS, XPS and TGA-FTIR experiments of discharged cathodes were compared with undischarged cathodes (base case). The undischarged cathodes were assembled in exactly same way as the

discharged cathodes and were soaked in the electrolyte system and exposed to a mixture of CO_2 and O_2 before washing with acetonitrile.

1.12 REFERENCES

1. R. Armstrong, C. Wolfram, K. de Jong, R. Gross, N. Lewis, B. Boardman, A. Ragauskas, K. Ehrhardt-Martinez, G. Crabtree and M. Ramana, The Frontiers of Energy. *Nature Energy* **1**, 1-8 (2016).
2. M. I. Hoffert, Farewell to Fossil Fuels? Science **329**, 1292-1294 (2010).
3. R. York, Do Alternative Energy Sources Displace Fossil Fuels. *Nature Climate Change* **2**, 441-443 (2012).
4. S. Chu, Carbon Capture and Sequestration. Science **325**, 1599 (2009).
5. R. S. Haszeldine, Carbon Capture and Storage: How Green Can Black Be? *Science* **325**, 1647-1652 (2009).
6. E. Z. Hamad, W. I. Al-Sadat, Reversible Solid Adsorption Method and System Utilizing Waste Heat for On-Board Recovery ad Storage of CO_2 from Motor Vehicle Internal Combustion Engine Exhaust Gases. *US Patent* 2013/0298532 A1, 2013.
7. G. A. Olah, B. Torok, J. P. Joschek, I. Bucsi, P. M. Esteves, G. Rasul, G. K. Surya Prakash, Efficient Chemoselective Carboxylation of Aromatics to Arylcarboxylic Acids with a Superelectrophilically Activated Carbon Dioxide-Al_2Cl_6/Al System. *J. Am. Chem. Soc.* **124**, 11379-11391 (2002).
8. A. N. Sarve, P. A. Ganeshpure, P. Munshi, Carboxylation of Toluene by CO_2 Generating p-Toluic Acid: A Kinetic Look. *Ind. Eng. Chem. Res.* **51**, 5174-5180 (2012).
9. R. Angamuthu, P. Byers, M. Lutz, A. L. Spek, E. Bouwman, Electrocatalytic CO_2 Conversion to Oxalate by a Copper Complex. *Science* **327**, 313-315 (2010).
10. K. Takechi, T. Shiga and T. Asaoka, A Li–O_2/CO_2 Battery. *Chem. Commun.* **47**, 3463-3465 (2011).

11. Y. Liu, R. Wang, Y. Lyu, H. Li, L. Chen, Rechargeable Li/CO_2–O_2 (2:1) Battery and Li/CO_2 Battery. *Energy Environ. Sci.* **7**, 677-681 (2014).
12. S. Xu, S. K. Das, L. A. Archer, The Li–CO_2 Battery: A Novel Method for CO_2 Capture and Utilization. *RSC Advances* **3**, 6656-6660 (2013).
13. S. K. Das, S. Xu, L. A. Archer, Carbon Dioxide Assist for Non-Aqueous Sodium–Oxygen Batteries. *Electrochemistry Communications* **27**, 59-62 (2013).
14. S. Xu, Y. Lu, H. Wang, H. D. Abru˜na, L. A. Archer, A Rechargeable Na–CO_2/O_2 Battery Enabled by Stable Nanoparticle Hybrid Electrolytes. *J. Mater. Chem. A* **2**, 17723-17729 (2014).
15. *Metal Prices in the United States through 2010: U.S. Geological Survey Scientific Investigations Report* (U.S. Geological Survey, 2013).
16. D. Linden, T. B. Reddy, *Handbook of Batteries* (McGraw-Hill Education, New York, ed. 3, 2011) chap. 1.
17. E. J. Rudd, D. W. Gibbons, High Energy Density Aluminum/Oxygen Cell. *J. of Power Sources* **47**, 329-340 (1994).
18. C. Li, W. Ji, J. Chen, Z. Tao, Metallic Aluminum Nanorods: Synthesis via Vapor-Deposition and Applications in Al/air Batteries. *Chem. Mater*. **19**, 5812–5814 (2007).
19. D. R. Egan, C. Ponce de León, R. J. Wood, R. L. Jones, K. R. Stokes, F. C. Walsh, Developments in Electrode Materials and Electrolytes for Aluminium-Air Batteries. *J. of Power Sources* **236**, 293-310 (2013).
20. M. Mokhtar, M. Z. Talib, E. H. Majlan, S. M. Tasirin, W. M. Wan Ramli, W. R. Wan Daud, J. Sahari, Recent Developments in Materials for Aluminum–Air Batteries: A Review. *J. of Industrial and Engineering Chemistry* **32**, 1-20 (2015).

21. C. Scordilis-Kelley, J. Fuller, R. T. Carlin, J. S. Wilkes, Alkali Metal Reduction Potentials Measured in Chloroaluminate Ambient-Temperature Molten Salts. *J. Electrochem. Soc.* **139**, 694-699 (1992).

22. J. J. Auborn, Y. I. Barberio, An Ambient Temperature Secondary Aluminum Electrode: Its Cycling Rates and Its Cycling Efficiencies. *J. Electrochem. Soc.* **132**, 598-601 (1985).

23. C. J. Dymek, Jr., J. L. Williams, D. J. Groeger, J. J. Auborn, An Aluminum Acid-Base Concentration Cell Using Room Temperature Chloroaluminate Ionic Liquids. *J. Electrochem. Soc.* **131**, 2887-2892 (1984).

24. R. Revel, T. Audichon, S. Gonzalez, Non-Aqueous Aluminium-Air Battery Based on Ionic Liquid Electrolyte. *J. of Power Sources* **272**, 415-421 (2014).

25. P. Wasserscheid, W. Keim, Ionic Liquids-New Solutions for Transition Metal Catalysis. *Angew. Chem. Int. Ed.* **39**, 3772-3789 (2000).

26. G. Cohn, L. Ma, L. A. Archer, A Novel Non-Aqueous Aluminum Sulfur Battery. *J. of Power Sources* **283**, 416-422 (2015).

27. N. Jayaprakash, S. K. Das, L. A. Archer, The Rechargeable Aluminum-Ion Battery. *Chem. Commun.* **47**, 12610-12612 (2011).

28. [52.] H. Wang, Y. Bai, S. Chen, X. Luo, C. Wu, F. Wu, J. Lu, K. Amine, Binder-Free V_2O_5 Cathode for Greener Rechargeable Aluminum Battery. *ACS Appl. Mater. Interfaces* **7**, 80-84 (2015).

29. X. Sun, Z. Bi, H. Liu, Y. Fang, C. A. Bridges, M. P. Paranthaman, S. Daiab, G. M. Browna, A High Performance Hybrid Battery Based on Aluminum Anode and $LiFePO_4$ Cathode. *Chem. Commun.* **52**, 1713-1716 (2016).

30. M. Lin, M. Gong, B. Lu, Y. Wu, D. Wang, M. Guan, M. Angell, C. Chen, J. Yang, B. Hwang, H. Dai, An Ultrafast Rechargeable Aluminium-Ion Battery. *Nature* **520**, 325-328 (2015).

31. D. Gelman, B. Shvartsev, Y. Ein-Eli, Aluminum–Air Battery Based on an Ionic Liquid Electrolyte. *J. Mater. Chem. A* **2**, 20237-20242 (2014).

32. A K. Abdul-Sada, A. M. Greenway, K. R. Seddon, T. Welton, A Fast Atom Bombardment Mass Spectrometric Study of Room-temperature 1-Ethyl-3-methylimidazolium Chloroaluminate (III) Ionic Liquids. Evidence for the Existence of the Decachlorotrialuminate (III) Anion. *Org. Mass. Spec.* **28**, 759-765 (1993).

33. G. Franzen, B. Gilber, G. Pelzer, E. DePauw, The Anionic Structure of Room-temperature Organic Chloroaluminate Melts from Secondary Ion Mass Spectrometry. *Org. Mass Spec.* **21**, 443-444 (1986).

34. A. Sala, F. Ferrario, E. Rizzi, S. Catinella, Pietro Traldi, Electron Ionization Mass Spectrometry of some 1-and 2-Alkylimidazoles and 1,3-Dialkylimidazole Iodides. *Rapid Comm. In Mass Spec.* **6**, 388-393 (1992).

35. S. Poetz, P. Handel, G. Fauler, B. Fuchsbichler, M. Schmuck, S. Koller, Evaluation of Decomposition Products of EMImCl-1.5$AlCl_3$ during Aluminium Electrodeposition with Different Analytical Methods. *RSC Adv.* **4**, 6685-6690 (2014).

36. J. Moulder, W. Stickle, P. Sobol, K. Bomben, *Handbook of X-ray Photoelectron Spectroscopy* (Perkin-Elmer Corporation, 1992).

37. J. R. Lindsay, H. J. Rose, W. E. Swartz, P. H. Watts, K. A. Rayburn, X-ray Photoelectron Spectra of Aluminum Oxides: Structural Effects on the Chemical Shift. *Applied Spectroscopy* **27**, 1-5 (1973).

38. R. T. Carlin, J. Fuller, W. K. Kuhn, M. J. Lysaght, P. C., Trulove, Electrochemistry of Room-Temperature Chloroaluminate Molten Salts at Graphitic and Nongraphitic Electrodes. *J. Appl. Electrochem.* **26**, 1147-1160 (1996).

39. V. Y. Young, K. R. Williams, X-Ray Photoelectron Spectroscopy of Aluminum Oxalate Tetrahydrate. *J. of Electron Spec. and Rel. Phen.* **104**, 221-232 (1999).

40. Hess, E. Kemnitz, A. Lippitz, W. E. S. Unger, D. H. Menz, ESCA, XRD, and IR Characterization of Aluminum Oxide, Hydroxyfluoride, and Fluoride Surfaces in Correlation with Their Catalytic Activity in Heterogeneous Halogen Exchange Reactions. *J. of Catalysis* **148**, 270-280 (1994).

41. G. Beamson, D. Briggs, *High Resolution XPS of Organic Polymers* (Wiley, New York, 1992).

42. F. Bernardi, J. D. Scholten, G. H. Fecher, J. Dupont, J. Morais, Probing the Chemical Interaction between Iridium Nanoparticles and Ionic Liquid by XPS Analysis. *Chemical Physics Letters* **479**, 113-116 (2009).

43. A. Foelske-Schmitz, D. Weingarth, R. Kötz, XPS Analysis of Activated Carbon Supported Ionic Liquids: Enhanced Purity and Reduced Charging. *Surface Science* **605**, 19791985 (2011).

44. B. B. Hurisso, K. R. Lovelock, P. Licence, Amino Acid-Based Ionic Liquids: Using XPS to Probe the Electronic Environment via Binding Energies. *Phys. Chem. Chem. Phys.* **13**, 17737-17748 (2011).

45. B. A. Sexton, N. R. Avery, Coordination of Acetonitrile (CH,CN) to Platinum (111): Evidence for an η2 (C, N) Species. *Surface Science* **129**, 21-36 (1983).

46. J. R. Stuff, Thermal Decomposition of 1-Methyl-3-Eethylimidazolium Chloride (MEIC)/Aluminum Chloride Molten Salts. *Thermochimica Acta* **152**, 421-425 (1989).

47. K. E. Hendrickson, L. Ma, G. Cohn, Y. Lu, L. A. Archer, Model Membrane-Free Li–S Batteries for Enhanced Performance and Cycle Life. *Adv. Sci.* **2**, 1500068-1500077 (2015).

48. I. Bauer, M. Kohl, H. Althues, S. Kaskel, Shuttle Suppression in Room Temperature Sodium–Sulfur Batteries Using Ion Selective Polymer Membranes. *Chem. Commun.* **50**, 3208-3210 (2014).

49. *Market Prospect and Production Application of Oxalic Acid-Organics* (China Chemical Reporter No. 21, 2003).

50. H. Yue, Y. Zhao, X. Ma, J. Gong, Ethylene Glycol: Properties, Synthesis, and Applications. *Chem. Soc. Rev.* **41**, 4218-4244 (2012).

51. G. Finnveden, M. Z. Hauschild, T. Ekvall, J. Guinee, R. Heijungs, S. Hellweg, A. Koehler, D. Pennington, S. Suh, Recent Developments in Life Cycle Assessment. *J. of Env. Man.* **91**, 1-21 (2009).

52. *The Environmental Footprint of Semi-Finished Aluminum Products in North America-A Life Cycle Assessment Report* (The Aluminum Association, 2013).

53. *Electric Power Annual 2014* (eia U.S. Energy Information Administration, 2016).

54. I. Fischer, Th. Lehmann, E. Heitz, The Production of Oxalic Acid from CO_2 and H_2O. *J. App. Electrochem.* **11**, 743-750 (1981).

55. W. Riemenschneider, M. Tanifuji, *Oxalic Acid* (Ullmann's Encyclopedia of Industrial Chemistry, Wiley-VCN, Weinheim, 2011) chap 25.

56. H. Lim, H. Lim, K. Park, D. Seo, H. Gwon, J. Hong, W. A. Goddard, H. Kim, K. Kang, Toward a Lithium−Air Battery: The Effect of CO_2 on the Chemistry of a Lithium−Oxygen Cell. *J. Am. Chem. Soc.* **135**, 9733-9742 (2013).

57. M. T. Carter, C. L. Hussey, S. K. Strubinger, R. A. Osteryoung, Electrochemical Reduction of Dioxygen in Room-Temperature Imidazolium Chloride-Aluminum Chloride Molten Salts. *Inorg. Chem.* **30**, 1149-1151 (1991).

58. Y. Katayama, H. Onodera, M. Yamagata, T. Miura, Electrochemical Reduction of Oxygen in Some Hydrophobic Room-Temperature Molten Salt Systems. *J. Electrochem. Soc*. **151**, A59-A63 (2004).

59. Md. M. Islam, T. Imase, T. Okajima, M. Takahashi, Y. Niikura, N. Kawashima, Y. Nakamura, T. Ohsaka, Stability of Superoxide Ion in Imidazolium Cation-Based Room-Temperature Ionic Liquids. *J. Phys. Chem. A* **113**, 912-916 (2009).

1.13 APPENDIX

Supporting Materials for Chapter 1

Table S1.1. DART Mass Spectroscopy detected species. Negative and positive ion fragments and corresponding cathodes.

Fragment	**Al/80%CO_2 Cathode**	**Al/100%O_2 Cathode**	**Undischarged Cathode**
Cl_2^-	●	●	●
HCl_2^-	●	●	●
$AlCl_4^-$	●	●	●
$AlCl_3(OH)^-$	●	●	●
$AlCl_2(OH)_2^-$	●	●	●
$AlCl(OH)_3^-$	●	●	●
$C_6H_{11}N_2Cl_2^-$	●	●	●
$C_6H_{11}N_2^+$	●	●	●
$C_5H_9N_2^+$	●	●	●
$C_4H_7N_2^+$	●	●	●
$C_3H_4N_2^+$	●	●	●
$Al(C_2O_4)^+$	●		
$Al(C_2O_4)_2^-$	●		
$Al(C_2O_4)(C_2O_3)^+$	●		
$Al(C_2O_4)O^-$	●		
$AlCl_2(C_2O_4)^-$	●		
$(C_6H_{11}N_2)(C_2O_4)^-$	●		
$(C_6H_{11}N_2)_3(C_2O_4)^+$	●		
$(C_6H_{11}N_2)_2(C_2O_4)Cl^-$	●		

Table S1.2. Typical DART Mass Spectroscopy results. Positive and negative ion mode detected and predicted species in discharged and undischarged cathodes.

Fragments	Detected	Predicted
Cl_2^-	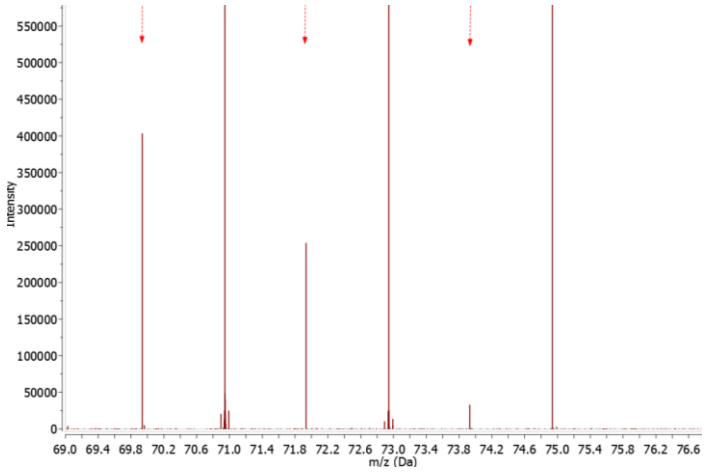	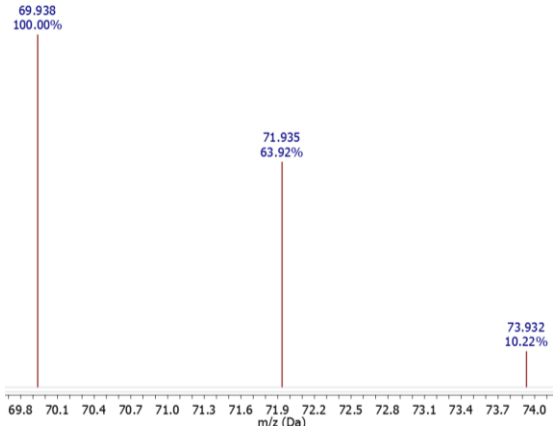
HCl_2^-	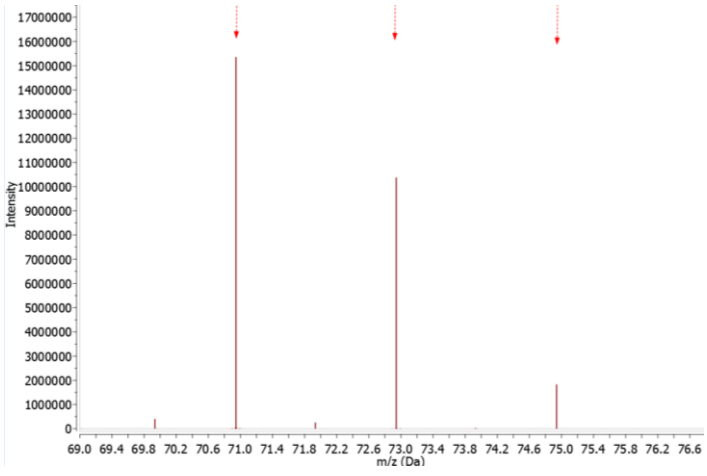	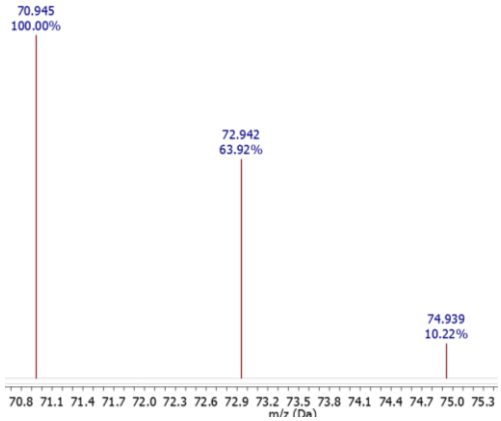

$AlCl_4^-$	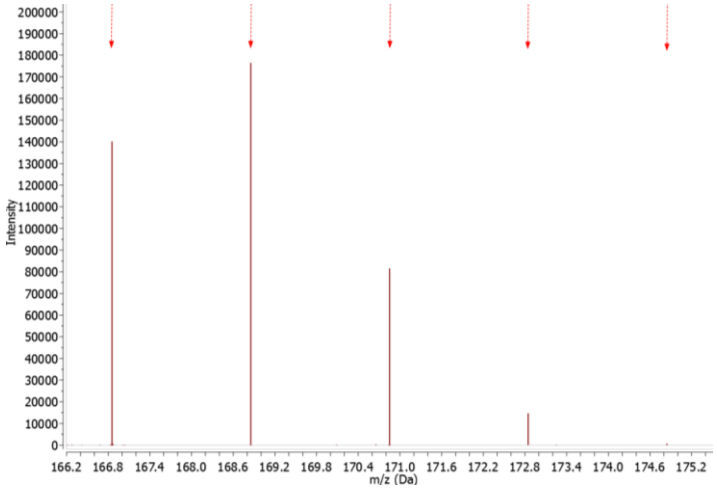	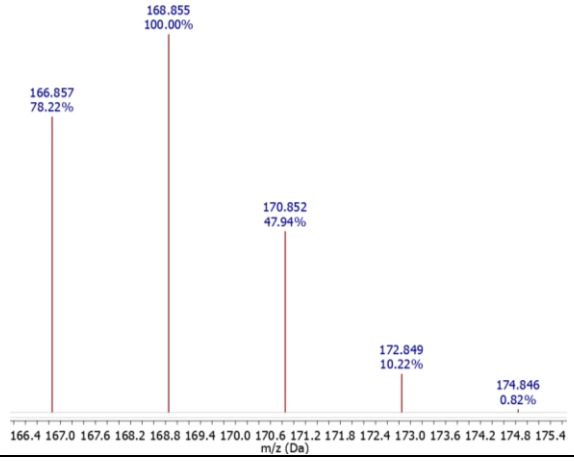
$AlCl_3(OH)^-$	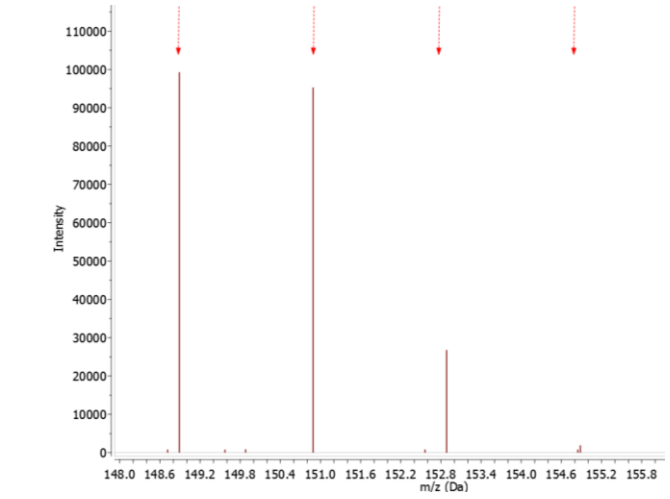	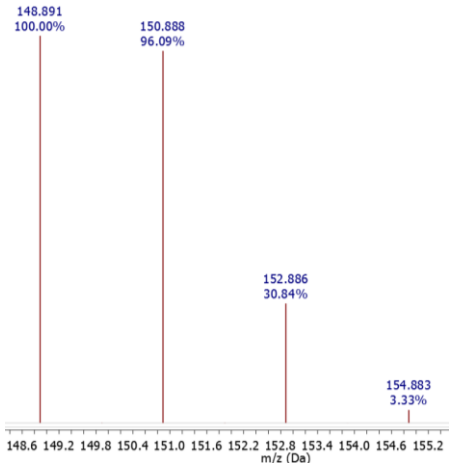
$AlCl_2(OH)_2^-$	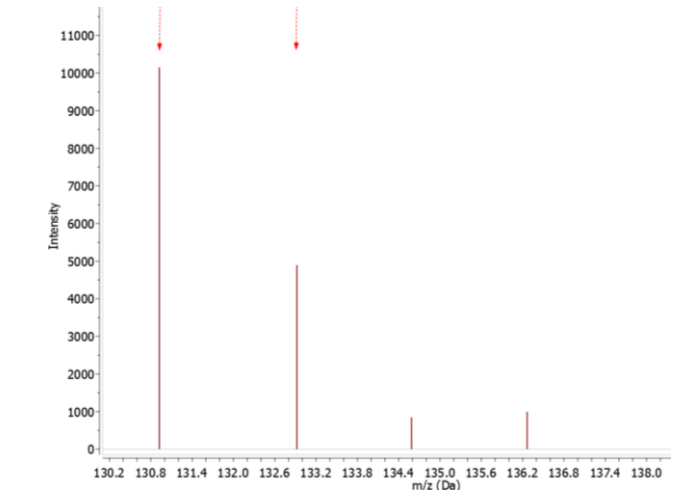	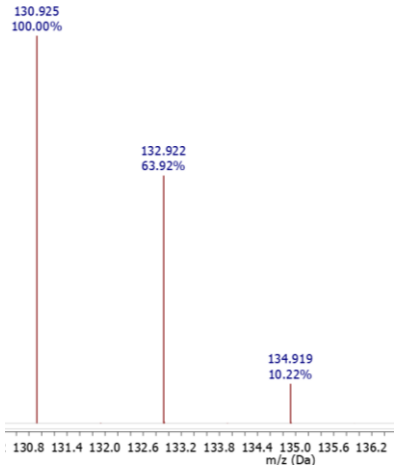

$AlCl(OH)_3^-$	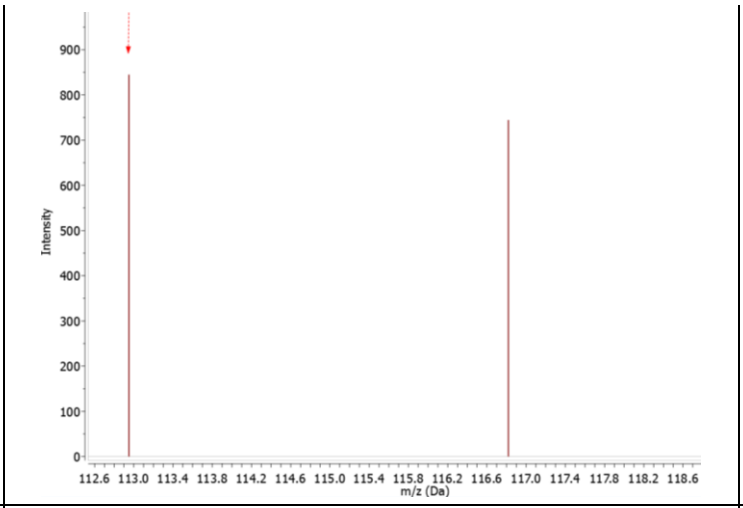	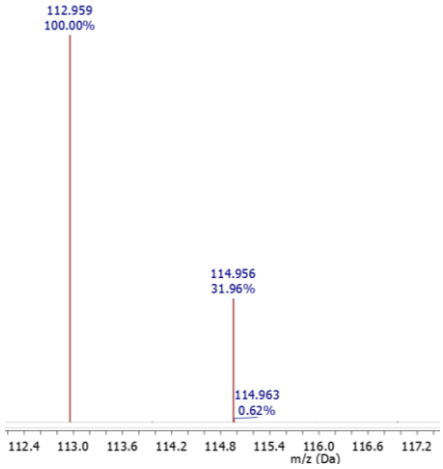
$C_6H_{11}N_2Cl_2^-$	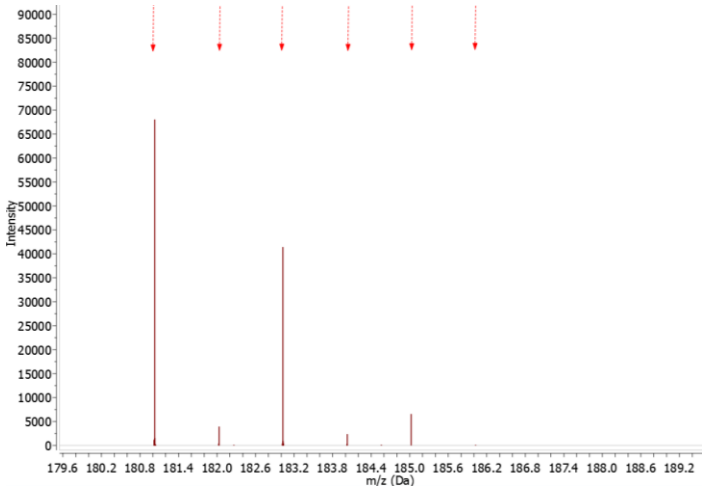	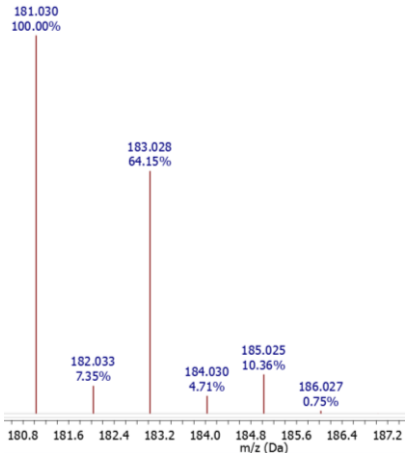
$C_6H_{11}N_2^+$	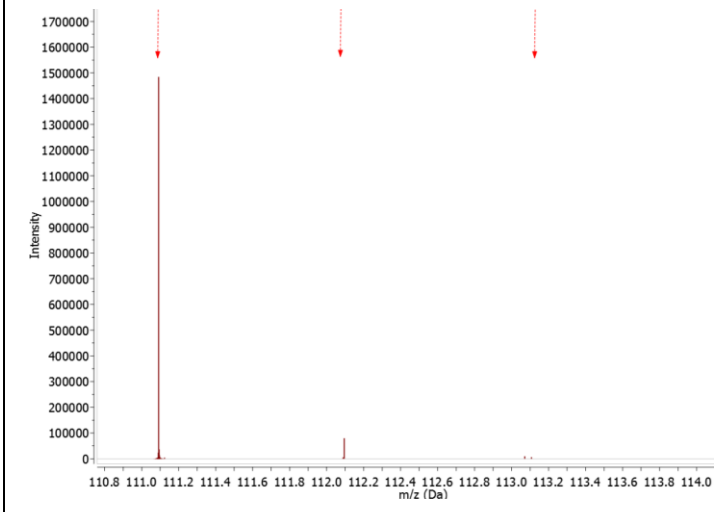	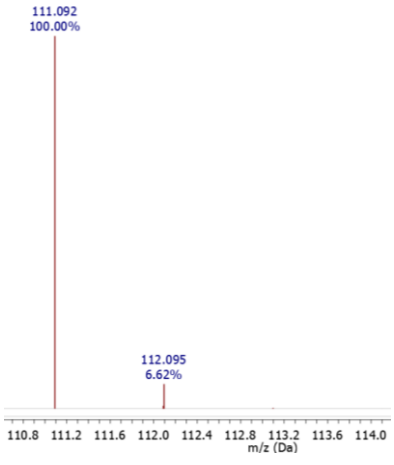

$C_5H_9N_2^+$	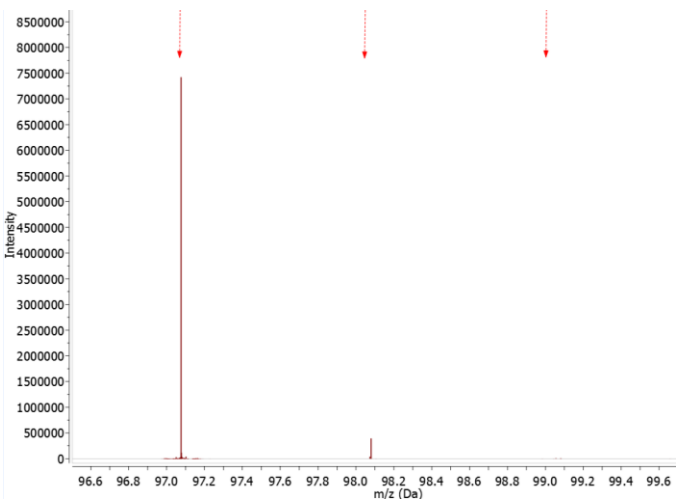	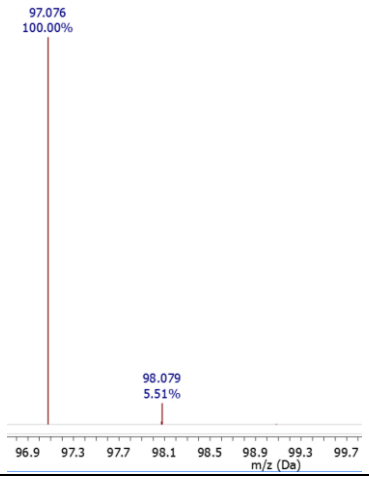
$C_4H_7N_2^+$	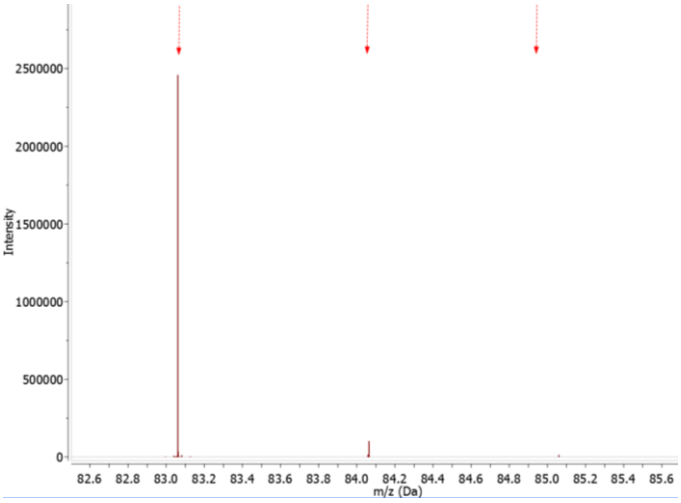	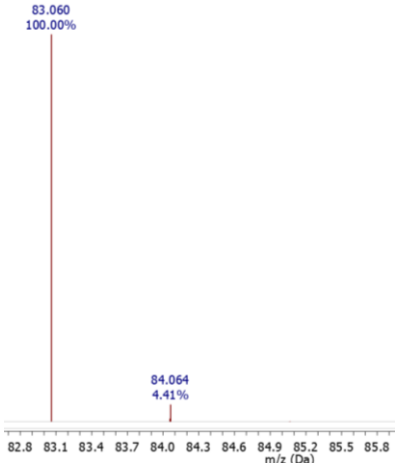
$C_3H_4N_2^+$	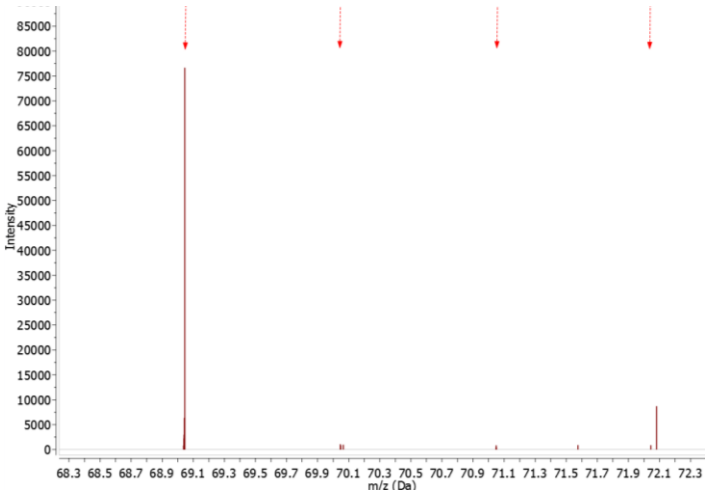	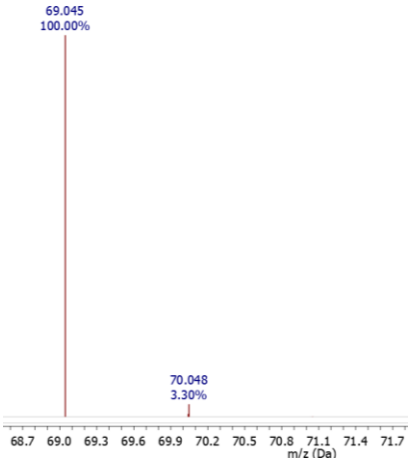

$Al(C_2O_4)^+$	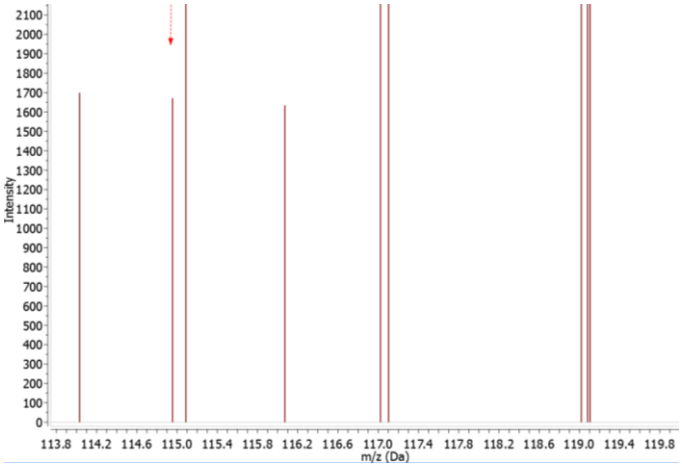	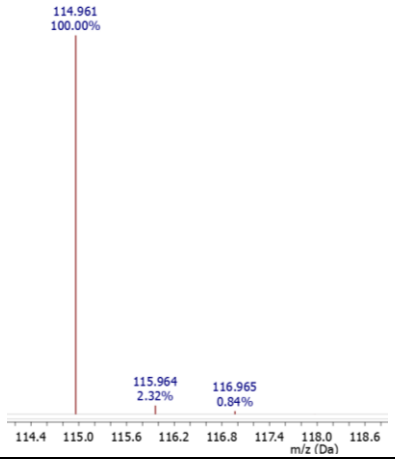
$Al(C_2O_4)_2^-$	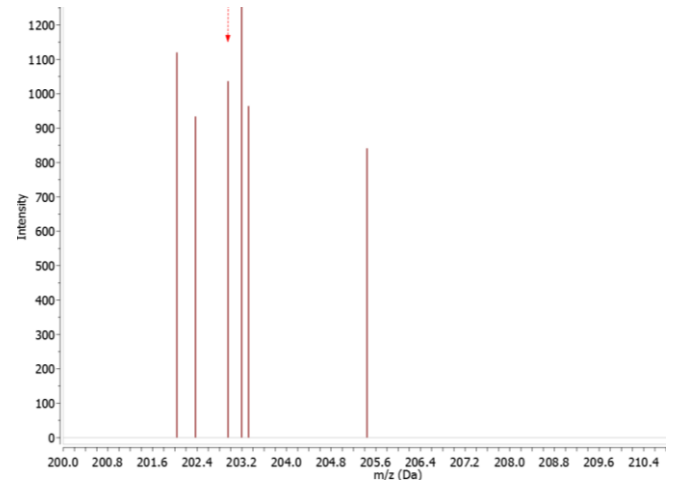	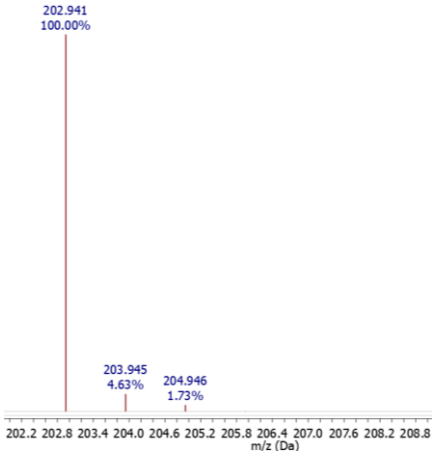
$Al(C_2O_4)\ (C_2O_3)^+$	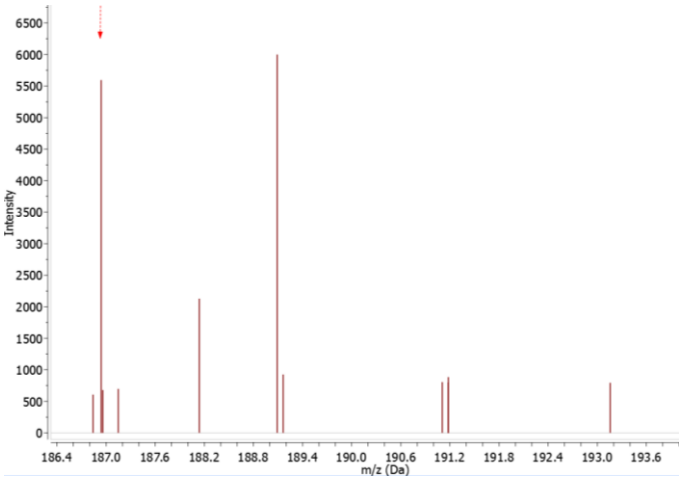	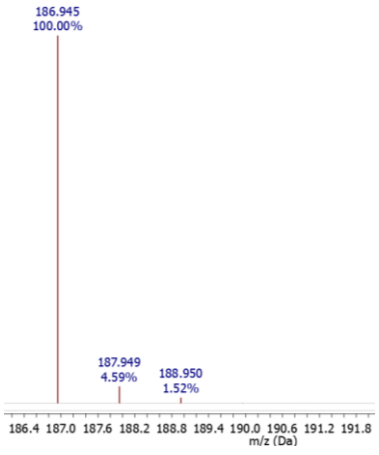

$Al(C_2O_4)O^-$	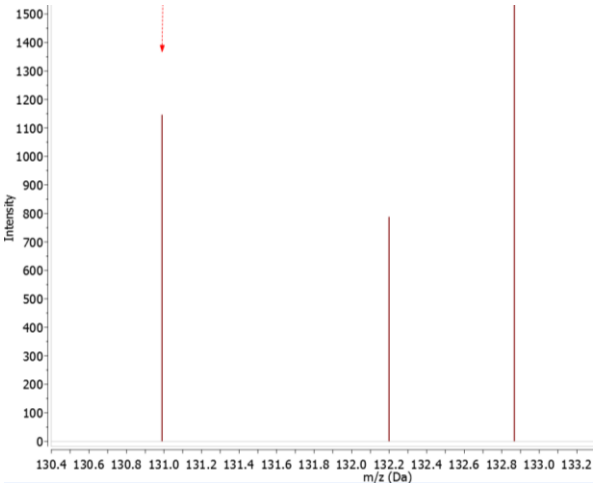	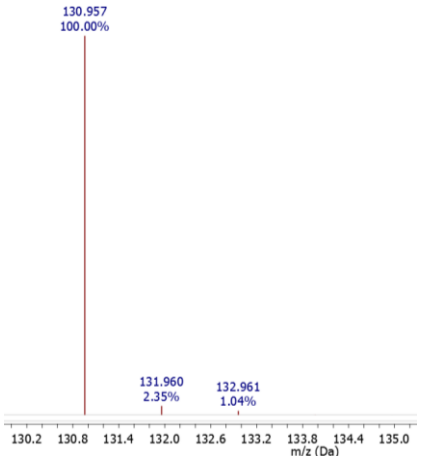
$AlCl_2(C_2O_4)^-$	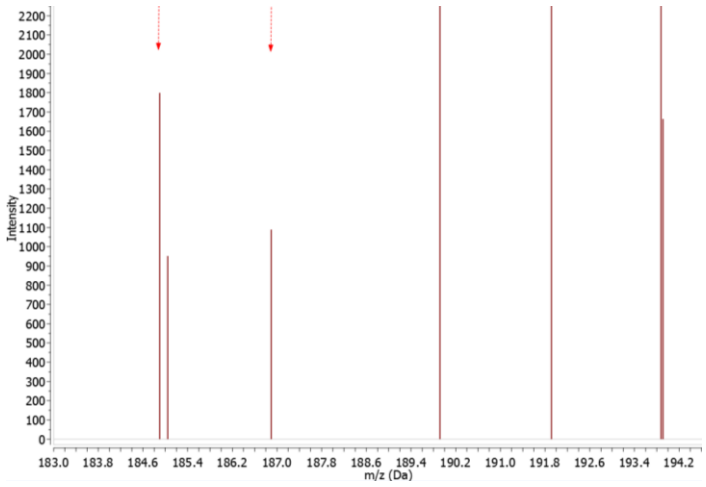	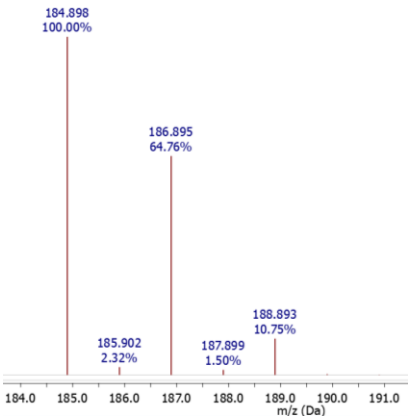
$(C_6H_{11}N_2)_3(C_2O_4)^+$	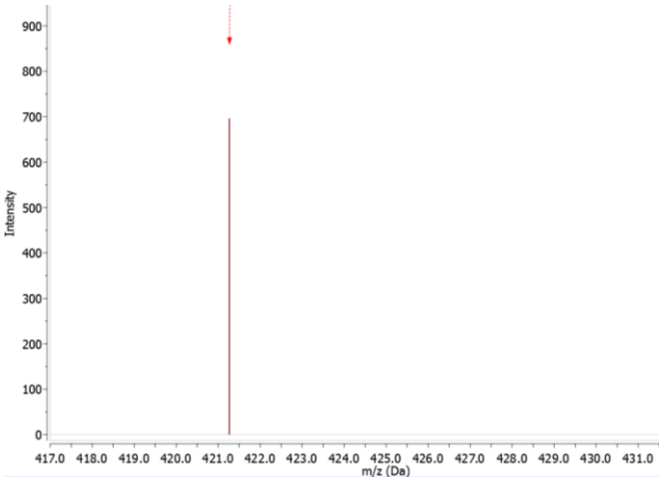	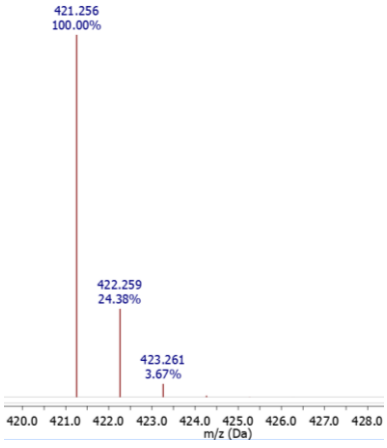

$(C_6H_{11}N_2)_2\ (C_2O_4)\ Cl^-$	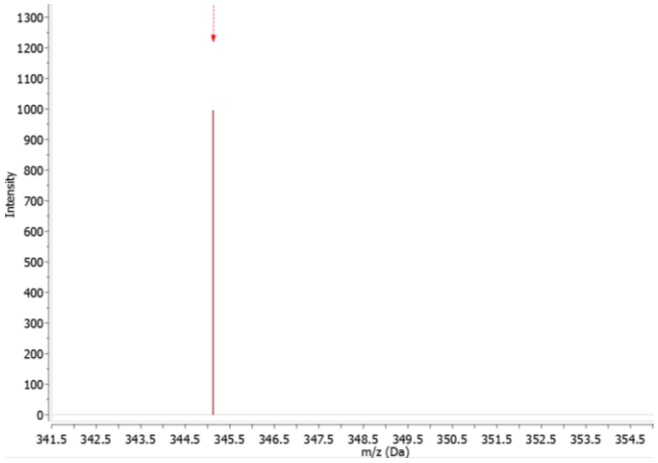	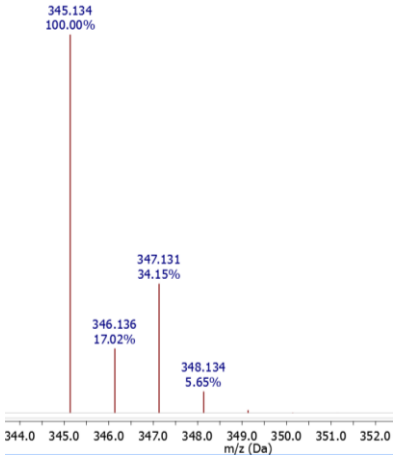
$C_6H_{11}N_2\ (C_2O_4)^-$	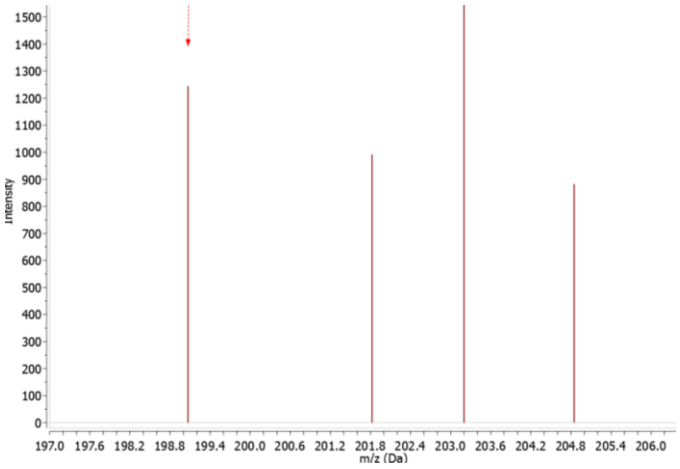	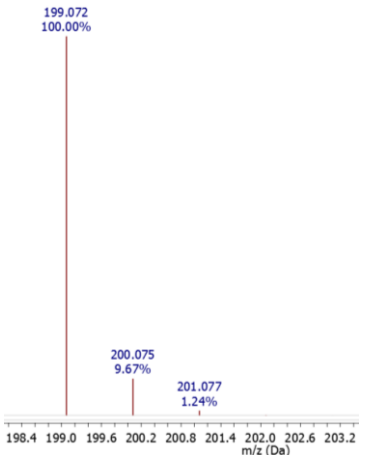

Table S1.3. EDXS spectra. Elemental detection (vs. count/sec) for discharged and undischarged cathodes.

Cathode	EDAX Spectra
Al/80%CO_2	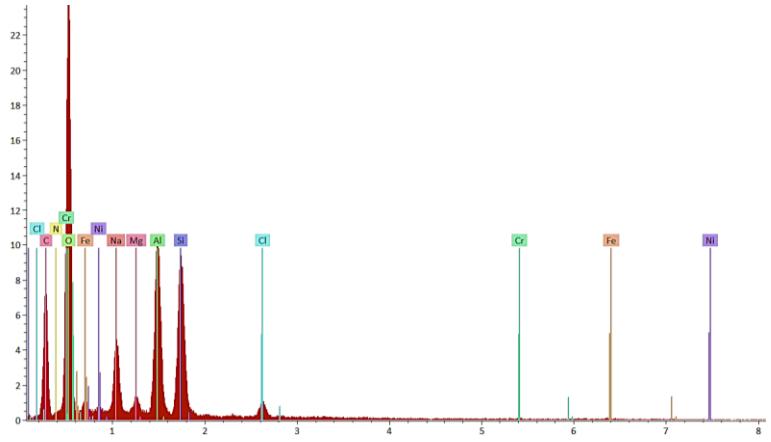
Al/100%O_2	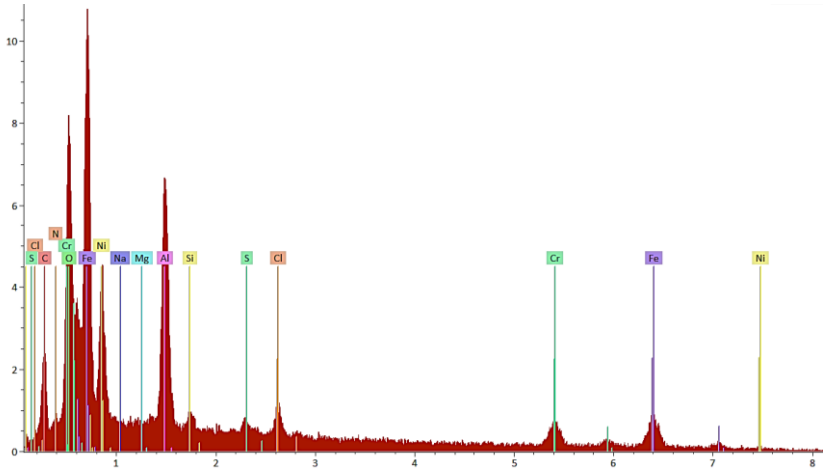
Undischarged	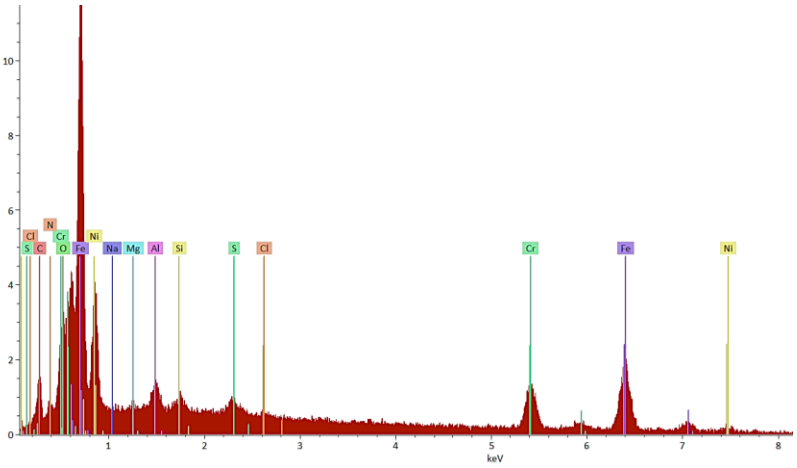

Table S1.4. XPS wide survey spectra. Scans (no. counts) for discharged, undischarged cathodes and chemically synthesized aluminum oxalate and identified elements.

Wide Survey Spectra	
Al/80%CO_2 Cathode	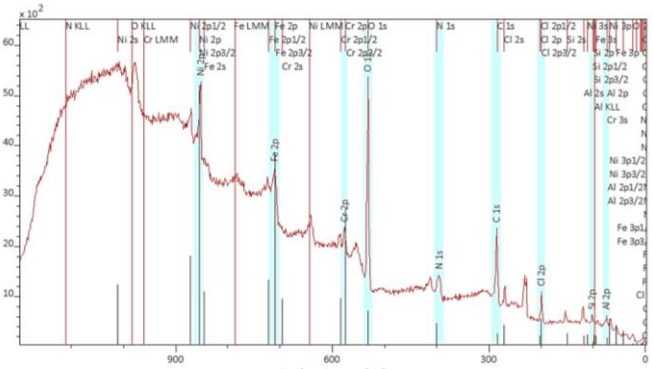
Al/100%O_2 Cathode	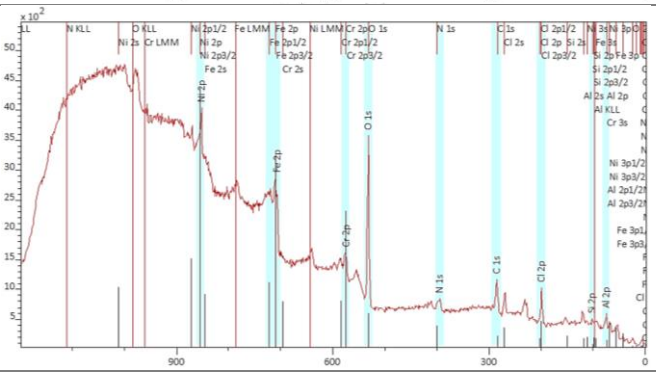
Undischarged Cathode	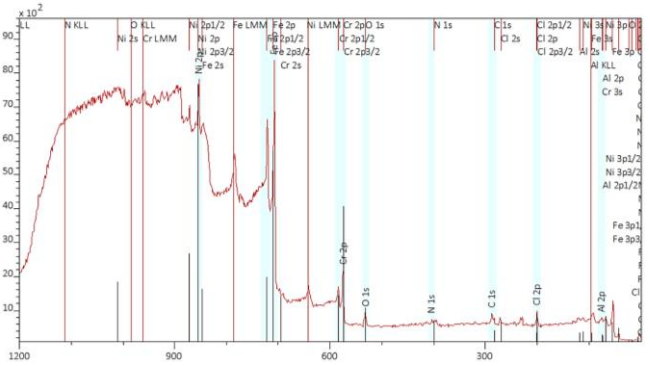
Aluminum Oxalate	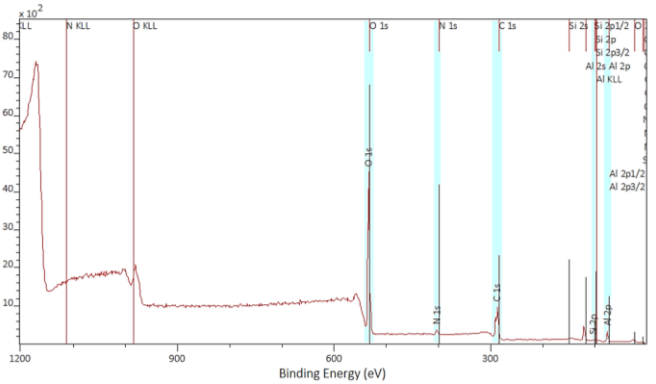

CHAPTER 2

Oligomerization, Isomerization and Carboxylation of Alkanes and Alkenes with Galvanostatically-Generated Superoxide in the Al/O_2 Electrochemical Cell

2.1 Abstract

Conversion of low-value, but thermodynamically stable chemical byproducts such as CO_2 or alkanes to more valuable feedstocks is of broad-based interest. These so-called up-conversion processes are expensive because they require energy-intensive and catalytically-driven processes to drive reaction against thermodynamic gradients. Here we show that the nucleophilic character of superoxides, generated galvanostatically in an Aluminum/O_2 electrochemical cell, can be used in tandem with the catalytic properties of an imidazolium/$AlCl_3$ electrolyte to facilely upgrade alkanes (n-decane), alkenes (1-decene) and CO_2 feeds. The Aluminum/O_2 electrochemical cell used to generate the superoxide intermediate also delivers large amounts of electrical energy in the process and as such offers a system for high-energy density storage and chemical up-conversion of low value compounds. Chronopotentiometry, mass spectrometry and nuclear magnetic resonance were used to investigate the electrochemical performance of the system and analyze the discharge products. We find that even at room temperature, alkanes and alkenes are facilely oligomerized and isomerized at high conversions (>97%), mimicking the traditionally produced refined products. Incorporating CO_2 in the alkane feed leads to formation of esters and formates at moderate yields (21%).

2.2 Introduction

The superoxide (O_2^-) specie is recognized for its importance in biological and chemical processes. Produced chemically, electrochemically, photocatalytically or biologically, superoxides are strongly nucleophilic reagents in aprotic solvents [1]. Superoxides are for this reason employed in many chemicals processes, including degradation of hazardous chemicals, hydrocarbon desulfurization, alcohol and amines carboxylation and hydrocarbon dehydrogenation [2-4]. As an example, paraffin conversion using chemically produced Ti(IV) superoxide, converts propane at moderate efficiency (12% conversion) mainly to acetone (80% yield), but only in the presence of H_2O_2 [2]. Chemically produced potassium superoxide has likewise been demonstrated to achieve complete conversion of aromatics to ketones [3]. MgO was used as a catalyst to convert alkanes and alkenes using chemically-produced superoxide, however mainly producing CO_2 (45% yield) and fragments of the starting hydrocarbons [4].

In a metal/O_2 electrochemical cell, superoxide is generated by the electrochemical reduction of oxygen on the cathode (typically high surface area porous carbon). In combination with high energy density metal anodes (such as Li [5], Na [6], Al [7] and Mg [8]) the conversion reaction produces large amounts of electrical energy, at specific energies competitive with those achieved by combusting liquid hydrocarbons. Exploiting highly reactive superoxide, metal/O_2 electrochemical systems has been proposed as a CO_2 capture technology. Discharging a mixture of O_2 and CO_2 has been demonstrated with Li [9-11], Na [12-13], Mg [9] and other metals, converting CO_2 and generating electrical energy. However, the main discharge product of metal/O_2+CO_2 electrochemical systems was carbonate based. Using Al as the anode and an imidazolium ionic liquid (IL)/aluminum chloride ($AlCl_3$) electrolyte, an Al/O_2+CO_2 electrochemical cell was previously shown to not only capture CO_2, but to convert the

captured material to an oxalate [14], a feedstock to useful chemicals supporting various markets/industries [15].

Compared to other high energy density metal anodes, Al is also attractive because of its greater abundance, inherently safer handling and higher volumetric capacity, making it ideal for conversion of low-value feedstocks as an Al/O_2 electrochemical systems. The imidazolium ionic liquid-based electrolyte is also important for multiple reasons. First, imidazolium-based ILs have been intensively studied for their ability to capture CO_2 by complexing with CO_2 [16-17]. Those studies favored the multistep chemisorption of CO_2 with the imidazolium cation and associated anion. Second, Ionic liquids have been reported to display catalytic activity in the conversion of hydrocarbons, and earlier studies have shown that when mixtures of high-value olefins and H_2 gas are used as feedstock, oligomerization and isomerization of the hydrocarbon can occur. For example, Jiang et al. have reported that in the presence of 1-butyl-3-methylimidazolium chloride/$AlCl_3$ (with higher $AlCl_3$ molar ratio), gaseous olefins (C_2H_4, C_3H_6, C_4H_8, H_2) were converted to C_8-C_{15} iso-paraffins with 80% selectivity [18]. Finally, imidazolium ILs serve as excellent hosts for $AlCl_3$, allowing the pH of the electrolyte to be facilely manipulated using salt or IL solvent concentrations to promote reversible stripping and plating of metallic aluminum under ambient conditions.

Here, we investigate chemical reactions of hydrocarbons with electrochemically generated aluminum superoxide in an ionic liquid solvent. We find that superoxide produced in an Al/O_2 electrochemical cell with a 2:1 ($AlCl_3$:1-ethyl-3-methylimidazolium chloride (EMImCl)) molar ratio of salt to electrolyte solvent oligomerizes and isomerizes alkane or alkene feedstock. Discharged in a mixture of O_2 and CO_2, the system is also shown to produce ester and formate in moderate yields,

demonstrating a path towards converting low-value hydrocarbon feedstocks and CO_2 emissions to higher value products.

2.3 Oligomerization and Isomerization of Alkane (n-Decane) Feed

To investigate the effect of electrochemically generated superoxide on hydrocarbons, an Al/O_2 electrochemical cell was discharged in a mixture of $AlCl_3$/EMImCl that is advantageous for its thermal and electrochemical stability [19]. The electrochemically prevalent species can be designated by adjusting the ratio of $AlCl_3$ to EMImCl [20-21]. An equimolar mixture will have $AlCl_4^-$ as the primary anion. Basic melts, where the EMImCl molar ratio is higher than $AlCl_3$, include Cl^- and $AlCl_4^-$ as the anions. Acidic melts, with higher $AlCl_3$ to EMImCl ratio have $AlCl_4^-$ and $Al_2Cl_7^-$ as the predominat anions. The acidic 2:1 ($AlCl_3$:EMImCl, molar ratio) electrolyte was primarily used in this study because it facilitates utilization of the electrochemically generated superoxide for conversion of a range of feedstocks.

Decane was used as a representative hydrocarbon and is typically used as a surrogate for fuels such as kerosene [22]. In the Al/O_2 electrochemical system, Al acts as the anode and O_2 diffuses through the porous carbon cathode into the electrolyte. The electrochemical reduction process takes place on the surface of the cathode, where superoxide (O_2^-) specie is generated (Figure 2.1). The Al anode is oxidized releasing an electrical current through an external circuit where electric energy can be harnessed.

Mixing n-decane with a 2:1 ($AlCl_3$:EMImCl) electrolyte results in the formation of two heterogenous fluid layers. Discharging the mixture under pure O_2, causes the two layers to merge to form a single homogenous fluid layer. During this process, the electrochemical cell generates 1,645mAh/g_{carbon} capacity at 0.7V potential as

demonstrated in Figure 2.1. The discharge potential is lower than that achieved by discharging the cell without hydrocarbons (1.4V [14]), but the discharge capacity is almost four-times higher. The difference in discharge potential can be attributed to the additional resistance of O_2 diffusion through the hydrocarbon layer and transport barriers imposed by the hydrocarbon layer to ion migration to the cathode. The alkane is therefore thought to act as a sacrificial material, reacting/complexing with the superoxide generated by reduction of O_2 at the cathode and lowering the production of the passivating aluminum oxide on the porous cathode, which explains the increase in capacity. The electrochemical reactions involve the oxidation of Al anode and reduction of O_2 on the surface of carbon cathode [14]:

Anode: $Al + 7\ AlCl_4^- \leftrightarrow 4\ Al_2Cl_7^- + 3\ e^-$

Cathode: $O_2 + e^- \leftrightarrow O_2^-$

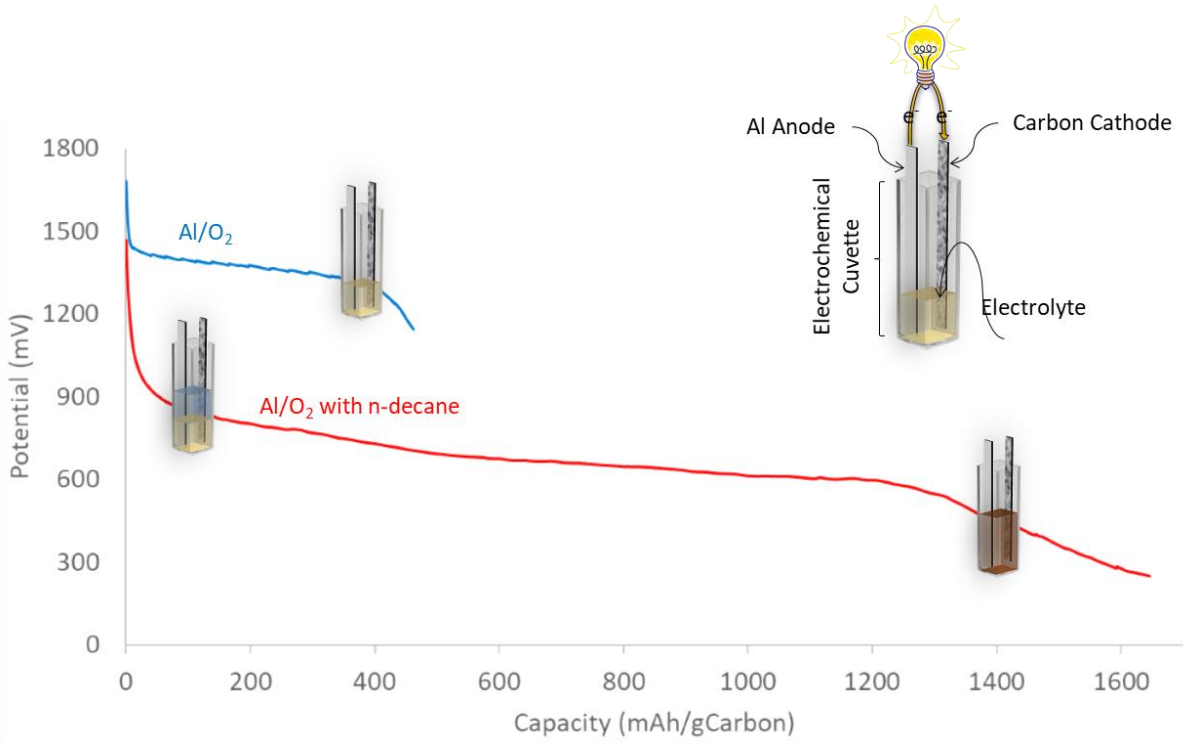

Figure 2.1: Galvanostatic discharge of Al/O_2 electrochemical cell. The cell was discharged in the presence and absence of n-decane layer using 2:1 ($AlCl_3$:EMImCl) electrolyte under 20mA current density. Insets shows the components of the electrochemical cuvettes. The n-decane layer merges with the electrolyte if discharged under O_2.

Gas Chromatography-Mass Spectrometry (GC-MS) of the homogenous electrolyte/hydrocarbon layer showed the conversion of n-decane ($C_{10}H_{22}$) to a distribution of longer alkanes (up to heptacosane, $C_{27}H_{56}$) as seen in Figure 2.2. Hydrocarbons of the same composition were detected at different retention times due to isomerization (branching and cyclization) taking place dynamically during discharge, as the hydrocarbons interact with the superoxide and electrolyte species. Typically, boiling point of alkanes with similar composition increases as they go from highly branched, to straight chains to cyclic [23]. In the liquid phase, 97.10% conversion of n-decane was achieved with the highest yield for pentadecane (17.48%), based on GC-MS. Unsaturated hydrocarbons were also detected in small yields (all unsaturated species less than 5%).

Mass spectrometry of the electrochemical cell's headspace, using Residual Gas Analysis (RGA), revealed that the solution phase process also generated smaller alkanes and CO_2 as side products. The difference between the RGA spectra of discharged n-decane in Al/2:1($AlCl_3$:EMImCl)/O_2 cell and mixed n-decane with the same electrolyte is presented in Figure 2.3. Discharging the electrochemical cell converted 3.41% of n-decane to gaseous alkanes (C_4 to C_1) and CO_2. The m/z signal associated with O_2 (32 and 16) is also seen to decrease, indicating the consumption of O_2 during discharge. The CO_2 yield is low and amount to at most 0.13%. This finding is significant as it demonstrates the ability of Al/O_2 cell to fractionate hydrocarbons, potentially producing light hydrocarbons from heavier, low value feedstocks, with minimal CO_2 emissions. The Al/O_2 electrochemical cell can also up-convert/upgrade alkanes under mild conditions. Previous investigations showed CO_2 as the main oxidation product (yield of 45%) when chemically-generated superoxides are used to chemically convert alkanes

[4]. Details of the RGA-MS results are provided in the Supplementary Materials section (Figure 2.S1).

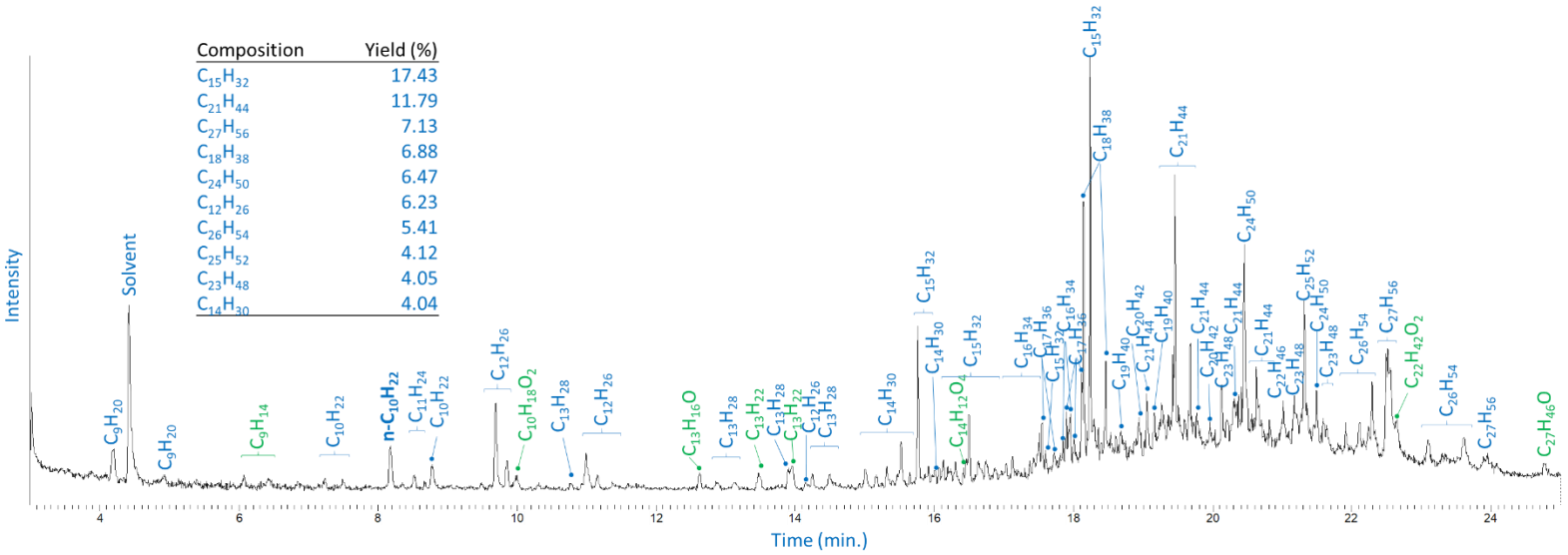

Figure 2.2: GC-MS Total ion count (TIC) chromatogram of hydrocarbons discharged galvanostatically in an Al/O_2 cell. The was discharged using 2:1 ($AlCl_3$:EMImCl) electrolyte. Detected hydrocarbons are denoted on the TIC (blue and green for saturated and unsaturated hydrocarbons, respectively). The insert table lists the yield of the main components.

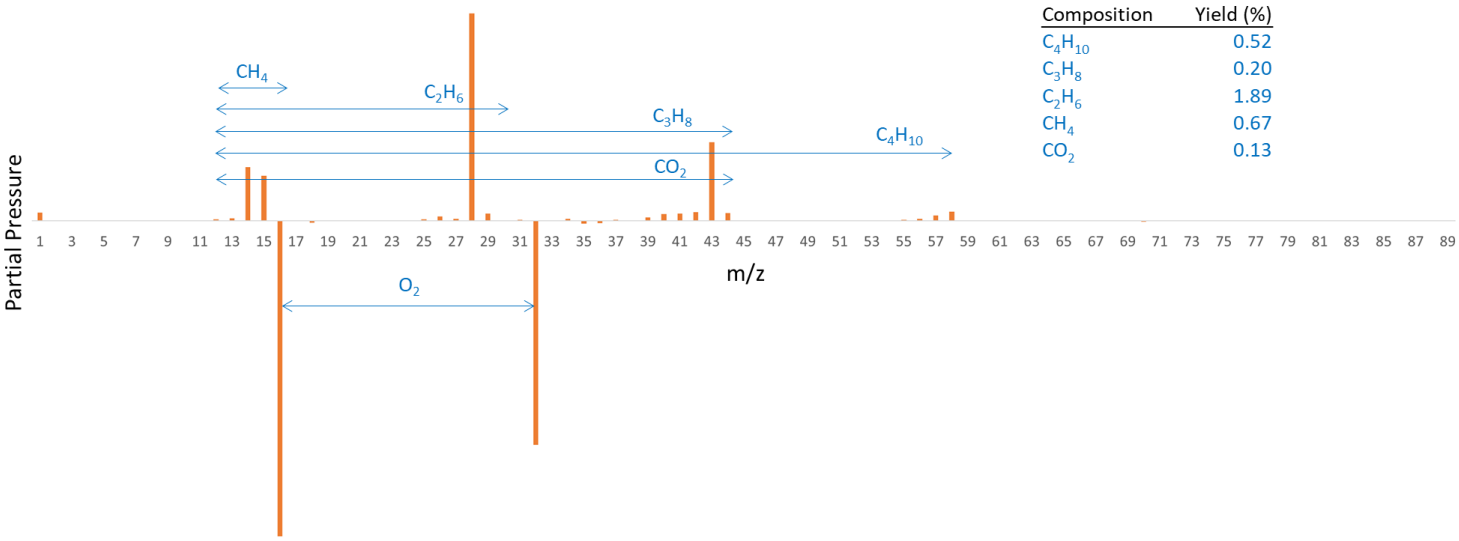

Figure 2.3: RGA-MS difference of the electochemical cell's headspace. The spectra demonstrate the difference between the Al/O_2 cell discharged with n-decane and only mixed case. The inset table lists the yields of the main components generated when Al/O_2 electochmical cell is disharged.

On the other hand, without electrochemical discharge, mixing n-decane and the 2:1 ($AlCl_3$:EMImCl) electrolyte and exposing the mixture to O_2, results in two layers (top-hydrocarbon and bottom-electrolyte). GC-MS of the top hydrocarbon layer shows the dominance of n-decane with a distribution of isomers that arise from interactions between the alkane and electrolyte (Figure 2.4). Hydrocarbons were also detected in the electrolyte layer but with n-decane accounting for only 8.39% of the GC-MS spectra, the remaining detected hydrocarbons were mainly unsaturated (Figure 2.5). The salt used in the electrochemical cell ($AlCl_3$) has been demonstrated to isomerize alkanes [24-25]. The conversion is typically low (<30%) and the selectivity depends on promoters.

Results from Proton Nuclear Magnetic Resonance Spectroscopy (^{1}H-NMR) agree with our findings from GC-MS and confirm the high degree of isomerization due to alkane-electrolyte interactions. Hydrocarbons isolated from the electrolyte (either only mixed or mixed/discharged) show the presence of alkenes. Aromatic protons were only detected when the alkane/electrolyte mixture is discharged in an Al/O_2 cell. ^{1}H-NMR results are detailed in the Supporting Materials section (Figure 2.S11). ^{27}Al-NMR confirms the rise of an aluminum chloride/hydrocarbon complex when the electrolyte is mixed with n-decane and the conversion of such complex during discharge (Figure 2.S20). These results therefore underscore the critical role the electrochemically generated superoxide plays in the conversion reaction.

Oligomerization and isomerization of the starting n-decane in an Al/2:1($AlCl_3$:EMImCl)/O_2 cell was also confirmed using Direct Analysis in Real Time (DART) Mass Spectrometry (MS) as demonstrated in Figures 2.S9, 2.S10 and 2.S11. Unsaturation was, particularly, highlighted by DART-MS in hydrocarbons isolated

from the bottom electrolyte layer when mixed with n-decane due to protonium/deuterium (H/D) exchange with the deuterated solvents ($CDCl_3/D_2O$).

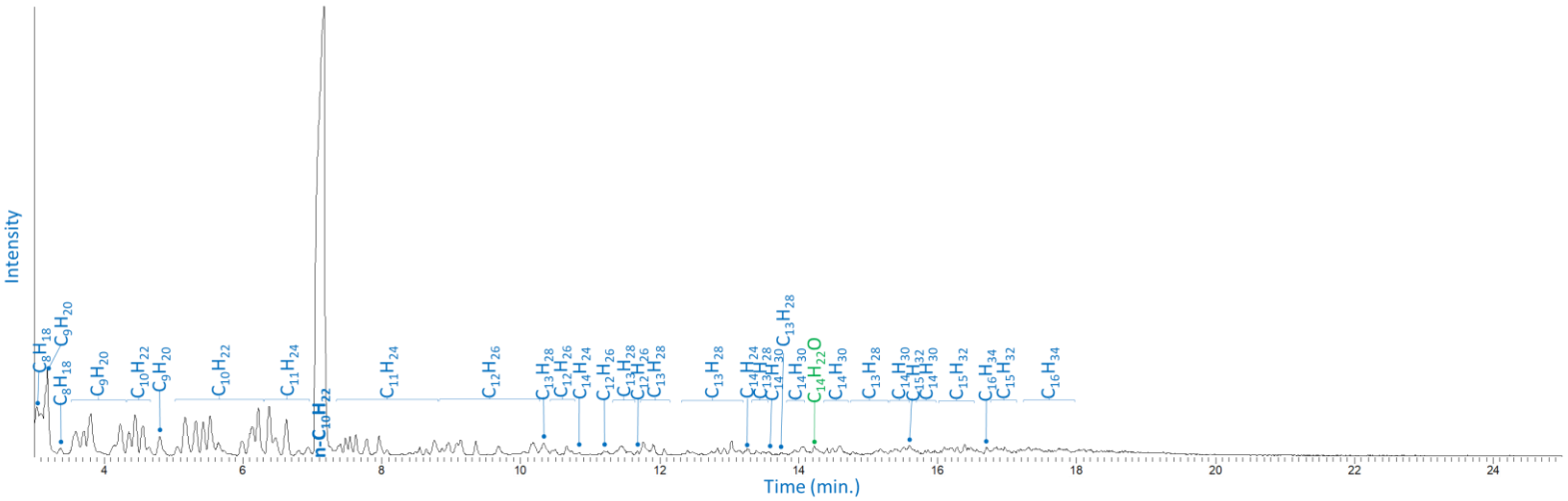

Figure 2.4: GC-MS TIC of the top n-decane layer. N-decane was mixed with 2:1 ($AlCl_3$:EMImCl) electrolyte and exposed to O_2. Detected hydrocarbons are denoted on the TIC (blue and green for saturated and unsaturated hydrocarbons, respectively).

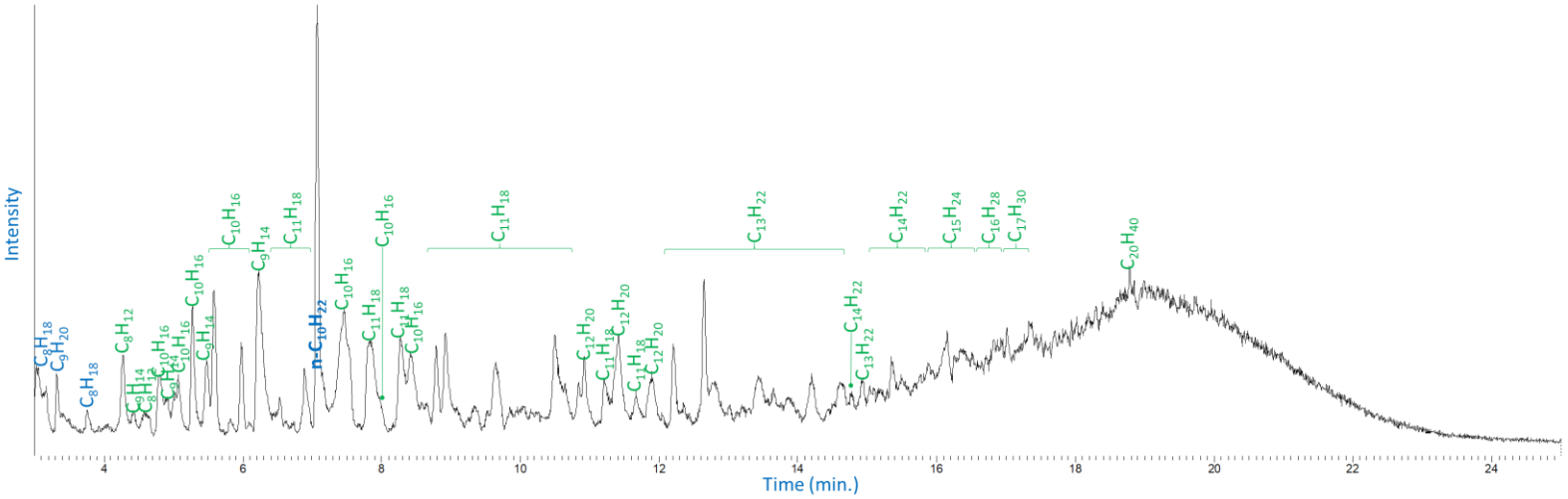

Figure 2.5: GC-MS TIC of the bottom 2:1 ($AlCl_3$:EMImCl) electrolyte layer. The electrolyte was mixed with n-decane and exposed to O_2. Detected hydrocarbons are denoted on the TIC (blue and green for saturated and unsaturated hydrocarbons, respectively).

2.4 Oligomerization and Isomerization of Alkene (1-Decene) Feed

To evaluate the effect of superoxide on unsaturated hydrocarbons, the Al/O_2 was discharged with an alkene feed. In contrast to the alkane/2:1($AlCl_3$:EMImCl) electrolyte mixture, the alkene-electrolyte mixture forms a single homogenous layer. Without discharge, 1-decene disappears giving rise to saturated hydrocarbons with the main signal for n-decane (Figure 2.6). Discharging 1-decene in the Al/O_2 cell also converted the 1-decene to saturated hydrocarbons. Distinctly, however, the main product is associated with pentadecane (36.95% yield), as demonstrated by GC-MS in Figure 2.7. The alkene was completely converted to saturated hydrocarbons due to interaction with the electrolyte. Dominance of up-converted species was driven by the electrochemically generated superoxide. ^{1}H-NMR confirm the disappearance of the alkene, when in contact with the 2:1($AlCl_3$:EMImCl) electrolyte (Figure 2.S15).

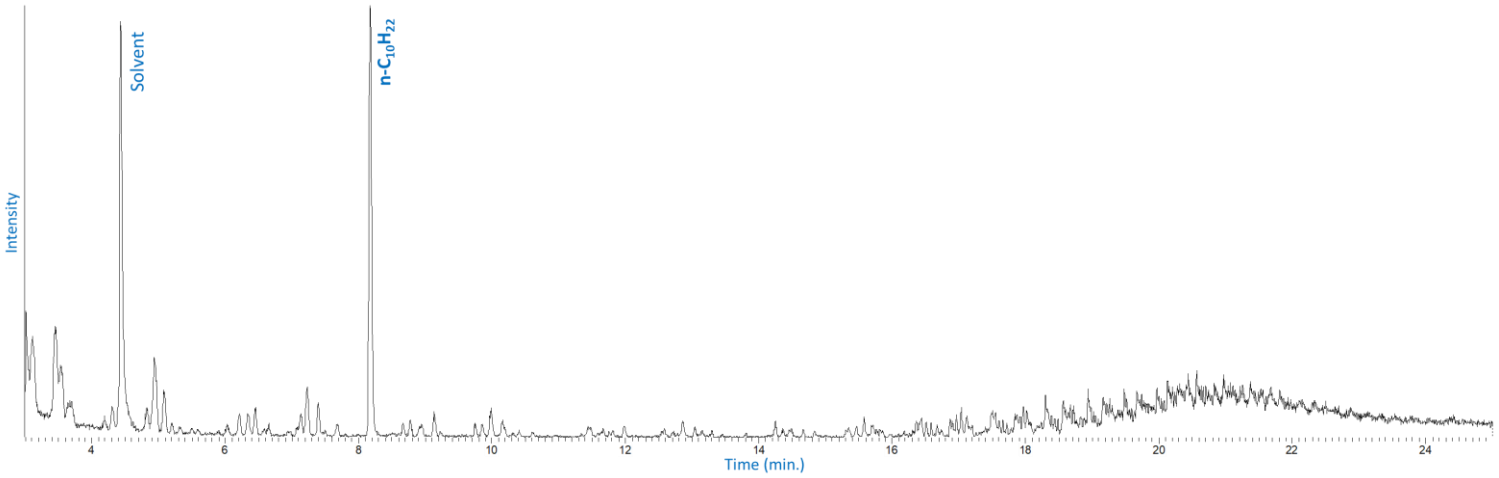

Figure 2.6: GC-MS TIC of 1-decene mixed with 2:1 ($AlCl_3$:EMImCl) electrolyte.

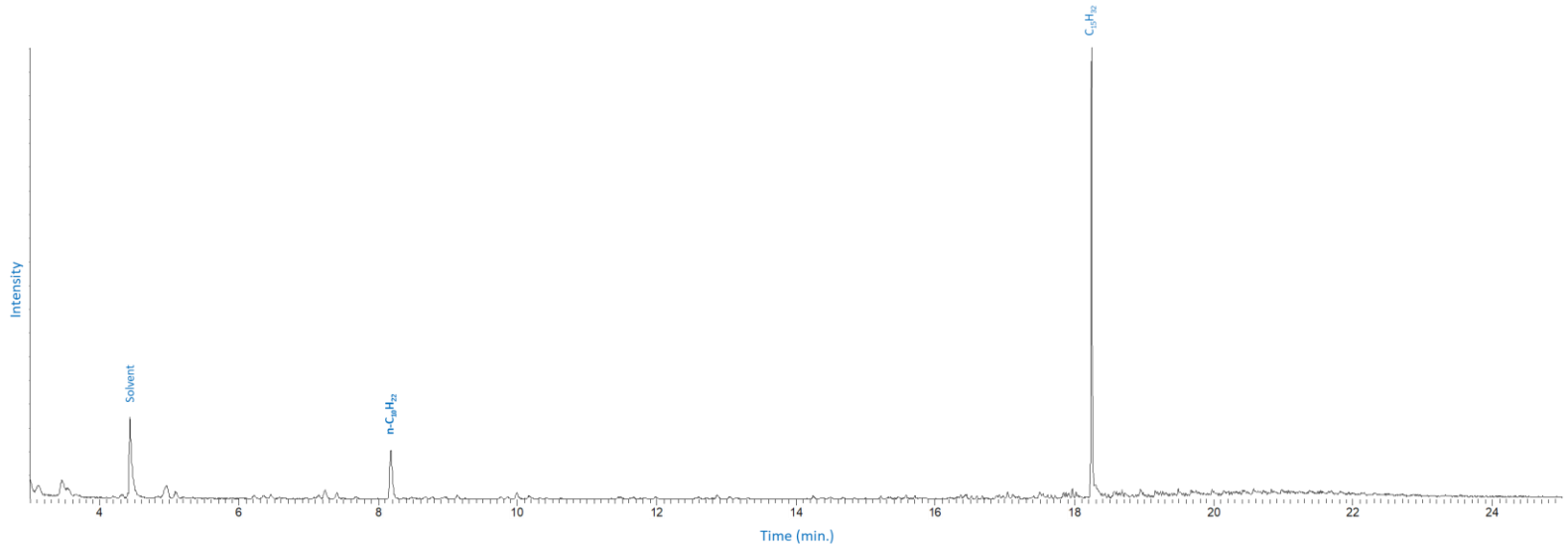

Figure 2.7: GC-MS TIC of 1-decene discharged in an Al/2:1($AlCl_3$:EMImCl)/O_2 cell.

2.5 Active Catalytical Species in the Electrolyte

Results in the previous sections show that the electrolyte plays a crucial role in converting the hydrocarbon feedstock using the electrochemically generated superoxide. This role can be understood further by manipulating the composition of $AlCl_3$ and EMImCl in the electrolyte to change the active anions present. In electrolytes with a large excess of EMImCl, the material forms a basic melt with $AlCl_4^-$ and Cl^- as the predominant anions. Notably, discharging this basic electrolyte with n-decane produced no change in the starting material as demonstrated by GC-MS (Figure 2.8). The two n-decane and electrolyte layers remained separate even after discharge. Only n-decane was detected in both top alkane and bottom 1:2.3($AlCl_3$:EMImCl) electrolyte layers with no evidence of isomerization, upgrade or branching as indicated by GC-MS (Figures 2.S3 and 2.S4). Remarkably, the introduction of an alkene to this electrolyte yielded a phase separated material with no evidence of interactions with the underlying melt. While the acidic electrolyte (2:1 $AlCl_3$:EMImCl) converted 1-decene to decane, the basic electrolyte has no effect as there is no evidence of conversion, isomerization or branching of the alkene (Figures 2.S5 and 2.S6). ^{1}H-NMR definitively confirms that the basic electrolyte 1:2.3 ($AlCl_3$:EMImCl) did not cause any change in the starting hydrocarbon (Figures 2.S16 and 2.S17).

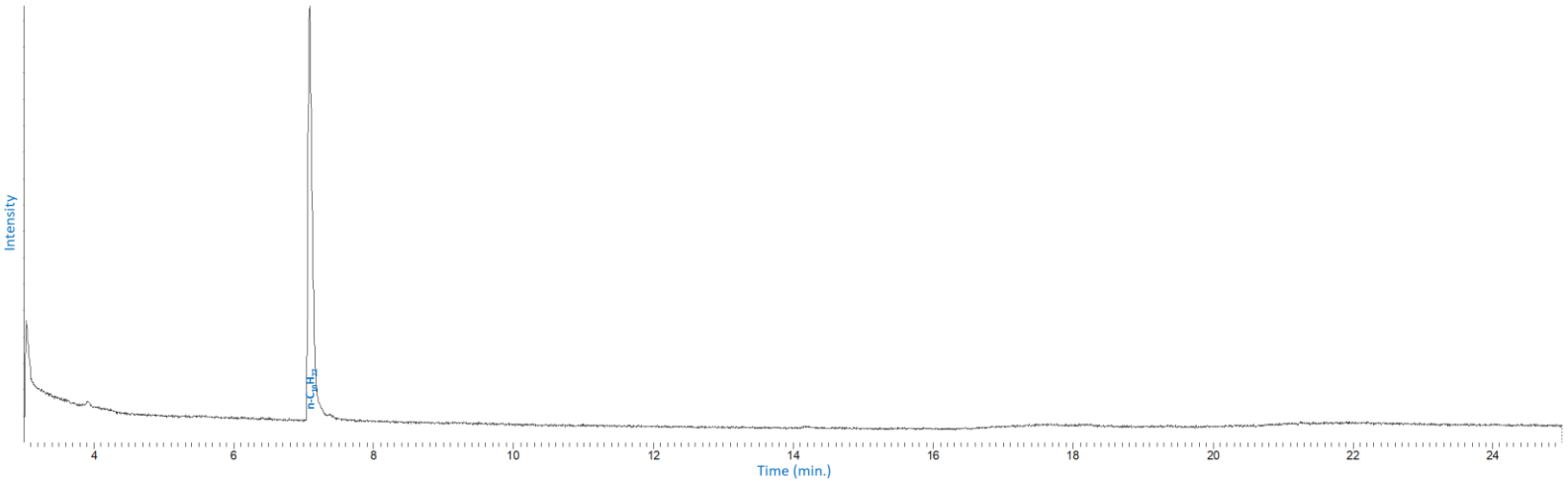

Figure 2.8: GC-MS TIC of the bottom 1:2.3 ($AlCl_3$:EMImCl) electrolyte layer. The electrolyte was mixed with n-decane and discharged in an Al/O_2 Cell.

2.6 Chemically Generated Superoxide

To understand the significance of electrochemical generation of the superoxide and the synergistic role the EMImCl-$AlCl_3$ electrolyte plays in the conversion process, we performed studies using metal superoxide generated chemically by reacting KO_2 and Dicyclohexo-18-Crown-6 in n-decane and 1-decene. In the absence of the EMImCl-$AlCl_3$ electrolyte, the chemically produced superoxide has no noticeable effect on n-decane, as demonstrated by Figure 2.9. However, as shown in Figure 2.10, it converts 1-decene to longer chains, up to hexadecane, but with much lower conversion (3.9%). The low alkene conversion is attributed to the short lifetime of superoxide in hydrocarbons compared to ionic liquid-based electrolyte [1]. Both results are confirmed by ^{1}H-NMR (see Figure 2.S18). These results not only demonstrate the synergistic effects of the superoxide and EMImCl-$AlCl_3$ electrolyte melt on conversion, but explains why electrochemical generation is required for high conversions.

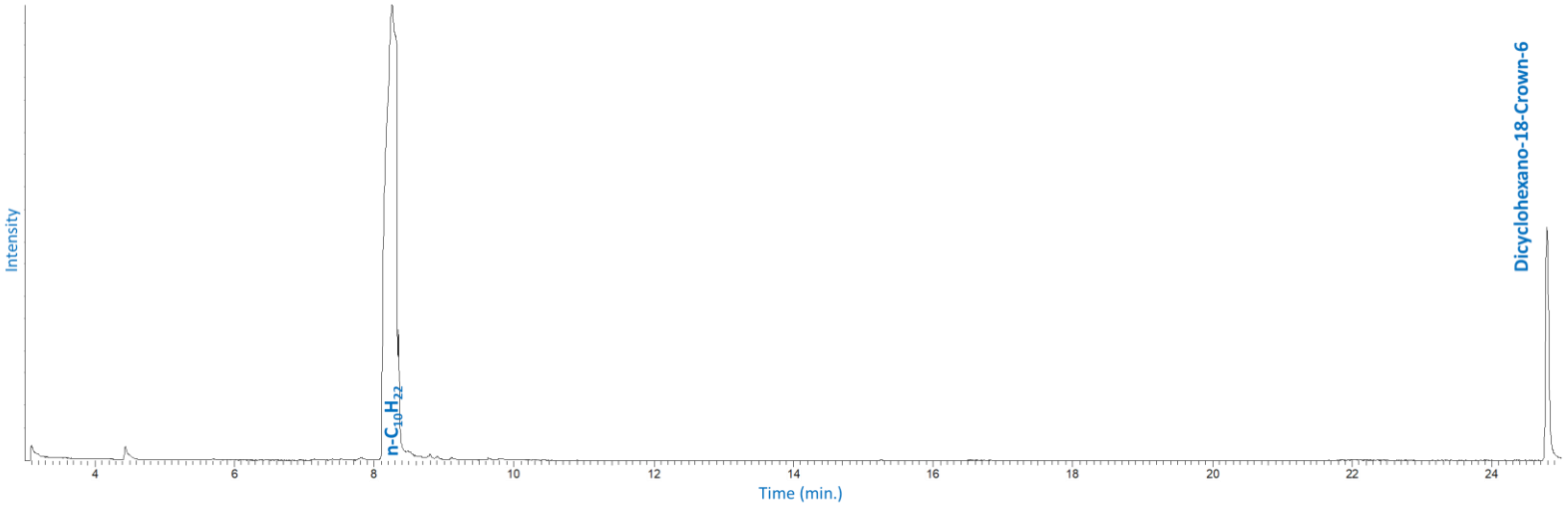

Figure 2.9: GC-MS TIC of n-decane exposed to chemically produced superoxide. The superoxide was produced by mixing KO_2 and Dicyclohexano-18-Crown-6.

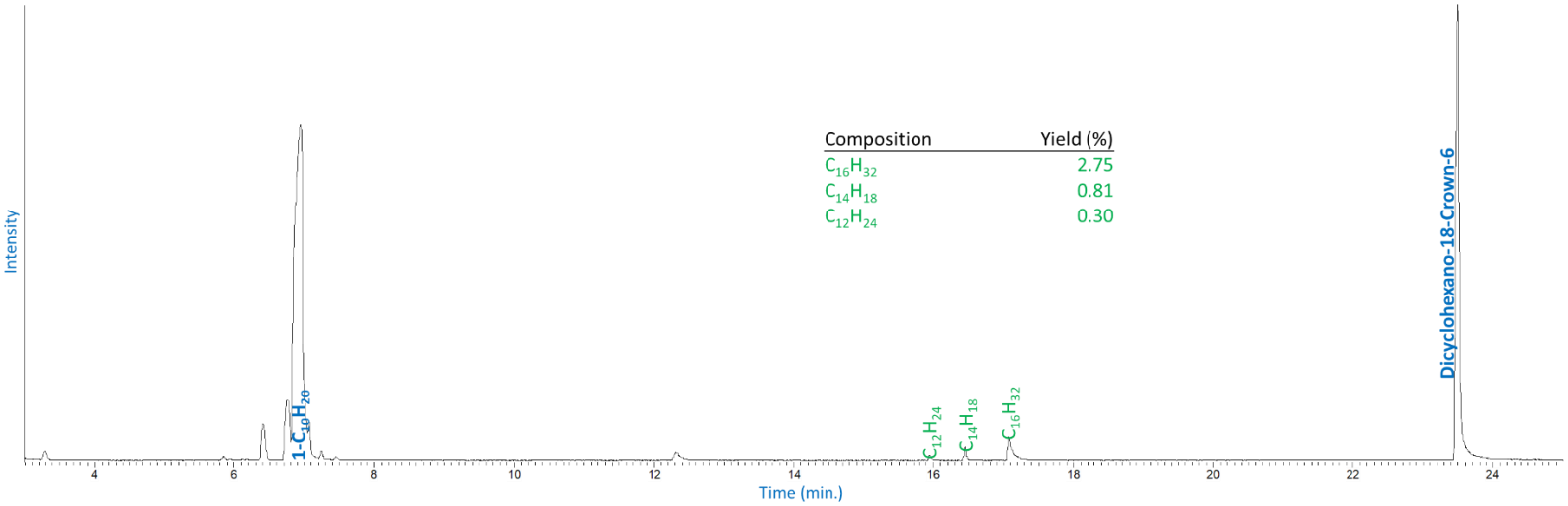

Figure 2.10: GC-MS TIC of 1-decene exposed to chemically produced superoxide. The superoxide was produced by mixing KO_2 and Dicyclohexano-18-Crown-6. The inset table lists the yields of the main produced hydrocarbons.

2.7 Carboxylation of Hydrocarbons (The Al/O_2+CO_2 Electrochemical Cell)

As a first step to understanding how an electrochemical process for up-converting hydrocarbon feeds might respond to other species, carbon dioxide was added to O_2 gas phase and its effects on the conversion reaction investigated. Significantly, it is found that CO_2 causes carboxylation of liquid hydrocarbons under specific circumstances. In particular, maintaining the same architecture of the electrochemical cell and discharging Al/80%CO_2 (denoting 80%CO_2 and 20%O_2) with n-decane or 1-decene resulted in identical products to discharging the hydrocarbons in an Al/O_2 cell. Figures 2.S7 (with n-decane) and 2.S8 (with 1-decene) present the GC-MS result for the Al/80%CO2 cells, identical to Figures 2.2 and 2.7, respectively. The results demonstrate that the superoxide preferentially reacts with the hydrocarbons and show little activity towards CO_2. This finding could be understood in terms of the thermodynamic stability of CO_2 and competing interaction of the hydrocarbons with the electrolyte. To improve the CO_2-electolyte interaction and superoxide's chance to react with CO_2, the electrochemical cell was modified to reduce the exposure of the hydrocarbons to the electrolyte. The hydrocarbons were introduced to the electrochemical cells through a capillary, limiting exposure of the bulk electrolyte. Discharging the Al/2:1($AlCl_3$:EMImCl)/80%CO_2 cell under such conditions wherein limited contact to n-decane was maintained, produced products of dramatically different chemistry as demonstrated in Figure 2.11. The conversion of n-decane was 77.35%, producing hydrocarbons as high as C_{18}. Remarkably, 21.27% of the products contained added CO_2 groups. The ^{1}H-NMR spectra (Figure 2.S19) corroborate the GC-MS results showing the detection of protons associated with formates and esters.

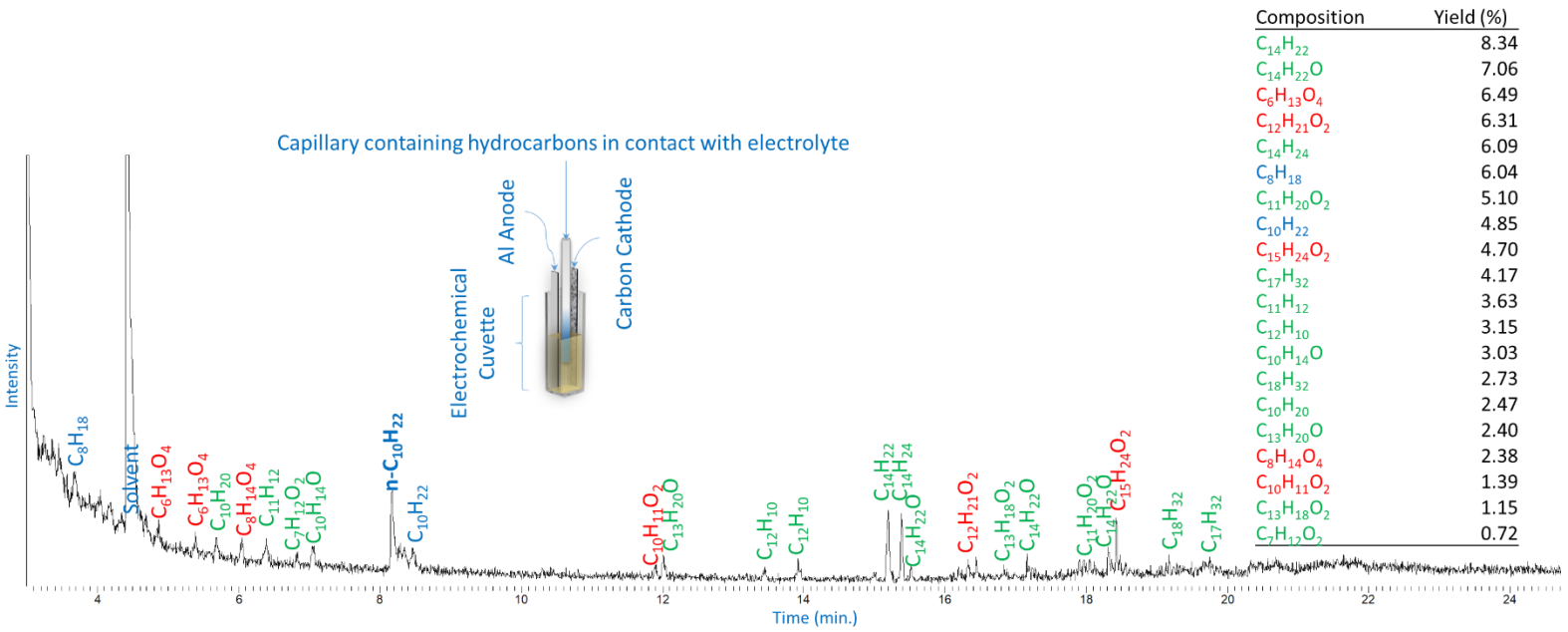

Composition	Yield (%)
$C_{14}H_{22}$	8.34
$C_{14}H_{22}O$	7.06
$C_6H_{13}O_4$	6.49
$C_{12}H_{21}O_2$	6.31
$C_{14}H_{24}$	6.09
C_8H_{18}	6.04
$C_{11}H_{20}O_2$	5.10
$C_{10}H_{22}$	4.85
$C_{15}H_{24}O_2$	4.70
$C_{17}H_{32}$	4.17
$C_{11}H_{12}$	3.63
$C_{12}H_{10}$	3.15
$C_{10}H_{14}O$	3.03
$C_{18}H_{32}$	2.73
$C_{10}H_{20}$	2.47
$C_{13}H_{20}O$	2.40
$C_8H_{14}O_4$	2.38
$C_{10}H_{11}O_2$	1.39
$C_{13}H_{18}O_2$	1.15
$C_7H_{12}O_2$	0.72

Figure 2.11: GC-MS TIC of n-decane discharged in an Al/80%CO_2 cell. The electrolyte is based on 2:1($AlCl_3$:EMImCl). The n-decane had limited exposure to the electrolyte. Detected hydrocarbons are denoted on the TIC (blue, green and red for saturated, unsaturated and carboxylated hydrocarbons, respectively). The insert table lists the yield of the main components. The inset figure presents the different components of an electrochemical cuvette with limited hydrocarbon/electrolyte exposure.

Discharging the Al/2:1($AlCl_3$:EMImCl)/80%CO_2 cell with limited contact of 1-decene changed the results as shown in Figure 2.12. The alkene was converted completely, producing compounds as large as C_{30}. Of the produced hydrocarbons, 21.30% of the yield contained added CO_2 groups. When starting with an alkene, GC-MS and ^{1}H-NMR (Figure 2.S19) results show the incorporation of CO_2 as esters.

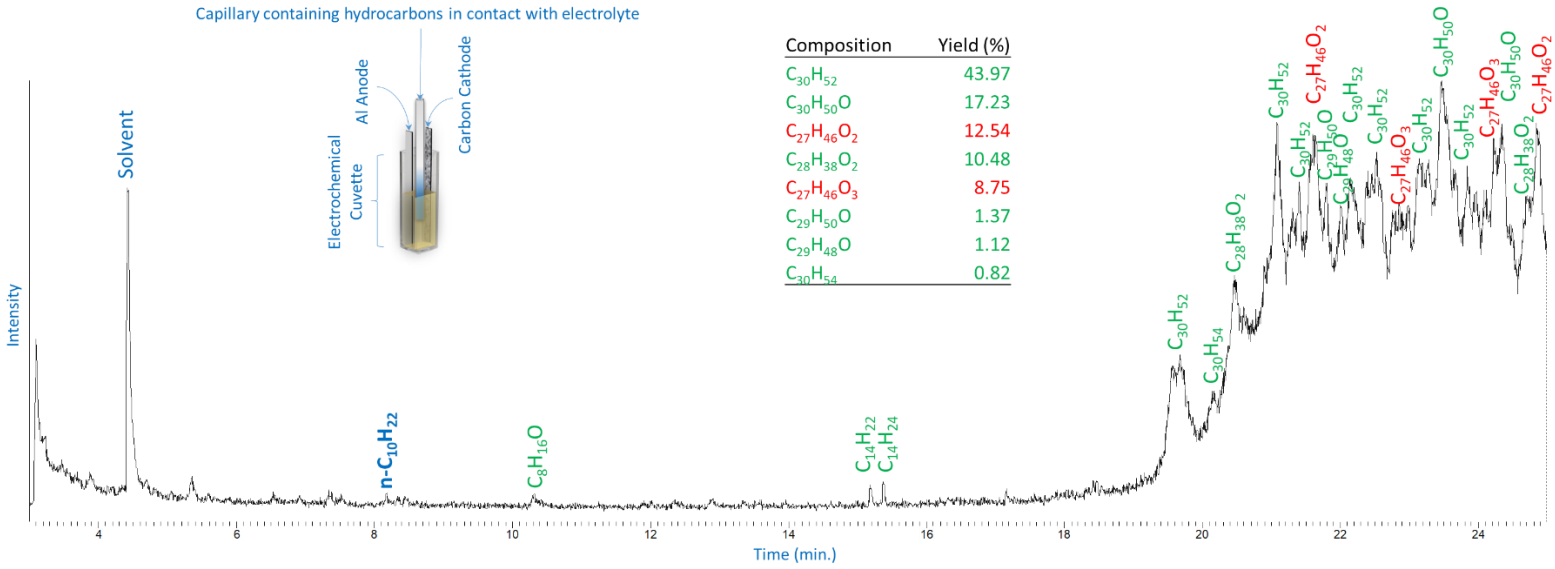

Composition	Yield (%)
$C_{30}H_{52}$	43.97
$C_{30}H_{50}O$	17.23
$C_{27}H_{46}O_2$	12.54
$C_{28}H_{38}O_2$	10.48
$C_{27}H_{46}O_3$	8.75
$C_{29}H_{50}O$	1.37
$C_{29}H_{48}O$	1.12
$C_{30}H_{54}$	0.82

Figure 2.12: GC-MS TIC of 1-decene discharged in an Al/80%CO_2 cell. The electrolyte is based on 2:1($AlCl_3$:EMImCl). The 1-decene had limited exposure to the electrolyte. Detected hydrocarbons are denoted on the TIC (blue, green and red for saturated, unsaturated and carboxylated hydrocarbons, respectively). The insert table lists the yield of the main components. The inset figure presents the different components of an electrochemical cuvette with limited hydrocarbon/electrolyte exposure.

We therefore conclude that discharging the cell in the presence of CO_2 and hydrocarbons produces a competition for reaction with electrochemically generated superoxide. Both materials may be thought to act as sacrificial agents and protect other components in the cell from superoxide. Limiting the exposure of the hydrocarbons to the electrolyte, allows CO_2 to complex with the acidic electrolyte and interact with the electrochemically generated superoxide, which favors its incorporation into hydrocarbon structures generated in the cell.

2.8 Conclusions

Conversion of thermodynamically stable chemicals (e.g. alkanes, CO_2) is typically energy intensive and catalytically driven [26]. To produce suitable fuels, hydrocarbons are upgraded through alkylation, isomerization, aromatization, blinding and other processes [27]. Highly branched, cyclic and aromatics isomers have higher octane rating and are blended with paraffins to upgrade the value of fuels. Carboxylation of hydrocarbons allows the capture of CO_2 and conversion to feedstocks of value to many industries/markets.

An Al/O_2 electrochemical system has been used to convert low-value feedstocks, utilizing the reactive superoxide and catalytic ability of the electrolyte. The system runs galvanostatically, producing considerable amount of energy. The $Al_2Cl_7^-$ anion in the imidazolium-based/$AlCl_3$ electrolyte is crucial to enable the activation of the hydrocarbons. With discharge, the generated superoxide allows for the oligomerization/isomerization of alkanes or alkenes with high conversion, increasing the value of the starting hydrocarbons. Discharging the electrochemical system under O_2 and CO_2, allows the conversion of CO_2 to esters and formates.

2.9 Materials and Methods

2.9.1 Electrolyte Preparation and Material Handling

The electrolyte was prepared by slowly mixing 1-ethyl-3-methylimidazolium chloride (EMImCl) (Sigma Aldrich, >95%) with aluminum chloride ($AlCl_3$) (Sigma Aldrich, 99.99%) in an Ar-filled glovebox. The electrolyte was vacuum heated at 130°C for 15 minutes to remove/reduce water and oxygen complexes before applying to the battery. N-decane (≥99%), 1-decene (94%), KO_2 (chunks), Dicyclohexano-18-Crown-6 (98%) were acquired from Sigma Aldrich and the deuterated solvents D_2O (D, 99.9%), $CDCl_3$ (D, 99.8%) and C_3D_6O (D, 99.9.%) were acquired from Cambridge Isotope Laboratories, Inc.

2.9.2 Electrochemical Cells Assembly and Post-Mortem Analysis

Cathodes were prepared by dissolving Ketjenblack (AkzoNobel EC600JD) with polyvinylidene floride (PVDF) binder (8:2 carbon to binder ratio) in n-methyl-2-pyrrolidone (NMP) solvent, ball milling and casting on carbon paper (Toray TGP-H-030). The cathodes were dried in vacuum oven overnight at 100°C. Typical loading of cathodes was 0.5-1.0mg_{Carbon}/cm^2. Al foil (Alfa Aesar, 99.99% 0.1mm thick) was used as the anode after mechanical cleaning with silicon carbide sandpaper and washing with acetone. The Al foil was dipped and scratched while in contact with the electrolyte before applying to the electrochemical cells. PMMA cuvettes (BRAND, 12.5mm x 12.5mm x 45mm) were used as electrochemical cells. The electrodes were prepared as 1mm strips and inserted in the cuvettes with Whatman filter paper as separator. 1mL electrolyte and equivalent hydrocarbon was supplied to the electrochemical cells. Custom-designed chambers were used to place the electrochemical cuvettes, exposing them to premixed gases at 1 atm.

An Ar-filled glovebox was used to store the electrodes, assemble the electrochemical cells, disassemble the cells for postmortem analysis and store samples. The neat electrolyte was used to conduct ^{27}Al-NMR. To separate the product hydrocarbons, 300µL of the hydrocarbon or electrolyte was dissolved in 5mL $CDCl_3$/5mL D_2O, mixed and centrifuged for 15min. The $CDCl_3$ layer was used to conduct DART-MS. 300µL of the $CDCl_3$ layer was dissolved in 1mL C_3D_6O to use for ^{1}H-NMR and GC-MS.

2.9.3 Electrochemical Experiments

Galvanostatic discharge experiments were conducted using a Neware CT-3008 battery testers at a fixed current density of 20mA/g_{Carbon}.

2.9.4 Gas Chromatography-Mass Spectrometry (GC-MS)

GC-MS was conducted using Agilent Technologies (Santa Clara, CA) 6890N gas chromatograph equipped with an Agilent 7683B autosampler and coupled to a JEOL (Peabody, MA) GCMate II double-focusing sector mass spectrometer. The injection volume was 1 µL. The split/splitless inlet was operated in split flow mode with 10:1 split ratio. Inlet temperature was maintained at 60°C. The oven program used was as follows: 60°C for 3 minutes; ramp to 120°C at 5°C/min; ramp to 270°C at 25°C/min; and a finally hold for 4 minutes for a total run time of 25 minutes. The GC column used was a DB-5 MS+DG capillary column (Agilent Technologies) with the dimensions 30m x 0.25mm ID, 0.25µm film thickness and a 10m DuraGuard guard column section. The MS was operated in positive ion mode at nominal resolving power of 500 (actual 670). Electron impact ionization was used with 70eV potential and 200mA filament current. Mass spectra were acquired from 35 to 500 m/z using a magnetic field sweep with 0.22s/scan and 0.1 s interscan delay to give 0.32s total scan duration. Data analysis was

performed using TSSPro 3.0 (Shrader Analytical and Consulting Laboratories Inc., Detroit, MI).

2.9.5 Residual Gas Analysis-Mass Spectrometry (RGA-MS)

RGA-MS was conducted using Extorr-XT200amu quadrupole residual gas analyzer (Extorr Inc., New Kensington, PA), measuring total gas and partial gases pressure up to 200amu. The RGA is equipped with a Pfeiffer turbo pump (Pfeiffer Vacuum Inc, Nashua, NH) to allow for sampling the gas of electrochemical chamber. The system was calibrated to the atmosphere before each run.

2.9.6 Direct Analysis in Real Time-High Resolution Mass Spectrometry (DART-MS)

DART high-resolution mass spectrometry analyses were carried out on a Thermo Scientific Exactive Orbitrap Mass Spec system operating at 100,000 resolution in positive mode. DART ion sources (IonSense, Saugus, MA) was operated with He gas at 350°C. MestReNova software (Mestrelab Research) was used to analyze the mass spec results and compare them to predicted spectra.

2.9.7 Nuclear Magnetic Resonance Spectroscopy (^{1}H and ^{27}Al NMR)

NMR was conducted using 500 MHz Bruker AVIII HD spectrometer equipped with a broadband Prodigy Cryoprobe and SampleXpress autosampler. Samples were prepared in acetone-d_6 and ^{1}H were referenced to residual acetone-d_5 at 2.07 ppm. ^{27}Al spectra were run neat without locking or shimming and were referenced to external aqueous $AlCl_3$ at 0 ppm. Spectra were acquired with probe-background suppression using the zgbs sequence provided in Bruker TopSpin 3.5 [28].

2.10 REFERENCES

1. Hayyan, M., Hashim, M. & AlNashef, I., Superoxide Ion: Generation and Chemical Implications. *Chem. Rev.* **116**, 3029-3085 (2016).
2. Heinrich, S., Plettig, M. & Klemm, E., Role of the Ti(IV)-Superoxide Species in the Selective Oxidation of Alkanes with Hydrogen Peroxide in the Gas Phase on Titanium Silicalite-1: An In Situ EPR Investigation. *Catal. Lett.* **141**, 251-258 (2011).
3. Lee-Ruff, E. & Timm, N., Superoxide mediated autoxidation of hydrocarbons. *J . Chem.* **58**, 2138-2141 (1980).
4. Iwamoto, M. & Lunsford, M., Surface Reactions of Oxygen Ions. 5. Oxidation of Alkanes and Alkenes by O_2^- on MgO. *J. Phys. Chem.* **84**, 3079-3084 (1980).
5. Peng, Z., Freunberger, S., Chen, Y. & Bruce, P., A Reversible and Higher-Rate Li-O_2 Battery. *Science* **337**, 563-566 (2012).
6. Das, S., Lau S. & Archer, L., Sodium–oxygen batteries: a new class of metal–air batteries. *J. Mater. Chem. A* **2**, 12623-12629 (2014).
7. Gelman, D., Shvartsev, B. & Ein-Eli,Y., Aluminum–air battery based on an ionic liquid electrolyte. *J. Mater. Chem. A* **2**, 20237-20242 (2014).
8. Muldoon, J., Bucur, C. & Gregory, T., Quest for Nonaqueous Multivalent Secondary Batteries: Magnesium and Beyond. *Chem. Rev.* **114**, 11683-11720 (2014).
9. Takechi, K., Shiga T. & Asaoka, T., A Li–O_2/CO_2 Battery. *Chem. Commun.* **47**, 3463-3465 (2011).
10. Liu, Y., Wang, R., Lyu, Y., Li, H. &, Chen, L., Rechargeable Li/CO_2–O_2 (2:1) Battery and Li/CO_2 Battery. *Energy Environ. Sci.* **7**, 677-681 (2014).
11. Xu, S., Das, S. & Archer, L., The Li–CO_2 Battery: A Novel Method for CO_2 Capture and Utilization. *RSC Advances* **3**, 6656-6660 (2013).

12. Das, S., Xu, S. & Archer, L., Carbon Dioxide Assist for Non-Aqueous Sodium–Oxygen Batteries. *Electrochemistry Communications* **27**, 59-62 (2013).
13. Xu, S., Lu, Y., Wang, Y., Abru˜na, H. & Archer, L., A Rechargeable Na–CO_2/O_2 Battery Enabled by Stable Nanoparticle Hybrid Electrolytes. *J. Mater. Chem. A* **2**, 17723-17729 (2014).
14. Al Sadat, W. & Archer, L., The O_2-assisted Al/CO_2 electrochemical cell: A system for CO_2 capture/conversion and electric power generation. *Sci. Adv.* **2**, e1600968 (2016).
15. Riemenschneider, W. & Tanifuji, M., Oxalic Acid *(Ullmann's Encyclopedia of Industrial Chemistry, Wiley-VCN, Weinheim, 2011)* chap **25**.
16. Mao, J., Steckel, J., Yan, F., Dhumal, N., Kimc, H. & Damodaran, K., Understanding the mechanism of CO_2 capture by 1,3 di-substituted imidazolium acetate based ionic liquids. *Phys. Chem. Chem. Phys.* **18**, 1911-1917 (2016).
17. Gurau, G., Rodriguez, H., Kelley, S., Janiczek, P., Kalb, R. & Rogers, R., Demonstration of Chemisorption of Carbon Dioxide in 1,3-Dialkylimidazolium Acetate Ionic Liquids. *Angew. Chem.* **123**, 12230-12232 (2011).
18. Jiang, P., Wu, X., Zhu, L., Ji, F., Li, J., Xia, T., Wang, T. & Li, Q., Production of jet fuel range paraffins by low temperature polymerization of gaseous light olefins using ionic liquid. *Energy Conversion and Management* **120**, 338-345 (2016).
19. Scordilis-Kelley, C., Fuller, J., Carlin, R. & Wilkes, J., Alkali Metal Reduction Potentials Measured in Chloroaluminate Ambient-Temperature Molten Salts. *J. Electrochem. Soc.* **139**, 694-699 (1992).
20. Auborn, J. & Barberio, Y., An Ambient Temperature Secondary Aluminum Electrode: Its Cycling Rates and Its Cycling Efficiencies. *J. Electrochem. Soc.* **132**, 598-601 (1985).

21. Dymek, C., Williams, J., Groeger, D. & Auborn, J., An Aluminum Acid-Base Concentration Cell Using Room Temperature Chloroaluminate Ionic Liquids. *J. Electrochem. Soc.* **131**, 2887-2892 (1984).
22. Westbrook, C., Pitz, W., Herbinet, O., Curran, H. & Silke, E., A comprehensive detailed chemical kinetic reaction mechanism for combustion of n-alkane hydrocarbons from n-octane to n-hexadecane. *Combustion and Flame* **156** 181-199 (2009).
23. Carl, Y., *Yaws' Thermophysical Properties of Chemicals and Hydrocarbons (Electronic Edition)*, Knovel, (2010).
24. Shilina, M., Bakharev, R. & Smirnov, V., Two Routes of Low-Temperature Conversion of Alkanes on Promoted Aluminum Chloride. *Doklady Physical Chemistry* **401,** 63-66 (2005).
25. Zinurov, D., Zinurov, R., Akhmed'yanova, R. & Liakumovich, A., Skeletal Isomerization of n-Pentane in the Presence of an $AlCl_3$-Based Ionic Liquid. *Petroleum Chemistry* **50**, 376-380 (2010).
26. Shah, N., Li, Z. & Ierapetritou, M., Petroleum Refining Operations: Key Issues, Advances, and Opportunities. *Ind. Eng. Chem. Res.* **50**, 1161-1170 (2011).
27. Alfke, G., Irion, W. & Neuwirth, O., Oil Refining *(Ullmann's Encyclopedia of Industrial Chemistry*, Wiley-VCN, Weinheim, 2012) vol. **25**.
28. Cory, D. & Ritchey, W., Suppression of Signals from the Probe in Bloch Decay Spectra. *J. Magn. Reson.* **80**, 128-132 (1988).

2.11 APPENDIX

Supporting Materials for Chapter 2

Residual Gas Analysis (RGA)-Mass Spectrometry (MS)

Mass spectrometry of the electrochemical cell's headspace was conducted using a Residual Gas Analyzer (RGA). RGA shows the presence of hydrocarbon fragments when n-decane is discharged in Al/O_2 with 2:1 ($EMImCl:AlCl_3$) electrolyte. Smiliar fragments were detected when n-decane is merely mixed with the electorlyte and exposed to O_2 for a duration similar to the dishcarge case. Some of the fragments orginate from n-decane in the headspace with m/z up to 85. Figure S2.1 presentes the mass spectrum results of the three cases.

To investigate the effect of electrochemically generated superoxide on the alkane, the difference between the discharged and mixed cases is ploted in Figure S2.2. Signals attributed to O_2 (32 and 16m/z) decrease dramatically while masses associated with hydrocarbons increase with dicharge. This indicates the consumption of O_2 and fragmentation of n-decane as the electochemical cell is discharged. The mass spectra indicate the generation of hydrocarbons from butane to methane.

Partial pressure of the detected hydrcarbons were used to determine the yield. Fragmentation patterns (from NIST database) were used to avoid double counting of fragments and relative sensitivity were taken into account [1]. No considerable CO_2 signal (44m/z) is detected after discharge. In the presence of hydrocarbons, HCl is generated from the electrolyte, indicated by fractions at 38, 37, 36 and 35 m/z.

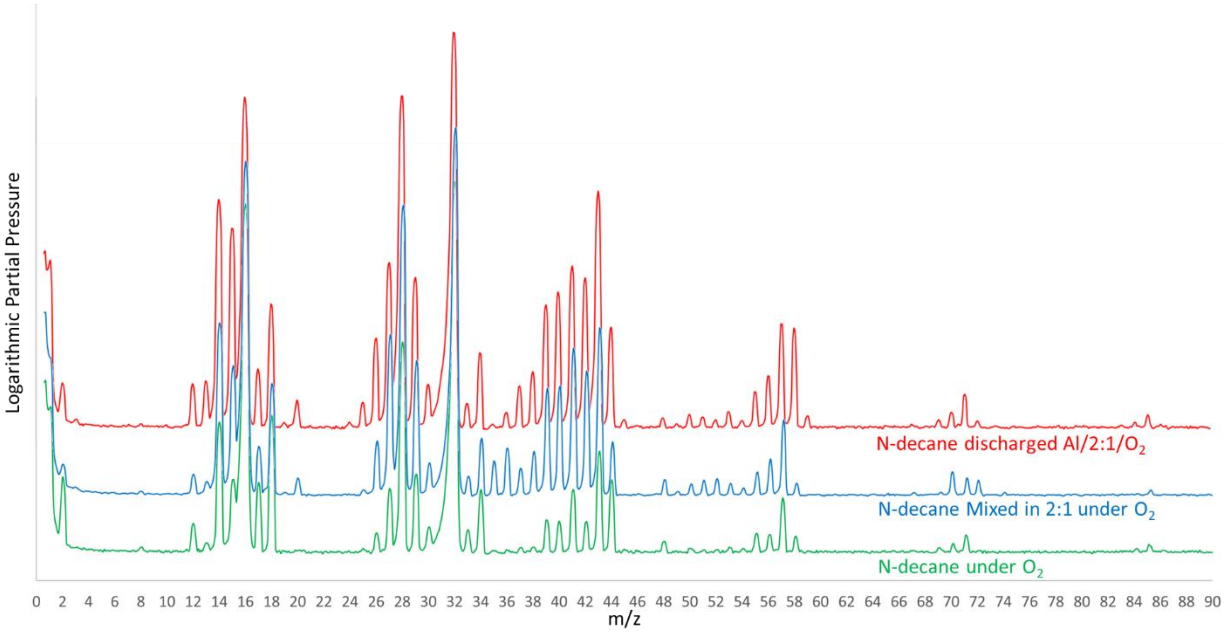

Figure S2.1: RGA-MS of electrochemical cell headspace. The spectra are for n-decane discharged under O_2, n-decane mixed with 2:1 ($AlCl_3$:EMImCl) electrolyte under O_2 and n-decane without the electolyte. Logarithmic scale was use to account for the large intensity difference between O_2 and hydrocarbons.

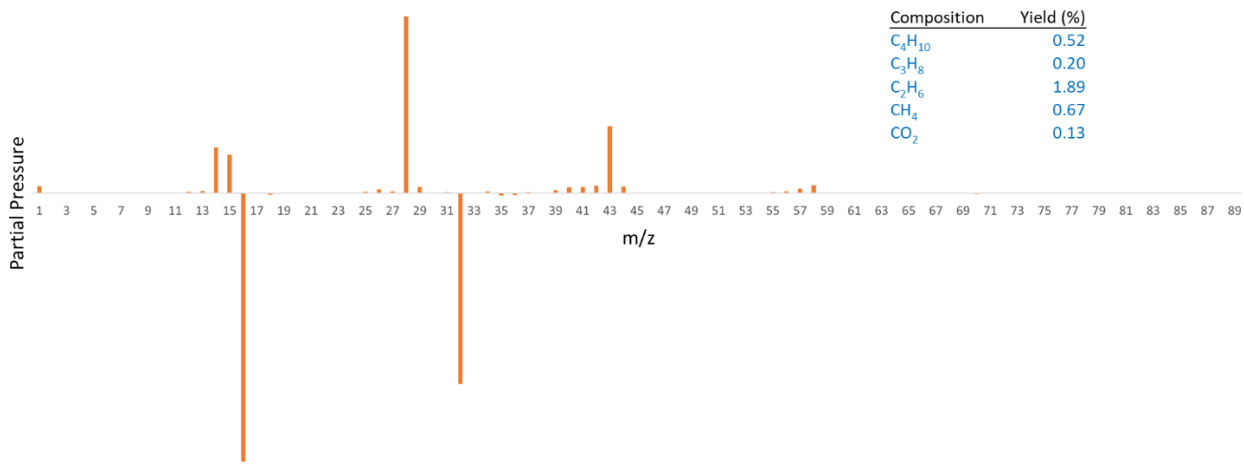

Figure S2.2: RGA-MS difference of the electochemical cell's headspace. The spectra shows the difference between the Al/O_2 cell discharged with n-decane and only mixed with n-decane. The electrolyte is based on 2:1 ($AlCl_3$:EMImCl). The inset lists the yields of the main components generated when Al/O_2 electochmical cell is disharged.

Gas Chromatography (GC)-Mass Spectrometry (MS)

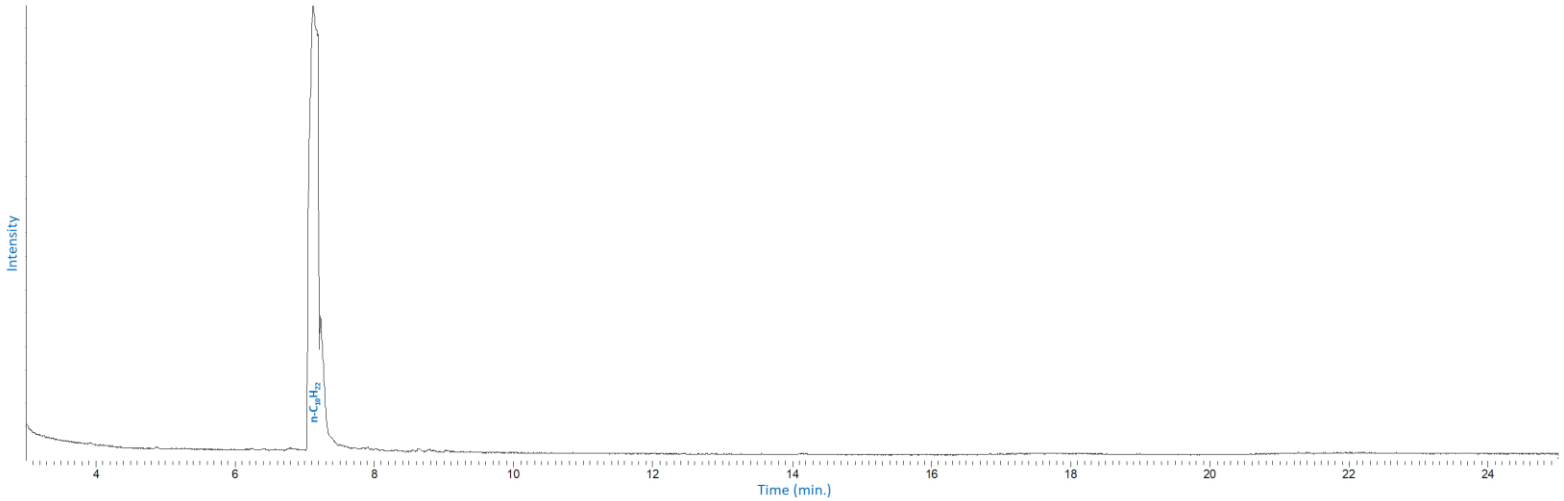

Figure S2.3: GC-MS Total Ion Count (TIC) chromatogram of top n-decane layer. N-decane was mixed with 1:2.3 ($AlCl_3$:EMImCl) electrolyte and exposed to O_2. Only n-decane was detected with no indication for fractionation, isomerization, branching or up-conversion.

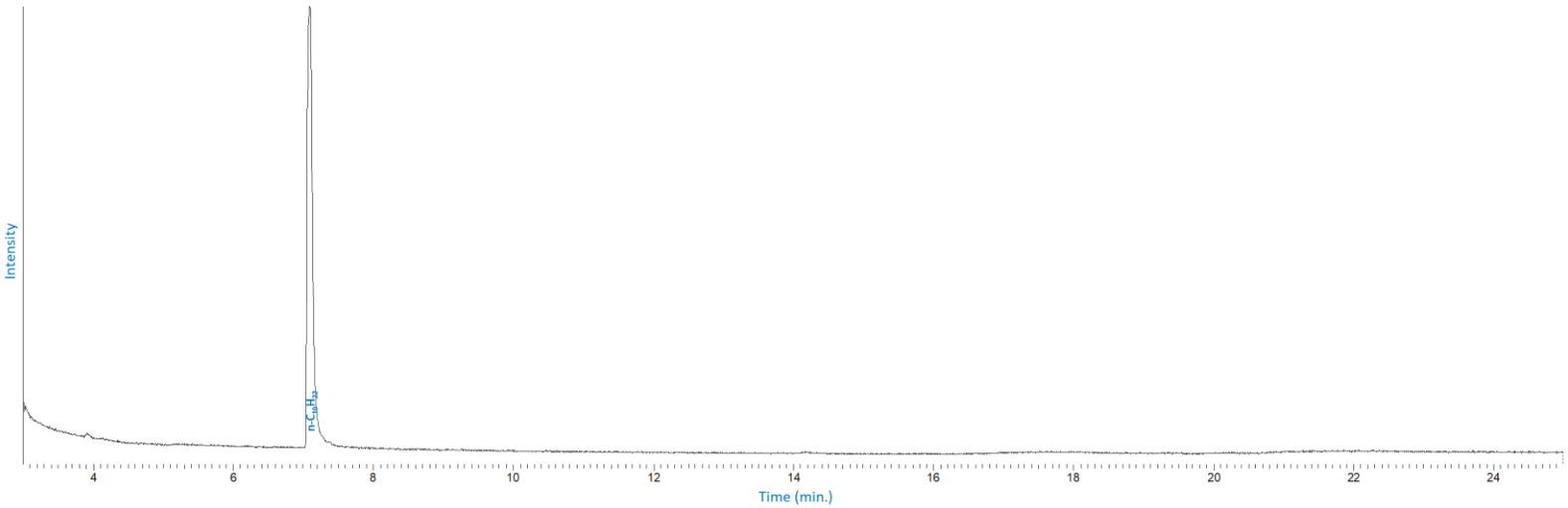

Figure S2.4: GC-MS TIC of bottom 1:2.3 ($AlCl_3$:EMImCl) electrolyte layer. The electrolyte was mixed with n-decane and exposed to O_2. Only n-decane was detected with no indication for fractionation, isomerization, branching or up-conversion.

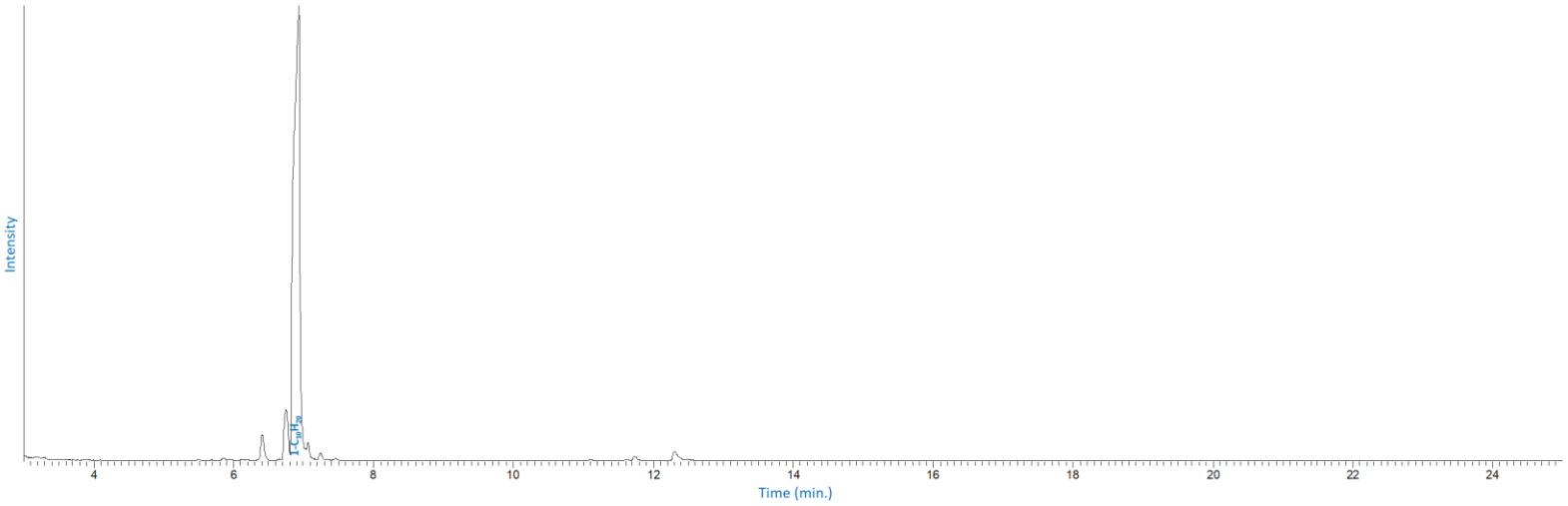

Figure S2.5: GC-MS TIC of top 1-decene layer. 1-decene was mixed with 1:2.3 ($AlCl_3$:EMImCl) electrolyte and exposed to O_2. No indication of conversion or hydrogenation.

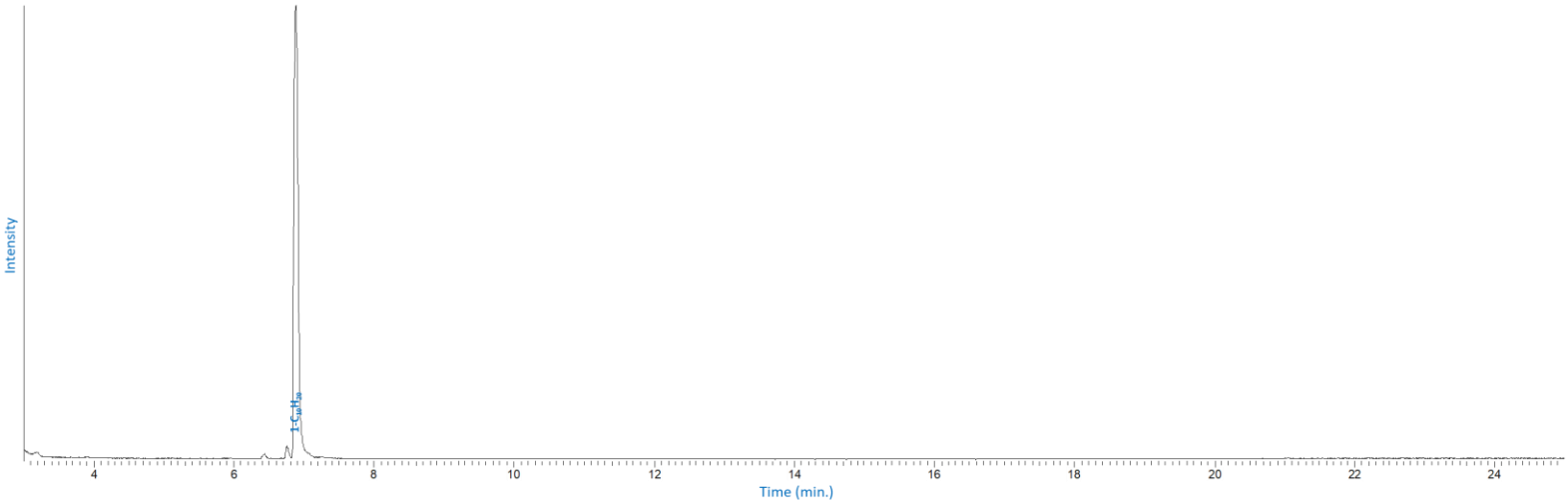

Figure S2.6: GC-MS TIC of bottom 1:2.3 ($AlCl_3$:EMImCl) electrolyte layer. The electrolyte was mixed with 1-decene and exposed to O_2. No indication of conversion or hydrogenation.

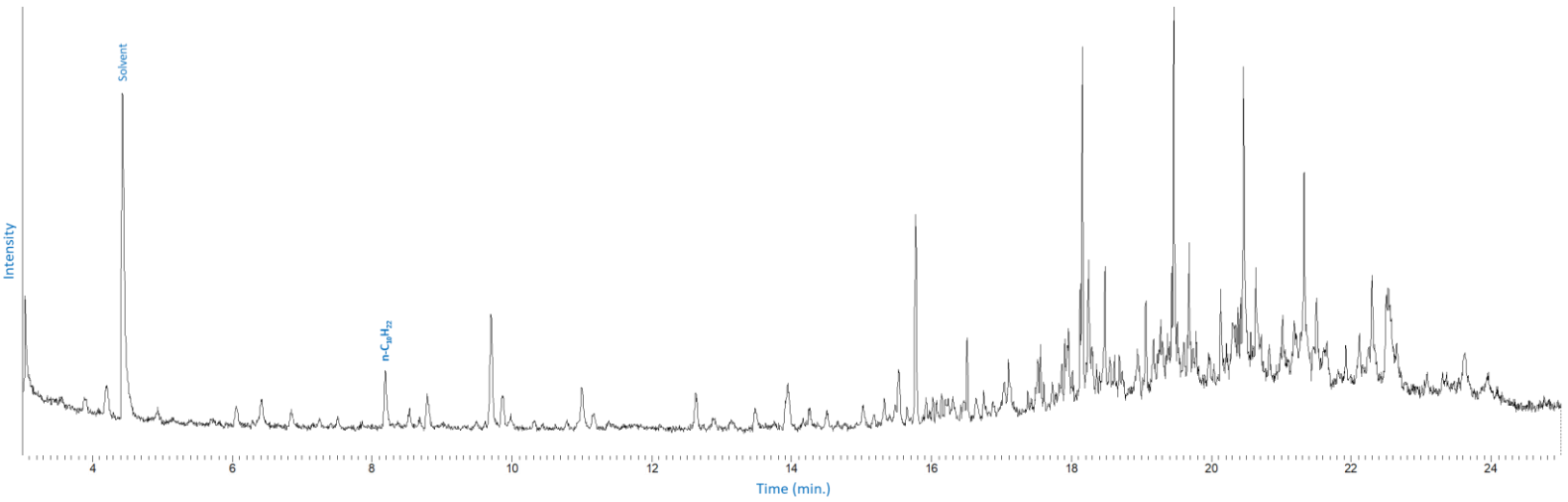

Figure S2.7: GC-MS TIC of n-decane discharged in an Al/80%CO_2 cell. The hydrocarbon was discharged using 2:1 ($AlCl_3$:EMImCl) electrolyte. The spectrum is identical to the Al/O_2 case.

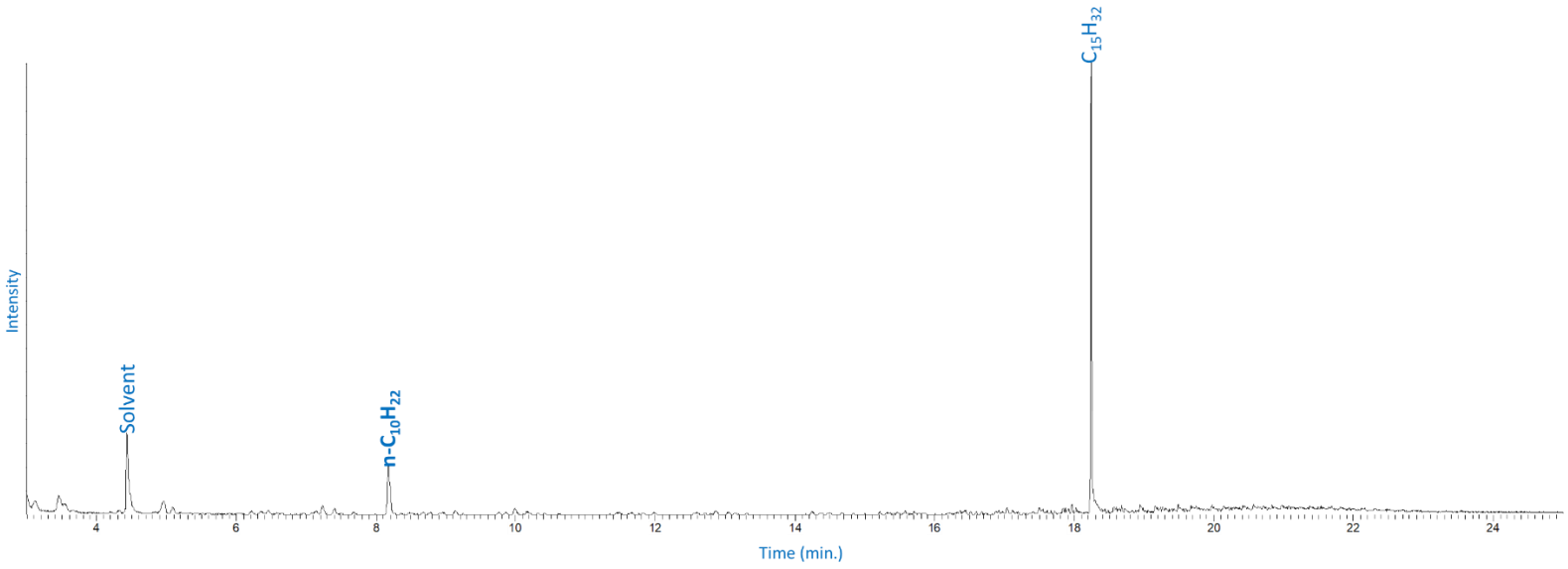

Figure S2.8: GC-MS TIC of 1-decene discharged in an Al/80%CO_2 cell. The hydrocarbon was discharged using 2:1 ($AlCl_3$:EMImCl) electrolyte. The spectrum is identical to the Al/O_2 case.

Direct Analysis in Real Time (DART)-Mass Spectrometry (MS)

DART-MS allows the ionization of different species in their original phase state, without the need for special separation or solvation requirements [2]. Complexity of the technique, however, is due to the strong signal of the ion source gas interacting and ionizing atmospheric species. Those active species can go on to interact with the sample and any solvents, if present. With no chromatography, the mass spectrum shows all ionized species. Sample species can be detected as directly ionized or fragmented with or without complexing with the background and solvent species. Particularly for hydrocarbons, DART ion source can cause the ionization of the main species (soft ionization) or fragmentation depending on the many parameters including ionizing gas temperature, interaction with solvent, and background species.

DART-MS has been reported to ionize atmospheric molecules to produce many ion species including NO^+, O_2^+ , H_2O^+, $(H_2O)_2^+$ and H_3O^+, which interact with the sample species to ionize or form ion complexes [3]. When ionizing alkanes [2, 4], the reported detected species included $[C_nH_{2n+2}]^+$, C_nH_{2n+2} $-H]^+$, $[C_nH_{2n+2}$ $-H$ $+O]^+$, $[C_nH_{2n+2}$ $-3H$ $+O]^+$, $[C_nH_{2n+2}$ $-H$ $+2O]^+$, $[C_nH_{2n+2}$ $-3H$ $+2O]^+$ and $[C_nH_{2n+2}$ $-H$ $+3O]^+$. Additionally, fragments of the alkane were detected as $C_nH_{2n+1}^+$, and $C_nH_{2n-1}^+$ ions. For example, when the ionizing gas temperature increased above 300°C, the $[C_nH_{2n+2}]^+$ ion of n-hexadecane accounted for only 20% intensity while fragmented ions dominated the results. Other studies reported interaction with other atmospheric ionized species including $+NO_2$, $+CO_3$, $+HCO_3$ and $+HCO_4$ [5].

Here, DART-MS was conducted for separated hydrocarbons after mixing with 2:1 ($AlCl_3$:EMImCl) electrolyte and after discharge. The results were in agreement with the GC-MS tests. The dominating saturated hydrocarbon species were detected as

$[C_nH_{2n+2}]^+$ ions and variations of $[C_nH_{2n+2} –(1 \text{ to } 4)H +(0 \text{ to}1)N +(0 \text{ to } 2)O]^+$. Some the saturated hydrocarbon species were detected interacting with imidazolium-based ionic liquid. The unsaturated hydrocarbons, however, were mainly detected as a distribution of $[C_nH_{2n-4} +H]^+$ to $[C_nHD_{(2n-3)} +H]^+$ species due to protonium/deuterium (H/D) exchange between deuterated solvents and unsaturated compounds. However, the complete H/D exchange was not detected for large compounds, potentially due to the low concentration of such species in the mixture. Similar H/D exchange was reported for alkenes but not alkanes [6]. Some of the unsaturated hydrocarbon species were also detected as $[C_nH_{2n-4} -H +2O]^+$.

After mixing n-decane with 2:1 ($AlCl_3$:EMImCl) electrolyte, DART-MS was conducted on the top hydrocarbon layer as demonstrated in Figure S2.9. The detected species are attributed mainly to $C_{10}H_{22}$ and associated fragments. The bottom layer, however, showed a different spectra, where the unsaturated species dominated (Figure S2.10). After discharge in an Al/O_2 electrochemical system, the DART-MS results changed dramatically (Figure S2.11) from the mixed cases. The distribution of detected species is spread to larger hydrocarbons, up to C_{24}. The unsaturated hydrocarbons are detected but to much lower intensities compared to the only mixed case. The dominating species are associated with saturated hydrocarbons, larger than the starting n-decane.

DART-MS was also conducted on hydrocarbons separated from Al/2:1($AlCl_3$:EMImCl)/80%CO_2 (denoting 80%CO_2 and 20%O_2 discharge gas mixture) cell, where the hydrocarbon/electrolyte interaction was limited using a capillary inside the electrochemical cuvette. When discharging n-decane, a distribution of species was detected in addition to ions that incorporate the carboxylic group (Figure S2.12). Discharging 1-decene shows the same pattern but the carboxylic-containing

hydrocarbons were detected at larger molecular weights (Figure S2.13), corroborating the GC-MS tests.

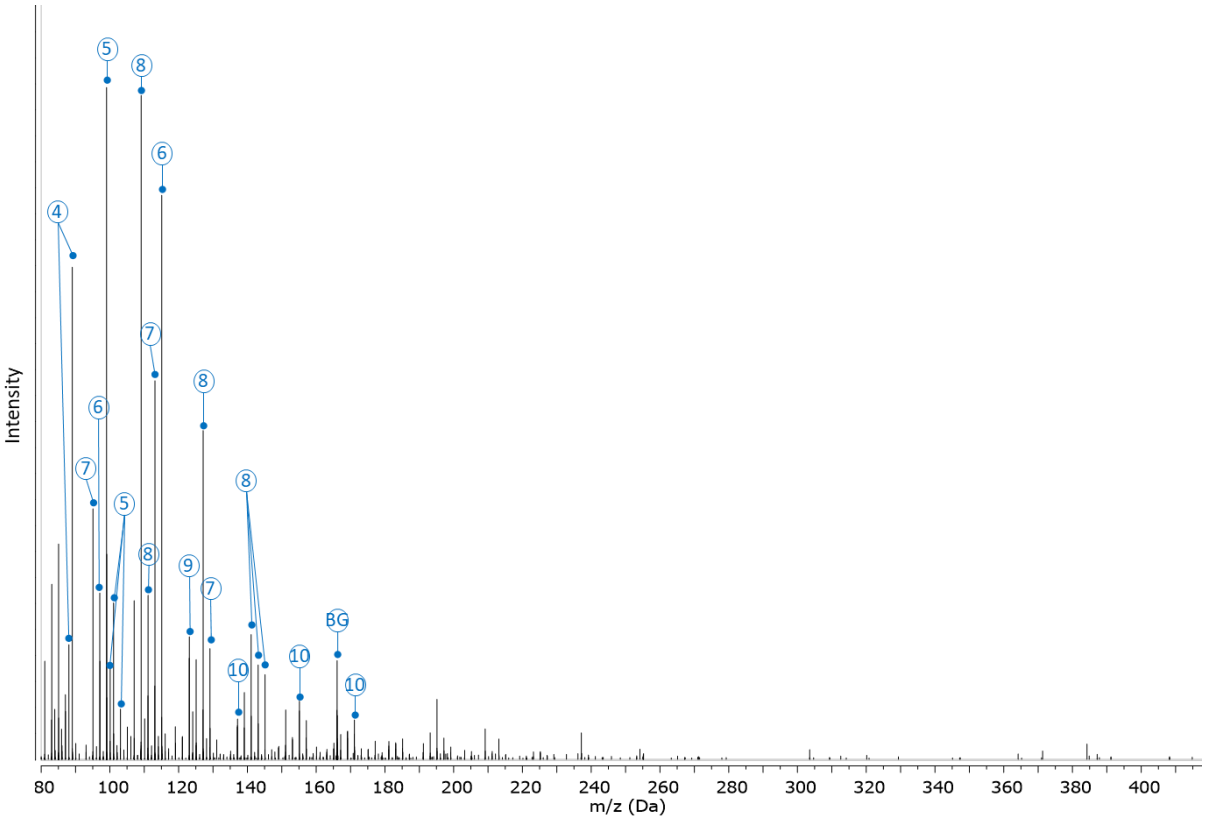

Figure S2.9: Positive-ion DART-MS spectra of top n-decane layer. The hydrocarbon was mixed with 2:1 ($AlCl_3$:EMImCl) electrolyte without discharge. The circled numbers refer to number of carbon atoms in an alkane.

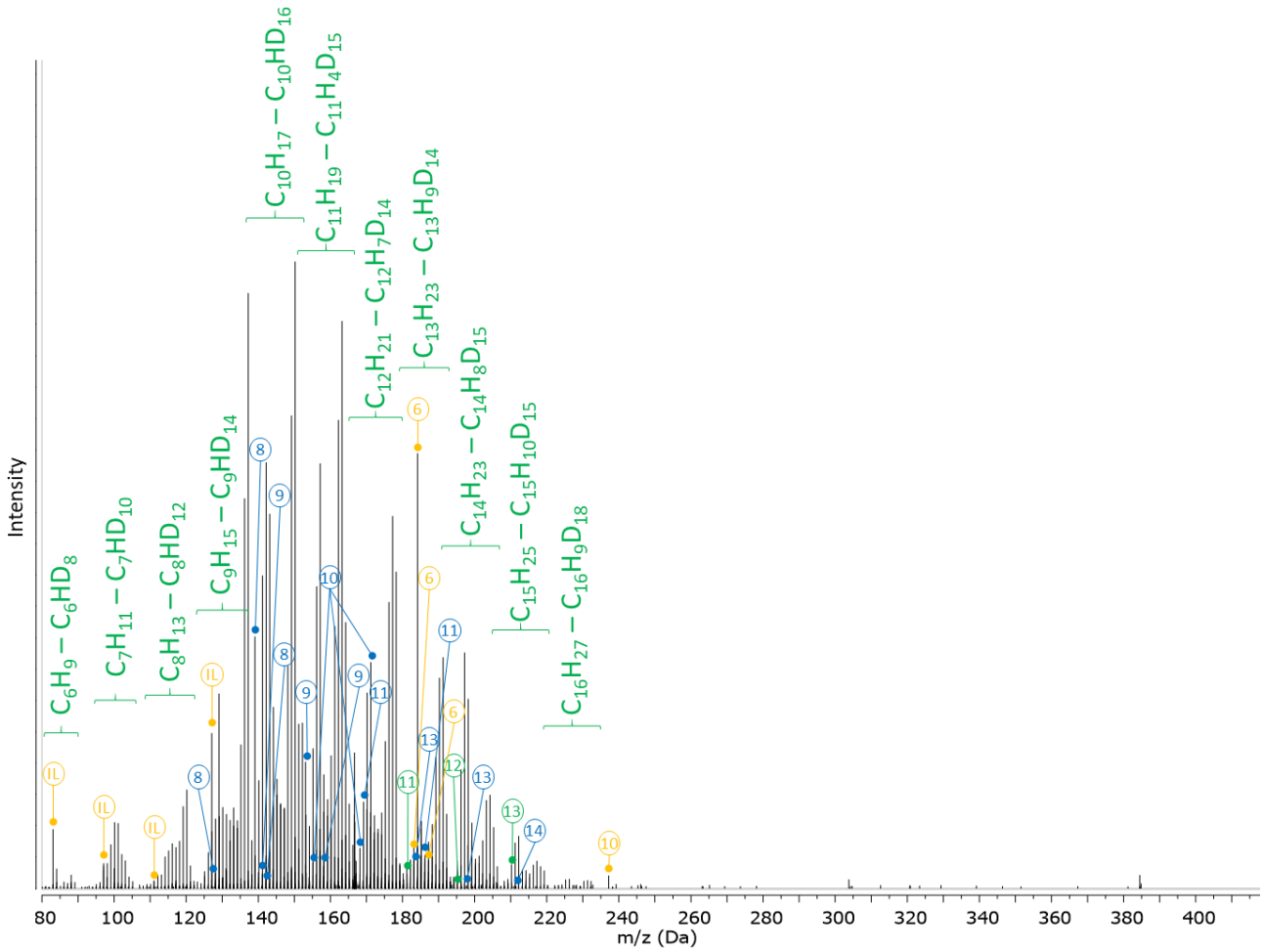

Figure S2.10: Positive-ion DART-MS spectra of bottom 2:1 ($AlCl_3$:EMImCl) electrolyte layer. The electrolyte was mixed with n-decane under O_2. The circled numbers refer to number of carbon atoms in the hydrocarbon. Blue, green and yellow refer to saturated, unsaturated and ionic liquid (IL)-associated species.

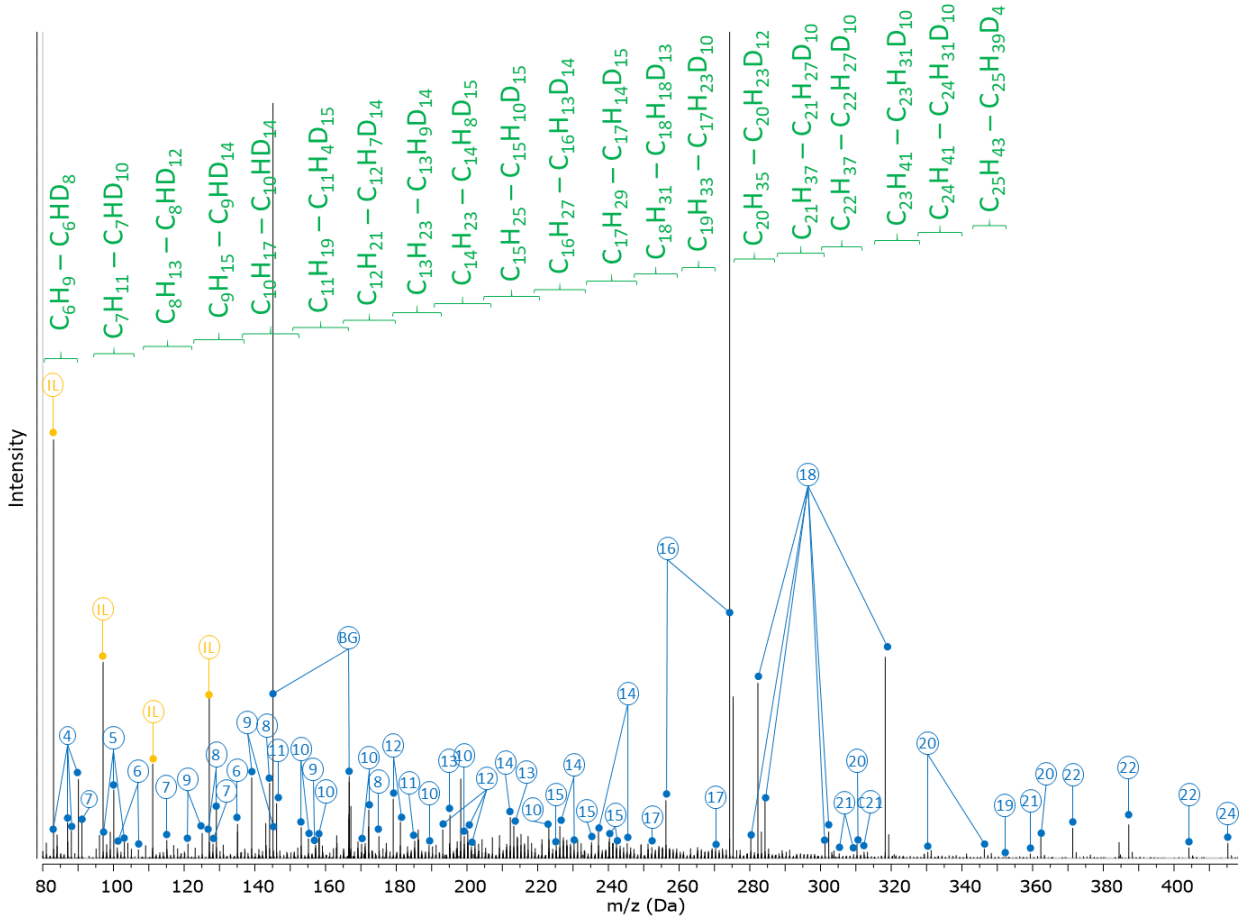

Figure S2.11: Positive-ion DART-MS spectra of discharged n-decane in an Al/O_2 cell. The electrolyte is based on 2:1 ($AlCl_3$:EMImCl). The circled numbers refer to number of carbon atoms in the hydrocarbon. Blue, green and yellow refer to saturated, unsaturated and ionic liquid (IL)-associated species.

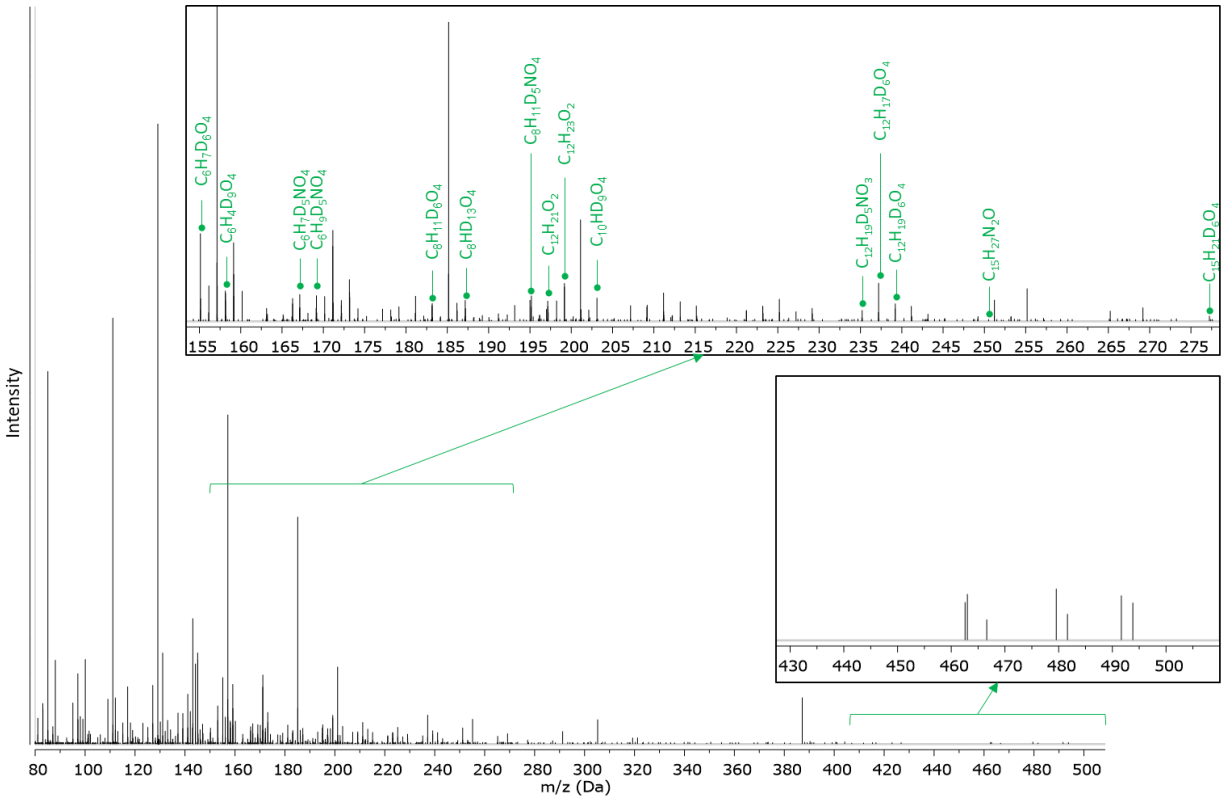

Figure S2.12: Positive-ion DART-MS spectra of discharged n-decane in an Al/80%CO_2 cell. The electrolyte is based on 2:1 ($AlCl_3$:EMImCl). Inset spectra show zoomed-in spectra and detected carboxylic-containing species.

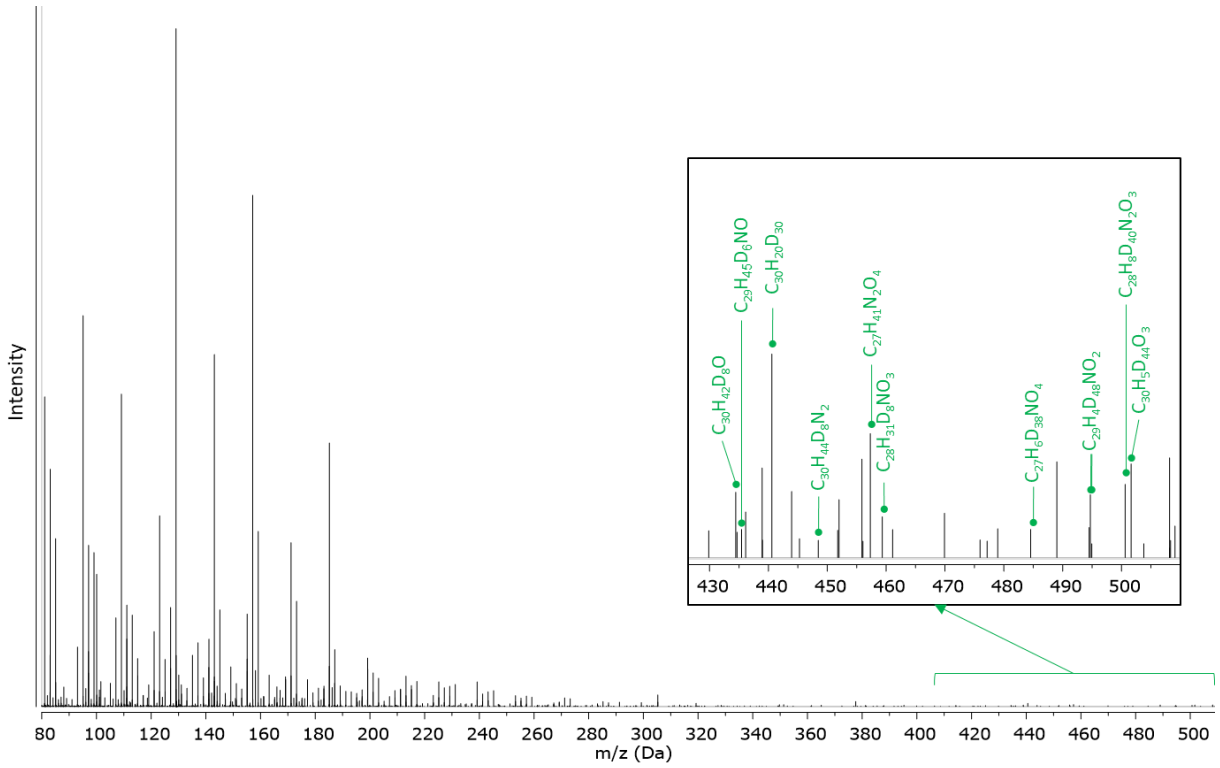

Figure S2.13: Positive-ion DART-MS spectra of discharged 1-decene in an Al/80%CO_2 cell. The electrolyte is based on 2:1 ($AlCl_3$:EMImCl). Inset spectra show zoomed-in spectra and detected carboxylic-containing species.

Proton Nuclear Magnetic Resonance (^{1}H-NMR) Spectroscopy

^{1}H-NMR was conducted to investigate the change in hydrocarbons as they interact/complex with electrolyte or superoxide during electrochemical discharge. When mixing n-decane with 2:1 ($AlCl_3$:EMImCl) electrolyte, the top hydrocarbon layer shows sharp peaks associated with methyl and methylene protons, which is in agreement with the GC-MS results of a dominating n-decane presence. ^{1}H-NMR (Figure S2.14) shows the dominance of methyl (0.8-1.2ppm), methylene (1.2- 1.8ppm) and methine (1.2-1.8ppm) protons. Hydrocarbons isolated from the electrolyte, whether discharged or just mixed with the electrolyte, show the protons associated with methyl, methylene and methine covering a wide distribution of chemical shifts, indicating a distribution of chemical structures. The ratio of methylene and methine to methyl protons for the three samples is smaller than the calculated value for n-decane (2.7), which indicates a high degree of isomerization. Uniquely, hydrocarbons isolated from the discharged electrolyte in an Al/2:1($AlCl_3$:EMImCl)/O_2 cell shows the presence of aromatic protons (7.1-7.5ppm). Alkenes (RC=C**H**R and $\mathbf{H_2}$C=CR_2) were detected in hydrocarbons isolated form the electrolyte discharged or only mixed with n-decane (4.5-7.0ppm). Ketones (R(C=O)C$\mathbf{H_3}$, R(C=O)C$\mathbf{H_2}$R) were also detected in hydrocarbons isolated form the electrolyte (2.1-2.75ppm). The typically broad O**H** peak was not detected due to H/D exchange, diminishing the peak. However, peaks at 3.7 and 3.8ppm could be associated with methylene groups adjacent to the hydroxyl (HOC$\mathbf{H_2}$R), confirming the small presence of alcohols.

When mixing 2:1 ($AlCl_3$:EMImCl) electrolyte with 1-decene, the signal associated or affected by the alkene disappear as presented in Figure S2.15. The ratio of methylene and methine to methyl protons for 1-decene discharged in an Al/2:1($AlCl_3$:EMImCl)/O_2 cell was 1.4, indicating high isomerization. When changing to the basic electrolyte 1:2.3

($AlCl_3$:EMImCl), hydrocarbons did not show any change from the starting alkane (Figure S2.16) or alkene (Figure S2.17). The ratio of methylene and methine to methyl protons depict the theoretically calculated for n-decane and 1-decene for the respective cases.

To isolate the effect of superoxide on the hydrocarbons, K_2O and Dicyclohexano-18-Crown-6 were mixed with n-decane and 1-decene (Figure S2.18). No discernable change was detected to the starting hydrocarbon. GC-MS showed that the introduction of chemically generated superoxide resulted in the conversion of only 3.86% of 1-decene to longer chains. Since the signal of methylene and methine groups dominate in the alkene it is difficult to detect the small increase of such groups.

Investigating the discharge of CO_2 and hydrocarbons in an Al/2:1($AlCl_3$:EMImCl)/O_2 electrochemical cell demonstrated the incorporation of CO_2 only if the hydrocarbon has limited exposure to the electrolyte (Figure S2.19). When discharging n-decane or 1-decene in an Al/2:1($AlCl_3$:EMImCl)/80%CO_2 cell with limited exposure to the electrolyte, the main proton peaks were also associated with methyl, methylene and methine groups. The ratio of methylene and methine to methyl was 1.1, for both n-decane and 1-decene. Alkenes, ketones and alcohols were detected as was the case n-decane discharged in Al/2:1($AlCl_3$:EMImCl)/O_2.

In the case of n-decane discharged with a limited exposure in an Al/2:1($AlCl_3$:EMImCl)/80%CO_2 cell, protons associated with aromatics and multiaromatic compounds were detected between 7.3 and 7.8ppm. A strong sharp signal was detected at 4.1ppm associated with R(C=O)OC$\mathbf{H_2}$R. Weak signals were detected between 3.2 and 3.7ppm attributed to RO(O=C)C$\mathbf{H_2}$R. The strong/sharp 9.47ppm was

only detected when an alkane is discharged in an Al/2:1($AlCl_3$:EMImCl)/80%CO_2 cell with limited exposure to the electrolyte. The peak is associated with R(C=O)**H** proton. The combination of such proton signals indicates the incorporation of CO_2 in the form of esters and formates. However, there was no indication of carboxylic acids formation considering that the typically wide peak associated with carbolic acid protons (**H**O(O=C)R, 10-13ppm) is not detected. A weak signal was detected between 4.5 and 7.0ppm showing the small presence of R**H**C=CR_2 and R_2C=C$\mathbf{H_2}$ protons.

In the case of 1-decene discharged with a limited exposure in an Al/2:1($AlCl_3$:EMImCl)/80%CO_2 cell, the strong signal associated with R**H**C=CR_2 and R_2C=C$\mathbf{H_2}$ protons disappear as the alkene interacts with the electrolyte. Peaks detected at 3.7, 4.1 and 4.6ppm could be attributed to R(CO=)OC$\mathbf{H_2}$R and at 3.2ppm attributed to RO(O=C)C$\mathbf{H_2}$R. When starting with an alkene, CO_2 was incorporated in the form of esters but not formates or carboxylic acids.

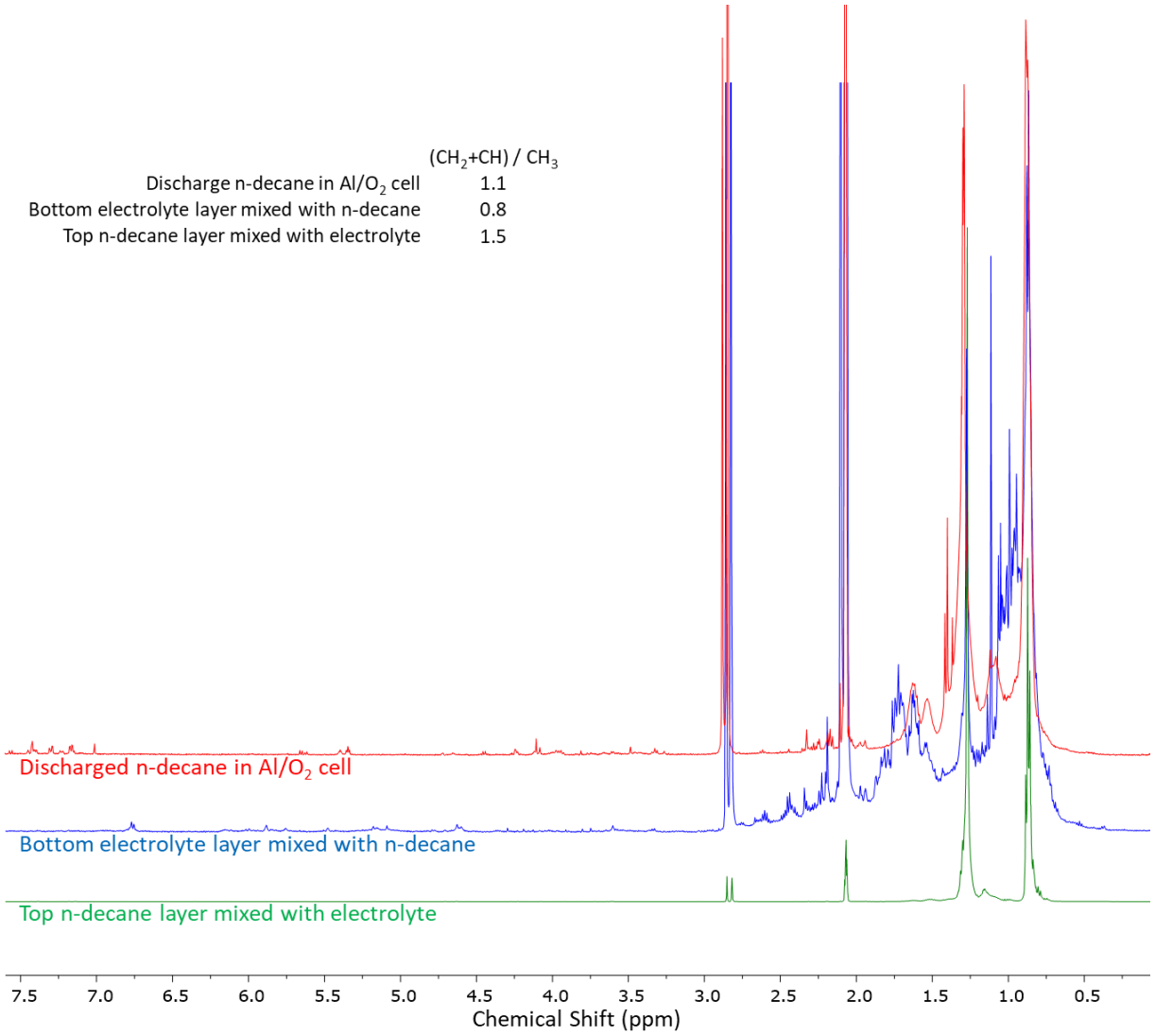

Figure S2.14: ^{1}H-NMR of 2:1 ($AlCl_3$:EMImCl) electrolyte with n-decane. The spectra are for the electrolyte discharged with n-decane in an Al/O_2 cell and of top and bottom layers of mixed n-decane and electrolyte exposed to O_2. The signal at 2.05 and 2.84ppm are associated with acetone and water solvents, respectively. The inset table lists the ratio of methylene and methine to methyl protons.

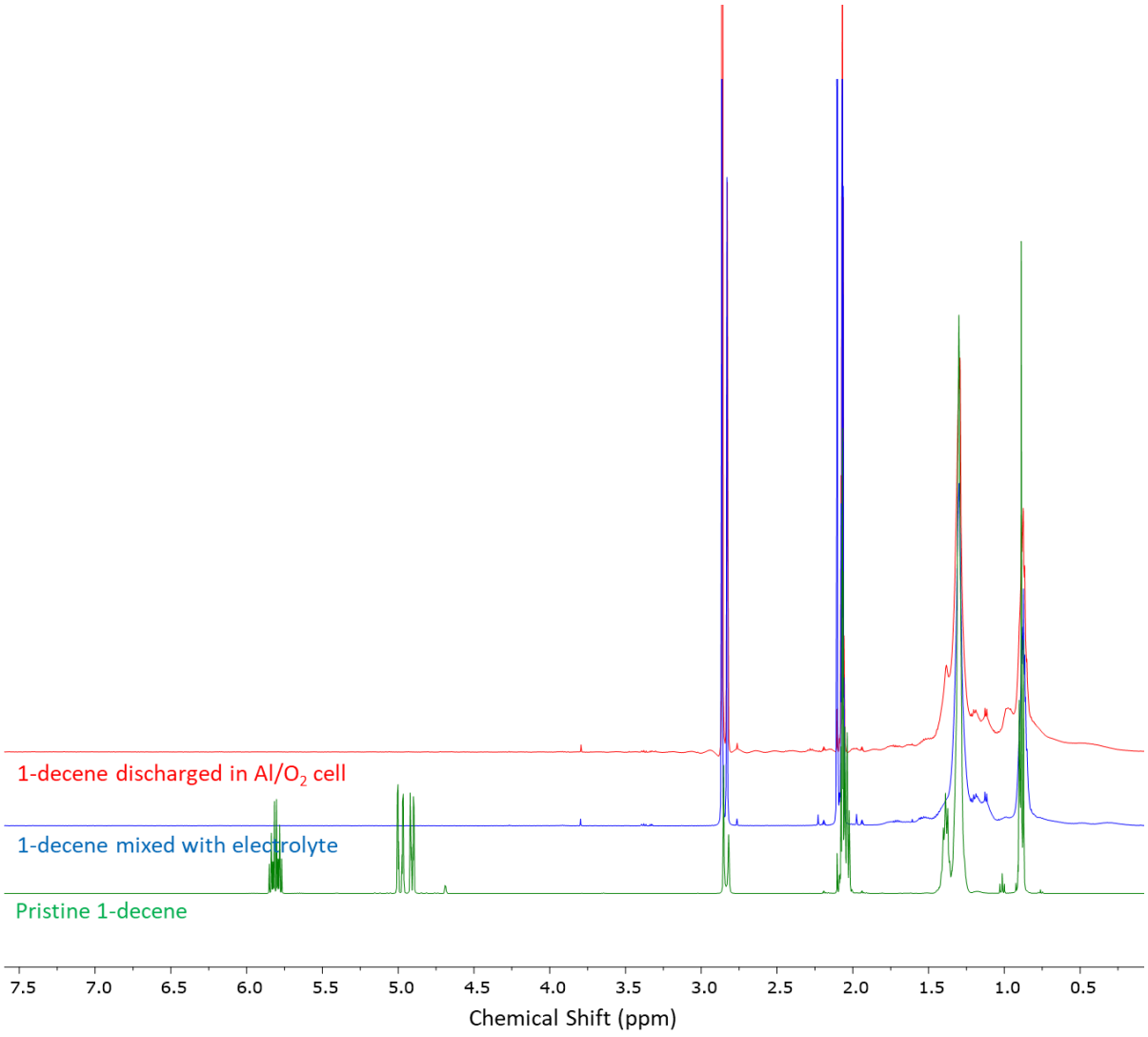

Figure S2.15: ^{1}H-NMR of 1-decene and 2:1 ($AlCl_3$:EMImCl) electrolyte. The spectra are for 1-decene mixed and mixed/discharged with 2:1 ($AlCl_3$:EMImCl) electrolyte in an Al/O_2 cell. The signal at 2.05 and 2.84ppm are associated with acetone and water solvents, respectively.

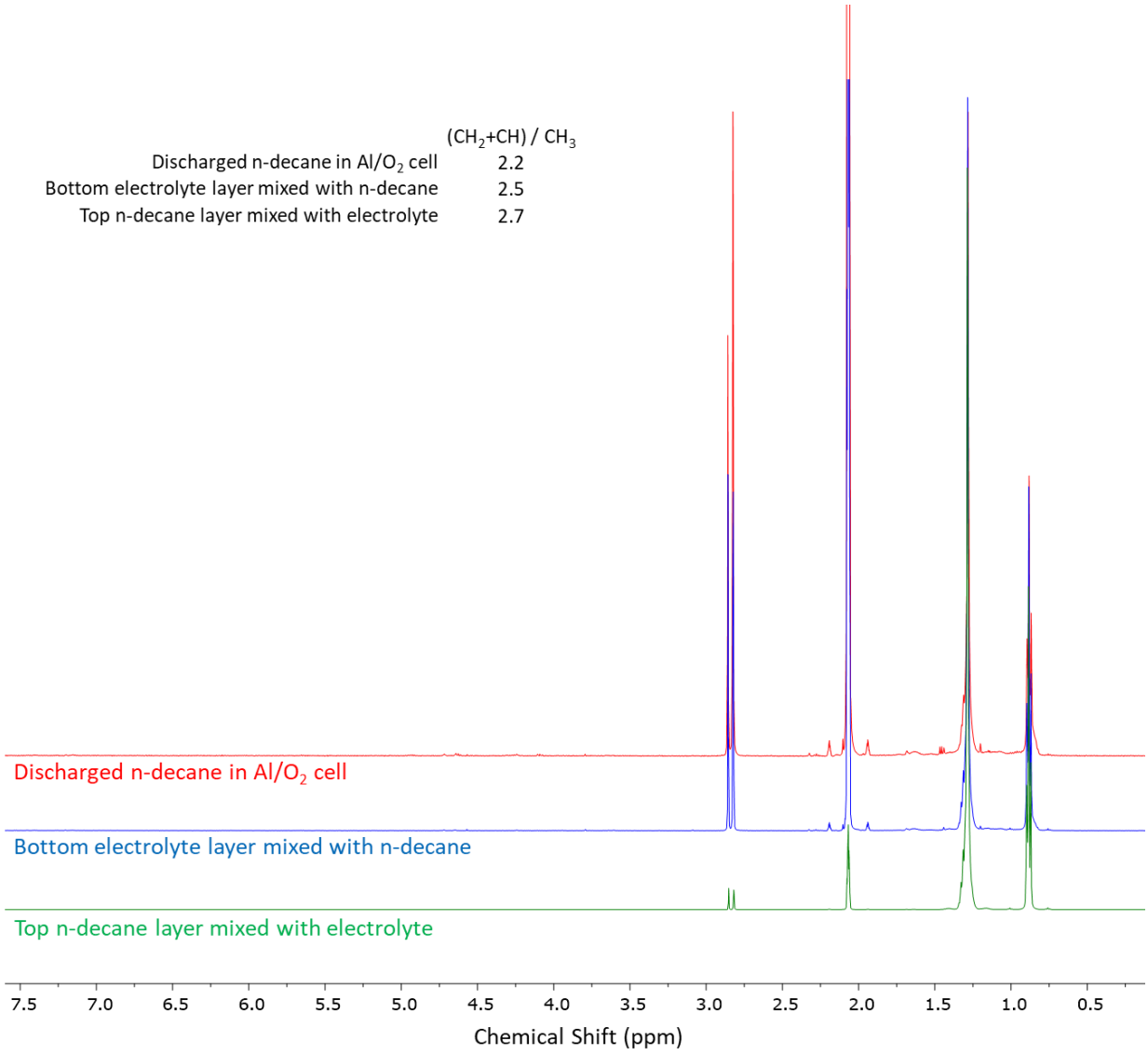

Figure S2.16: ^{1}H-NMR of 1:2.3 ($AlCl_3$:EMImCl) electrolyte and n-decane. The spectra are for the electrolyte discharged with n-decane in an Al/O_2 cell and of top and bottom layers of mixed n-decane and electrolyte exposed to O_2. The signal at 2.05 and 2.84ppm are associated with acetone and water solvents, respectively. The inset table lists the ratio of methylene and methine to methyl protons.

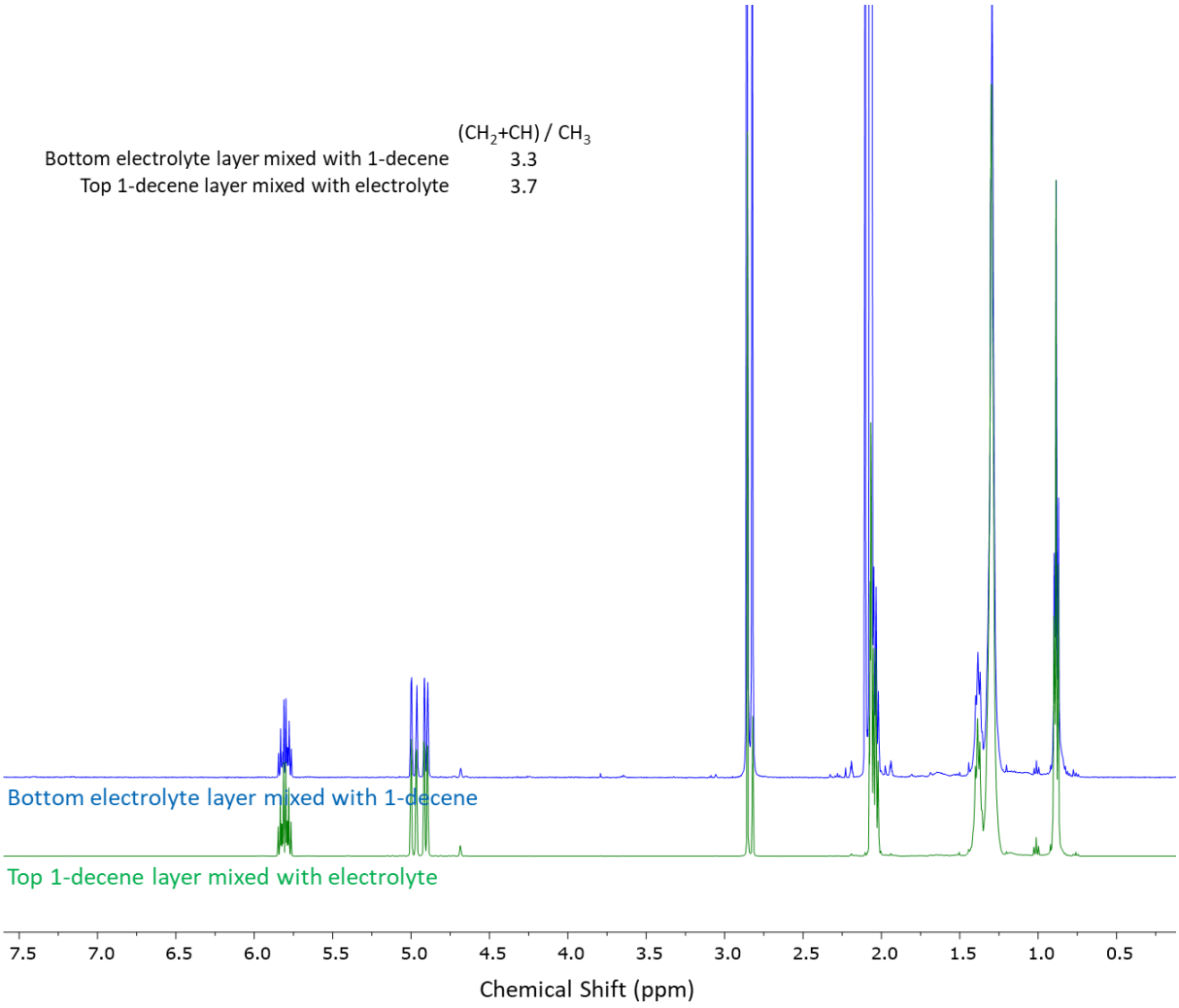

Figure S2.17: ^{1}H-NMR of 1-decene and 1:2.3 ($AlCl_3$:EMImCl) electrolyte. The spectra are for 1-decene mixed and mixed/discharged with the electrolyte in an Al/O_2 cell. The signal at 2.05 and 2.84ppm are associated with acetone and water solvents, respectively. The inset table lists the ratio of methylene and methine to methyl protons.

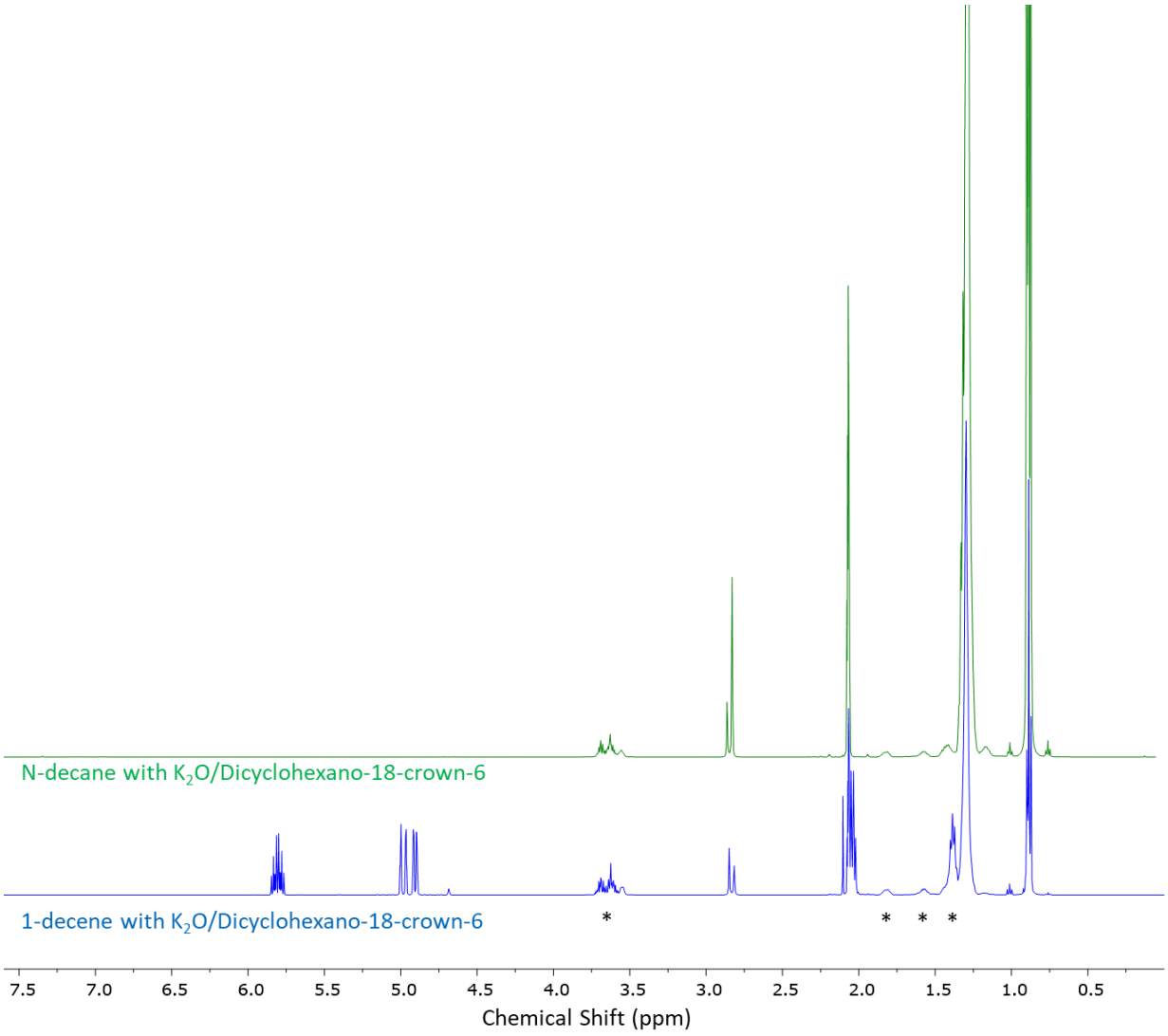

Figure S2.18: ^{1}H-NMR for chemically produced superoxide with hydrocarbons. The spectra are for n-decane and 1-decene with chemically generated superoxide using K_2O and Dicyclohexano-18-crown-16. The signal at 2.05 and 2.84ppm are associated with acetone and water solvents, respectively. * corresponds to protons associated with Dicyclohexano-18-Crown-6.

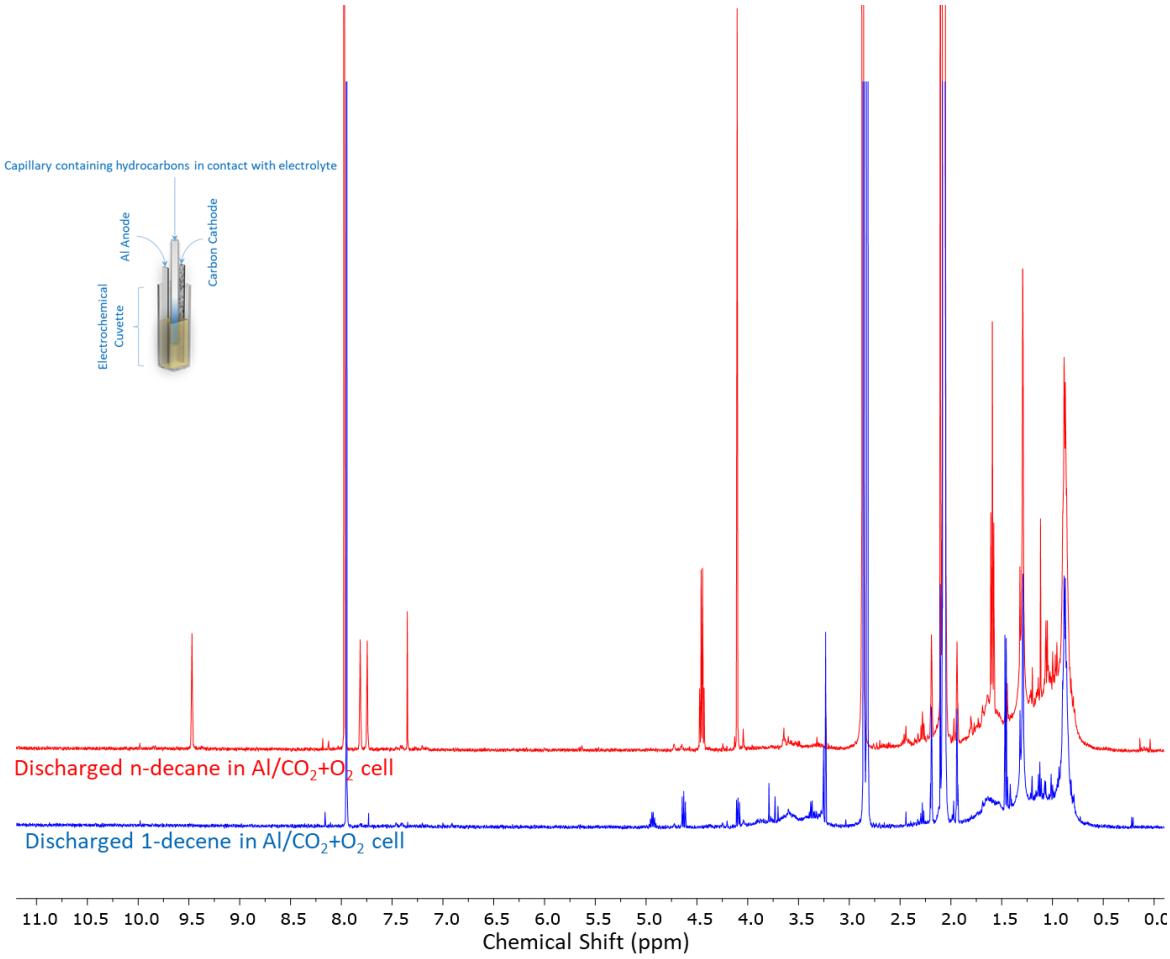

Figure S2.19: ^{1}H-NMR of Al/O_2+CO_2 (80%CO_2) cell. The spectra are for 2:1 ($AlCl_3$:EMImCl) electrolyte discharged with n-decane and 1-decene in an Al/O_2+CO_2 (80%CO_2) cell. The inset shows the hydrocarbon introduced inside a capillary in the electrochemical cell. The signal at 2.05, 2.84 and 7.6ppm are associated with acetone, water and chloroform solvents, respectively.

Aluminum Nuclear Magnetic Resonance (^{27}Al-NMR) Spectroscopy

^{27}Al-NMR was conducted to study the interaction between the n-decane with the present aluminum chloride species (Figure S2.20). The pristine 2:1 ($AlCl_3$:EMImCl) electrolyte demonstrated the presence of a single broad peak at 103ppm, as expected for the only $Al_2Cl_7^-$ specie [7-8]. Mixing with n-decane changed the spectra to reveal two Al environments for the $AlCl_4^-$ (98ppm) and an aluminum chloride/hydrocarbon complex (104ppm). Similar interaction has been reported for unsaturated hydrocarbons with an acidic triethylamine hydrochloride/$AlCl_3$ melt [9]. After discharge in an Al/O_2 electrochemical cell, the broad 103ppm peak dominates again while the sharper 98ppm peak persists, indicating the conversion of aluminum chloride/hydrocarbon complex.

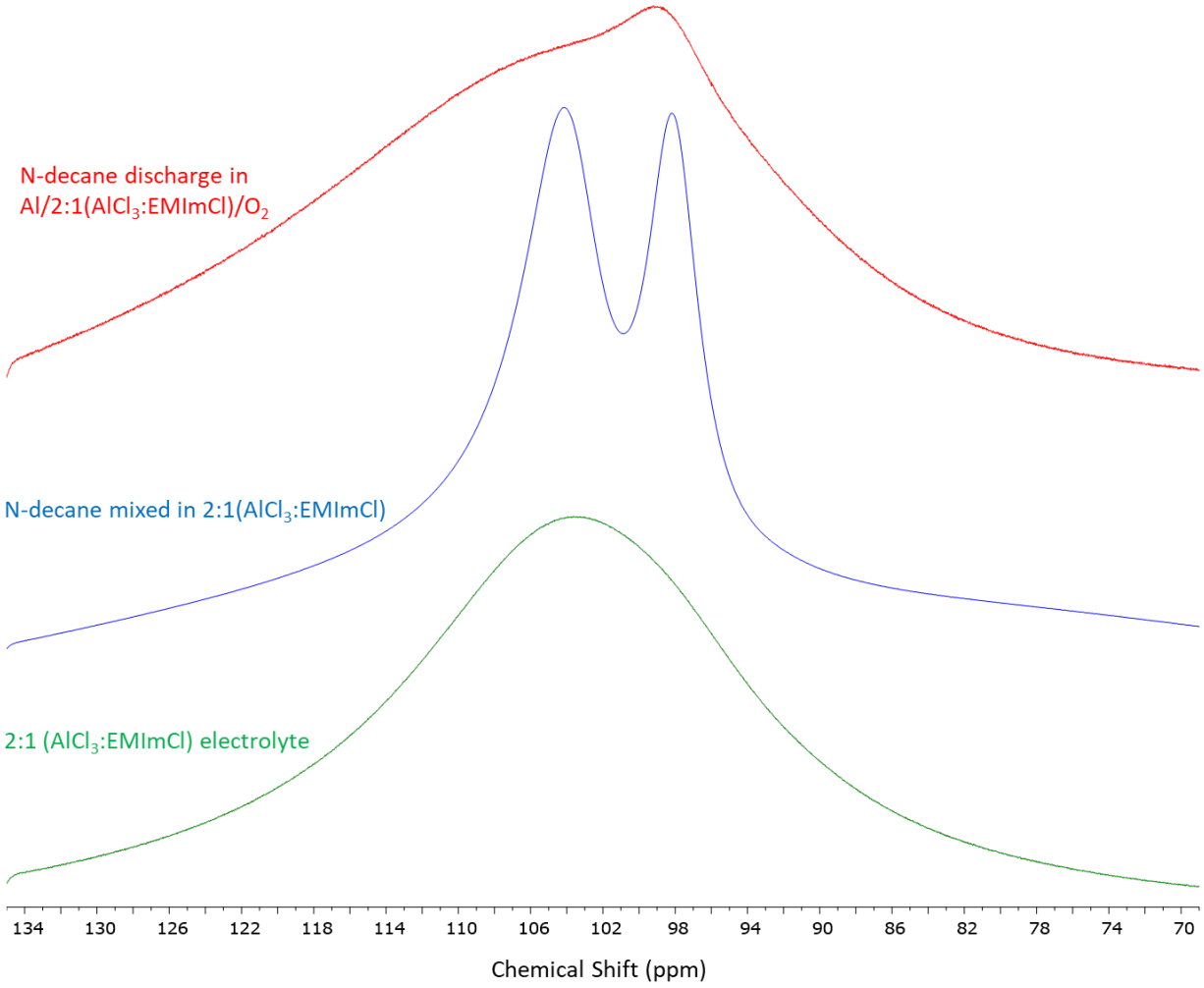

Figure S2.20: ^{27}Al-NMR of 2:1 ($AlCl_3$:EMImCl) electrolyte. The spectra are for the electrolyte with and without n-decane and after discharge in an Al/O_2 cell.

REFERENCES

1. Bartmess, J. & Georgiadis, R., Empirical Methods for Determination of Ionization Gauge Relative Sensitivities for Different Gases. *Vacuum* **33**, 149-153 (1983).
2. Cody, R., Larame´e, J. & Durst, H., Versatile New Ion Source for the Analysis of Materials in Open Air under Ambient Conditions. *Anal. Chem.* **77**, 2297-2302 (2005).
3. Cody, R., Observation of Molecular Ions and Analysis of Nonpolar Compounds with the Direct Analysis in Real Time Ion Source. *Anal. Chem.* **81**, 1101-1107 (2009).
4. Wu, C., Qian, K., Nefliu, M. & Cooks, R., Ambient Analysis of Saturated Hydrocarbons Using Discharge-Induced Oxidation in Desorption Electrospray Ionization. *J. Am. Soc. Mass Spectrom.* **21**, 261-267 (2010).
5. Cody, R. & Dane, A., Soft Ionization of Saturated Hydrocarbons, Alcohols and Nonpolar Compounds by Negative-Ion Direct Analysis in Real-Time Mass Spectrometry. *J. Am. Soc. Mass Spectrom.* **24**, 329-334 (2013).
6. Yang, Z. & Attygalle, A., Aliphatic Hydrocarbon Spectra by Helium Ionization Mass Spectrometry (HIMS) on a Modified Atmospheric-Pressure Source Designed for Electrospray Ionization. *J. Am. Soc. Mass Spectrom.* **22**, 1395-1402 (2011).
7. Gray, J. & Maciel, G., Aluminum-27 Nuclear Magnetic Resonance Study of the Room-Temperature Melt $AlCl_3$/n-Butylpyridinium Chloride. *J. Am. Chem. Soc.* **103**, 7147-7151 (1981).
8. Wilkes, J., Frye, J. & Reynolds, G. ^{27}Al and ^{13}C NMR Studies of Aluminum Chloride-Dialkylimidazolium Chloride Molten Salts. *Inorg. Chem.* **22**, 3870-3872 (1983).

9. Zhang, J., Huang, C., Chen, B., Ren, P. & Pu, M., Isobutane/2-butene alkylation catalyzed by chloroaluminate ionic liquids in the presence of aromatic additives. *J. of Catalysis* **249**, 261-268 (2007).

CHAPTER 3

Conclusion and Future Work

To summarize, we've demonstrated a high-energy density metal/O_2 electrochemical cell as a system to convert low-value feedstocks into higher value products. Results in the previous chapters show that the conversion is facilitated by an electrochemically generated superoxide (O_2^-) specie and by specific, possibly catalytic interactions of molecules in the feed with the Ionic Liquid/Lewis acid salt electrolyte. From the perspective of energy storage, results reported in the theses show how sacrificial agents might be used to increase specific capacity of metal/oxygen cells by 2 to 10 folds. These sacrificial agents appear to achieve this function, by protecting other components of the cell (salt, electrolyte) from reactions with the highly nucleophilic superoxide intermediates at the cathode. Electrochemical and physical analytical techniques were used to understand the synergistic effects of electrolyte and superoxide in converting several low-value feedstocks of contemporary interest. With a CO_2 co-feed, an Al/O_2 electrochemical cell was shown to convert the CO_2 to a valuable C_2 species, demonstrating a novel approach to carbon capture and conversion. The Al/O_2 electrochemical cell oligomerized and isomerized an alkane feed, showing the system's ability to upgrade low octane-rating hydrocarbons to higher octane-rating. Combining CO_2 and hydrocarbon feedstocks, the system carboxylated the hydrocarbon.

3.1 Water Insensitive Electrolyte

One of the major drawbacks to direct industrial adoption of the proposed Al/($AlCl_3$:EMImCl)/O_2 electrochemical system is the hygroscopic characteristics of the

electrolyte. To use as this system as a platform for carbon capture and conversion from exhaust streams, water must be separated to avoid degradation of the electrolyte. As pointed in Chapter 1, variations in the aluminum salt and ionic liquid have been studied in the literature [1-2] as paths for creating water-insensitive electrolytes. Alternatives will have to be investigated for CO_2, hydrocarbon and other feedstocks activation as well as electrochemical suitability. Noticeably, when discharging the $AlCl_3$:EMImCl electrolyte in an Al/O_2 electrochemical cell while maintaining a layer of alkane on top, the hydrocarbon layer acts as a barrier protecting the electrolyte from moisture penetration and degradation.

3.2 Incorporation of Low-Value Feedstock

We demonstrated the application of metal/O_2 to upgrade CO_2 and hydrocarbon feedstocks. The system's scalability and economic advantages potentially lends it to other conversion processes, including conversion of sulfur-containing hydrocarbons, heavy refining products, natural gas and toxic chemicals. The architecture of the electrochemical cell and individual components will have be changed to accommodate these different feedstocks.

3.3 Theoretical Modeling of Mechanism

The physical analytical techniques adopted in this work provide a process for rigorously investigating reaction products and through careful experiments identifying elements of a plausible reaction mechanism. More detailed information about reaction mechanisms, including the role played by specific components in the electrolyte in interaction/complexing with molecules in the feed require greater access to the distribution of molecular species formed and to time-dependent changes in structure and composition of these species. How the complexes go on to react with the

electrochemically produced superoxide likewise remains an open question. Complementary theoretical and computational studies able to simultaneously elucidate changes in molecular structure and solvent environment are particularly expected to provide fruitful directions for additional inquiry. Among the benefits of such efforts would be deeper knowledge of the interactions that might be used to produce products of desired chemical composition. This knowledge can be used for conversion systems designed to handle mixed feedstocks to control competition for nucleophilic reaction with the superoxide to form specific, desired products.

3.4 REFERENCES

1. Veder, J., Horne, M., Rüther, T., Bondc, A. & Rodopoulos, T., The influence of thermal degradation on the electrodeposition of aluminium from an air- and water-stable ionic liquid. *Phys. Chem. Chem. Phys.* **15**, 7470-7474 (2013).
2. El Abedin, S., Moustafa, E., Hempelmann, R., Natter, H., & Endres, F., Electrodeposition of Nano- and Microcrystalline Aluminium in Three Different Air and Water Stable Ionic Liquids. *ChemPhysChem.* **7**, 1535-1543 (2006).